MASTER

A wideband circularly polarized microstrip antenna array

Vrinten, M.L.A.

Award date:
1988

TECHNISCHE UNIVERSITEIT EINDHOVEN

FACULTEIT ELEKTROTECHNIEK

VAKGROEP Theoretische Elektrotechniek

A wideband circularly polarized microstrip antenna array

door

M.L.A. Vrinten

ET-4-88

Verslag van een afstudeeronderzoek,
verricht in de vakgroep ET, onder
leiding van dr. M.E.J. Jeuken,
in de periode mei 1987 - april 1988.

Eindhoven, 15 april 1988.

Abstract.

Microstrip antennas are likely to become increasingly important in the areas of antenna design for mobile communications. Especially in the lower frequency bands, where conventional antennas, such as horns, will become very bulky, use of microstrip antennas appears to be advantageous. The development of a multiple-beam antenna for mobile satellite communication services is a project, with which the group 'Electromagnetics' at the Eindhoven University of Technology is concerned. A specific project requirement was to develop a circularly polarized antenna array with good axial ratio over the frequency band 1.5 GHz to 1.6 GHz.

The major operational disadvantage of microstrip antennas is their narrow frequency bandwidth. When microstrip antennas are used to obtain circular polarization, the axial ratio bandwidth appears to be the limiting factor.

However, recent developments have shown that, when the antennas are placed in a sequentially rotated fashion, a considerable improvement in axial ratio bandwidth is obtained. The gain loss appears now to be the limiting factor.

In this report important theoretical and practical properties of microstrip antennas and feeding networks are considered, resulting in a practical design of a four element sequentially rotated array.

With this array, good circular polarization is obtained over a relatively wide frequency band and wide azimuthal angle in all planes and can be summarized as

Axial ratio < 1 dB : 1.42 GHz < f < 1.54 GHz in broadside direction.

: $|\theta| < 35^\circ$ f = 1.5 GHz

Contents

1. Introduction.

In recent years, the use of microstrip antennas and microstrip antenna arrays has become of great importance. Especially in satellite communications services, the benefit of this antenna is obvious, due to its lightweight and thin planar configuration. As the used frequency is rather low, the advantage of microstrip antenna technology becomes even more evident, because the conventional antennas, usually horn antennas, will become very bulky and cumbersome.
Part of the group 'Electromagnetism' is concerned with the investigation to a multiple beam antenna for mobile satellite communications service. This investigation is dealt with an offset parabolic reflector with an antenna array as feed. One of the outcomes of this investigation is, that the spacing of the feed elements is required to be very small. Application of conventional antennas is not suitable anymore, because of their large dimensions at the specified frequencies (1.5 GHz and 1.6 GHz). Microstrip antennas are much more tractable in its dimensional design, because the patch size is strongly dependent of the substrate dielectric constant. It seems therefore worthwhile to investigate the properties of an array consisting of these elements.
The aim of the investigation, discussed in this report, is to develop a circularly polarized microstrip antenna, suitable for the frequencies 1.5 GHz to 1.6 GHz. We will see, that the necessary bandwidth is not easy to realize, because the microstrip antenna is a narrow band device.

This report is organized as follows. In Chapter 2, the fundamental characteristics concerning polarization are defined and applied to antenna arrays. A brief discussion of polarization measurements is included in this chapter.
The principal operation of the microstrip antenna is discussed in Chapter 3. Only the rectangular antenna is considered, because this is the type of antenna we shall deal henceforth. The interior fields are obtained with the cavity model. Other important features are the input impedance, bandwidth, radiation pattern and occurring losses, to be discussed in consecutive sections.
The antenna feeding network is performed in microstrip, to maintain the specific advantages of microstrip antenna technology. This network consists of power splitters and phase shifters to provide equal amounts of power and appropriate phasings to the antenna input ports. Chapter 4 is primarily concerned with the theoretical analysis and practical design of the Wilkinson power splitter.

In Chapter 5 general methods to obtain circular polarization with microstrip antennas are discussed. Advantages and disadvantages of these methods are considered, resulting in a practical design of a four element sequentially rotated array. This antenna configuration is expected to give a considerable improvement in axial ratio bandwidth.
Experimental results are discussed in Chapter 6. The measured reflection coefficients and polarization patterns of the sequentially rotated array are compared with those of a single element.

2. Concepts of circular polarization.

The basic principles concerning circular polarization will be given in this chapter.
Important features in elliptical polarization are the co- and crosspolarization and axial ratio. A definition of them will be given in the first part.
These concepts will be applied to antenna arrays in the second part. There are several possibilities to obtain circular polarization by making use of antenna arrays. Some examples are given in a next chapter with their respective advantages and disadvantages.
A FORTRAN-computerprogram that calculates the mentioned characteristics is added to this report [Appendix A].

2.1 Characteristics of circularly polarized radiation.

The spherical co-ordinate system is shown in Fig.2.1.

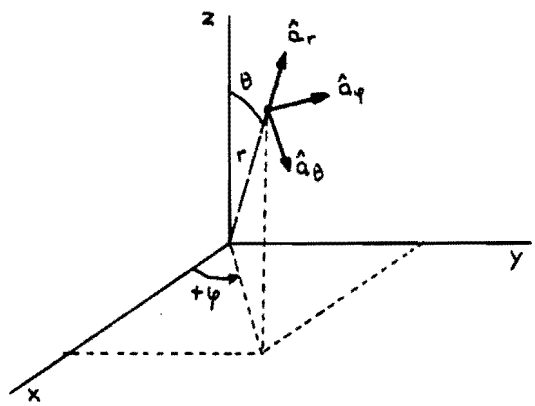

Fig. 2.1 The spherical co-ordinate system.

The co-ordinate transformation from the cartesian to the spherical co-ordinate-system is given by the relations

$$\hat{a}_r = \sin\theta\cos\varphi\,\hat{a}_x + \sin\theta\sin\varphi\,\hat{a}_y + \cos\theta\,\hat{a}_z \qquad (2.1.a)$$

$$\hat{a}_\theta = \cos\theta\cos\varphi\,\hat{a}_x + \cos\theta\sin\varphi\,\hat{a}_y - \sin\theta\,\hat{a}_z \qquad (2.1.b)$$

$$\hat{a}_\varphi = -\sin\varphi\,\hat{a}_x + \cos\varphi\,\hat{a}_y \qquad (2.1.c)$$

We consider an arbitrary antenna placed in the origin of the co-ordinate system. From antenna theory [11] we know that the radiation field can be written as

$$\bar{E}(r,\theta,\varphi) = E_\theta(r,\theta,\varphi)\,\hat{a}_\theta + E_\varphi(r,\theta,\varphi)\,\hat{a}_\varphi \qquad (2.2.a)$$

$$\bar{H}(r,\theta,\varphi) = H_\theta(r,\theta,\varphi)\,\hat{a}_\theta + H_\varphi(r,\theta,\varphi)\,\hat{a}_\varphi \qquad (2.2.b)$$

These relations are given in complex phasor notation. Moreover, the relation between E and H is given by

$$Z_o\,\bar{H} = \hat{a}_r \times \bar{E} \qquad (2.3)$$

with Z_o the wave impedance in vacuum.
Now we are ready to define the polarization of the wave [1].
Let $\bar{\mathcal{E}}(r,\theta,\varphi,t)$ and $\bar{\mathcal{H}}(r,\theta,\varphi,t)$ be the time dependent field components. The polarization of a wave is that property describing the time varying direction and relative magnitude of $\bar{\mathcal{E}}$- or $\bar{\mathcal{H}}$-vector; specifically, the figure traced as a function of time by the extremity of the vector at a fixed location, and the sense in which it is traced, as observed along the direction of propagation (Fig.2.2).

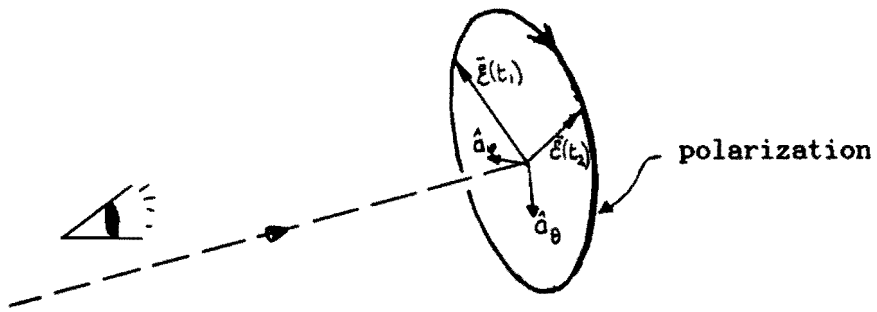

Fig.2.2 Polarization of a wave.

We are only dealing with time-harmonic waves of the same frequency. We write the complex E-vector as

$$\bar{E} = |E_\theta| e^{j\psi_\theta} \hat{a}_\theta + |E_\varphi| e^{j\psi_\varphi} \hat{a}_\varphi = e^{j\psi_\theta} \left\{ |E_\theta|\,\hat{a}_\theta + |E_\varphi|\, e^{j\psi} \hat{a}_\varphi \right\} \qquad (2.4)$$

with $\psi = \psi_\varphi - \psi_\theta$

The polarization is linear when $\psi = 0$. The electric vector describes a straight line in a specified point in space as a function of time.
We are primarily concerned with circular polarization. This type of polarization is obtained when

$$|E_\theta| = |E_\varphi| \tag{2.5.a}$$

$$\psi = \pm \pi/2 \tag{2.5.b}$$

With the conditions (2.5) equation (2.4) can be written as

$$\bar{E} = e^{j\psi_\theta} |E_\theta| \left\{ \hat{a}_\theta \pm j \hat{a}_\varphi \right\} \tag{2.6}$$

Returning to the instantaneous form gives

$$\bar{\mathcal{E}}(r,t) = |E_\theta| \left\{ \cos(\omega t + \psi_\theta) \hat{a}_\theta \mp \sin(\omega t + \psi_\theta) \hat{a}_\varphi \right\} \tag{2.7}$$

Applying the minus-sign in (2.5.b) leads to rotation in the counterclockwise sense. We will call it left-hand circular polarization (LHC). The plus-sign gives right-hand circular polarization (RHC).
For the general case, $|E_\theta| \neq |E_\varphi|$ or $\psi \neq 0$ or $\psi \neq \pm \pi/2$, the polarization appears to be elliptic. The polarization ellipse arises from the vectorial addition of the extremities of two oppositely rotating vectors, representing the contributions of the left-hand and right-hand circular polarization. The sense of circular polarization that predominates is called the copolarization, the other is referred to as the crosspolarization.
Eq.2.2.a can be written as follows

$$\bar{E} = E_\theta \hat{a}_\theta + E_\varphi \hat{a}_\varphi = E_L \hat{a}_L + E_R \hat{a}_R \tag{2.8}$$

with complex unit-vectors

$$\hat{a}_L = \frac{1}{\sqrt{2}} (\hat{a}_\theta + j \hat{a}_\varphi)$$

$$\hat{a}_R = \frac{1}{\sqrt{2}} (\hat{a}_\theta - j \hat{a}_\varphi)$$

E_L and E_R represent the LHC-, respectively the RHC-component. Writing out eq.2.8, we obtain

$$E_L = \frac{1}{\sqrt{2}} (E_\theta - j E_\varphi) \tag{2.9.a}$$

$$E_R = \frac{1}{\sqrt{2}} (E_\theta + j E_\varphi) \tag{2.9.b}$$

A graphical representation is given in Fig.2.3.

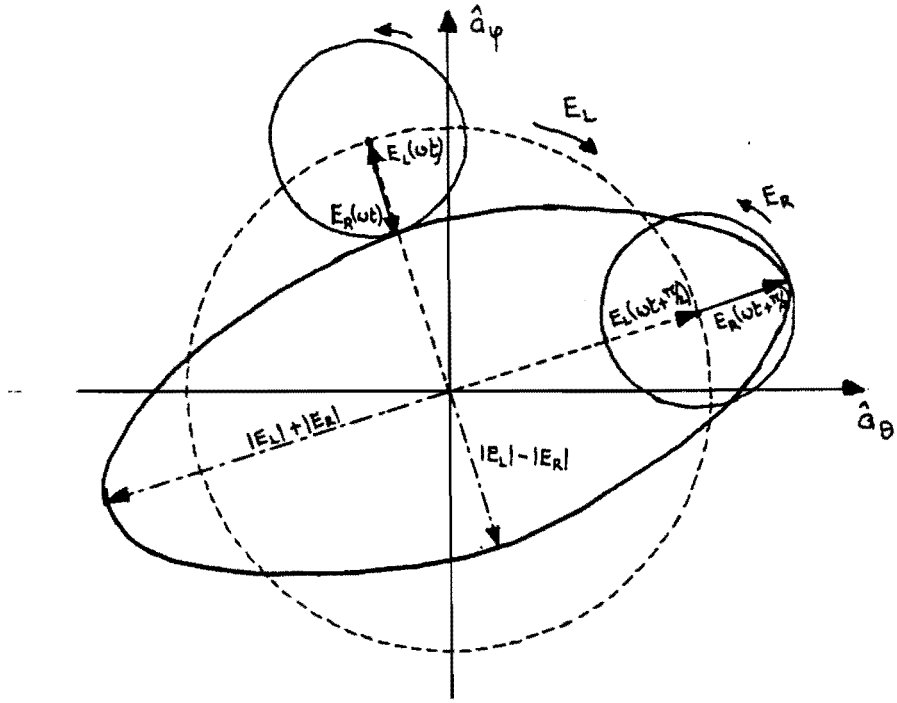

Fig.2.3 Polarization ellipse as a result of the vectorial addition of two oppositely rotating vectors. Wave propagation out of the paper.

Another important feature of the polarization ellipse is the axial ratio, defined as

$$AR = \left| \frac{|E_L| + |E_R|}{|E_L| - |E_R|} \right| \qquad (2.10)$$

From Fig.2.3 you can see that the axial ratio represents the length ratio of the longest and shortest axis of the ellipse.
The defined characteristics are usually given in decibell (dB).
Suppose we have a wave, predominantly LHC-polarized. We can write

copolarization $$|E_L|_{dB} = 20\,{}^{10}\log \frac{|E_L|}{|E_L|_{max}} \qquad (2.11.a)$$

crosspolarization $$|E_R|_{dB} = 20\,{}^{10}\log \frac{|E_R|}{|E_L|_{max}} \qquad (2.11.b)$$

axial ratio $$AR_{dB} = 20\,{}^{10}\log AR \qquad (2.11.c)$$

For a RHC-polarized wave we have to change the indices L and R.

2.2 Circularly polarized antenna arrays.

In this chapter we will derive general formulas for the radiation pattern of a two-dimensional antenna array.
To do this, we write the radiation pattern of an arbitrary antenna placed in the origin of the co-ordinate system as follows.

$$\bar{E} = \frac{-jke^{-jkr}}{4\pi r} \left\{ f_\theta(\theta,\varphi)\,\hat{a}_\theta + g_\varphi(\theta,\varphi)\,\hat{a}_\varphi \right\} \qquad (2.12)$$

We consider this antenna as a reference antenna. Rotating the antenna over an angle φ_o as depicted in Fig.2.4 leads to modification of eq.2.12 as

$$\bar{E} = \frac{-jke^{-jkr}}{4\pi r} \left\{ f_\theta(\theta,\varphi-\varphi_o)\,\hat{a}_\theta + g_\varphi(\theta,\varphi-\varphi_o)\,\hat{a}_\varphi \right\} \qquad (2.13)$$

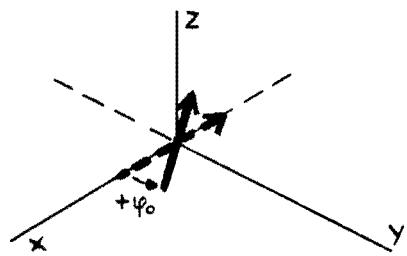

Fig.2.4 Rotation of the reference antenna.

Let's now consider an antenna as mentioned above placed somewhere in the xy-plane (Fig.2.5).

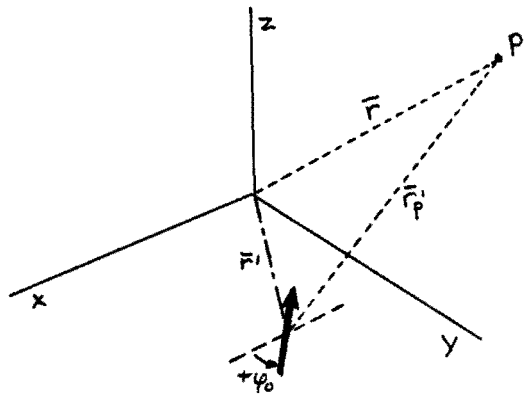

$r_p = |\bar{r}_p|$

Fig.2.5 Antenna placed in the xy-plane.

For this antenna, eq.2.13 has to be written as

$$\bar{E} = \frac{-jke^{-jkr_p}}{4\pi r_p} \left\{ f_\theta(\theta,\varphi-\varphi_0)\hat{a}_\theta + g_\varphi(\theta,\varphi-\varphi_0)\hat{a}_\varphi \right\} \qquad (2.14)$$

In the denominator, r_p can be approximated by r . However, this is not permitted for the 'phase term' e^{-jkr_p} ,in which r_p must be approximated by [11]

$$r_p \simeq r - (\hat{r}\cdot\bar{r}') \qquad (2.15)$$

with $\hat{r} = \frac{\bar{r}}{r}$

which is valid for $$r > \frac{2D^2}{\lambda} \qquad (2.16)$$

the well known far field criterion. In eq.2.16, D is the maximum size of the antenna system and λ represents the wavelength in vacuum.
Consequently, the approximate contribution for a single antenna to the far field becomes

$$\bar{E} \simeq \frac{-jke^{-jkr}}{4\pi r} e^{jk(\hat{r}\cdot\bar{r}')} \left\{ f_\theta(\theta,\varphi-\varphi_0)\hat{a}_\theta + g_\varphi(\theta,\varphi-\varphi_0)\hat{a}_\varphi \right\} \qquad (2.17)$$

Now consider N antennas arbitrarily placed in the xy-plane, each of them having a specific rotation φ_i with regard to a reference antenna thought in the origin.
Since the antennas are excited sinusoidally, we can also choose the phase ψ_i, and the amplitude A_i.
Summarizing, suppose a reference antenna in the origin with field components

$$E_\theta(r,\theta,\varphi) = \frac{-jke^{-jkr}}{4\pi r} f_\theta(\theta,\varphi) \qquad (2.18.a)$$

$$E_\varphi(r,\theta,\varphi) = \frac{-jke^{-jkr}}{4\pi r} g_\varphi(\theta,\varphi) \qquad (2.18.b)$$

Then the field components of an N-element two dimensional array, neglecting the effects of mutual coupling, can be written as

$$E_\theta^N(r,\theta,\varphi) = \frac{-jke^{-jkr}}{4\pi r} \sum_{i=1}^{N} A_i e^{j(\psi_i + k(\hat{r}\cdot\bar{r}_i'))} f_\theta(\theta,\varphi-\varphi_i) \qquad (2.19.a)$$

$$E_\varphi^N(r,\theta,\varphi) = \frac{-jke^{-jkr}}{4\pi r} \sum_{i=1}^{N} A_i e^{j(\psi_i + k(\hat{r}\cdot\bar{r}_i'))} g_\varphi(\theta,\varphi-\varphi_i) \qquad (2.19.b)$$

From eqs.2.9 and 2.10 , we find the co-,crosspolarization and axial ratio for the array.
A FORTRAN-computerprogram based on (2.19) is described in appendix A. This program calculates the CP-characteristics for an N-element antenna array.

2.3 Theory of measurement.

Several possibilities to measure the characteristics of circular polarization are discussed in this chapter.
Our purpose is, to measure the copolarization, crosspolarization and axial ratio as a function of the polar angle θ and as a function of the frequency. If possible, we want to determine the sense of rotation too.
The first method we consider is the so-called polarization pattern method [1]. This method requires, that a linearly polarized antenna, usually a dipole, be used to probe the polarization in the plane, that contains the direction of the desired polarization. The arrangement is shown in Fig.2.6. The dipole is rotated in the plane of the polarization, which is taken to be normal to the direction of the incident field and the output voltage of the probe is recorded. In this case, the rotating dipole is used as the receiving antenna, and the antenna under test is used as the transmitting antenna. However, the opposite arrangement is possible as well.

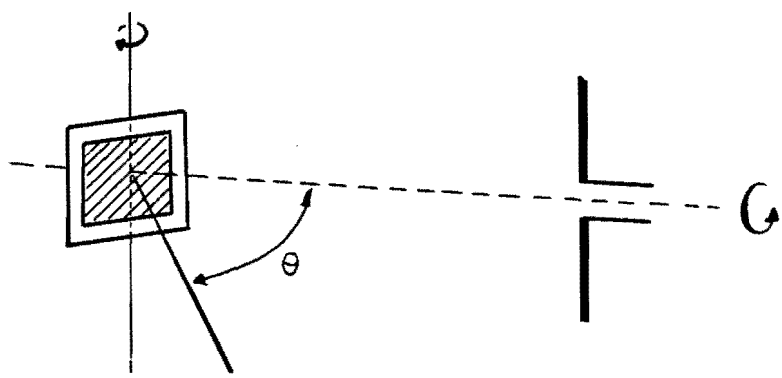

antenna under test rotating dipole

Fig.2.6 Polarization measuring system.

A typical polarization pattern using this method is given in Fig.2.7. The angular frequency of the rotating dipole is required to be much greater than the angular frequency of the antenna under test.

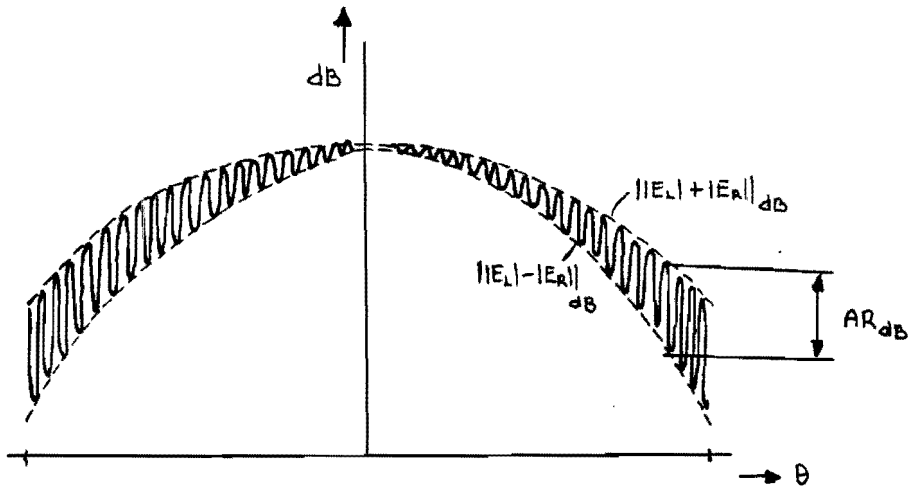

Fig.2.7 Typical polarization pattern.

With this method the axial ratio is easily extracted as indicated in Fig.2.7. However, the copolarization and crosspolarization are not obvious. Another disadvantage of this method is that the sense of rotation cannot be determined.

A more elaborate method in which even the sense of rotation can be determinedis the following. With the measurement system installed, it is possible to do both amplitude and phase measurements at once. Using a linearly polarized antenna in the transmitting mode and the antenna under test in the receiving mode, we have to do two measurements as indicated in Fig.2.8.

In the first measurement, position A of the transmitting antenna (H-plane), we obtain the E_θ-components as a function of the angle φ. The second measurement, in which the transmitting antenna is rotated over 90° in a predetermined way (position B, E-plane) delivers the E_φ-components as a function of the angle φ.

Note, that the angle φ as depicted in Fig.2.8 has the same function as the polar angle θ in the co-ordinate system of Fig.2.1.

The results of both measurements are stored in different files as complex numbers in the computer, one file containing the H-plane measurements (E_θ-components), the other containing the E-plane measurements (E_φ-components). The acquired data can be converted to the demanded characteristics with the eqs.2.9 and 2.10.

A FORTRAN-computerprogram that accomplishes this, is added to this report [Appendix B].

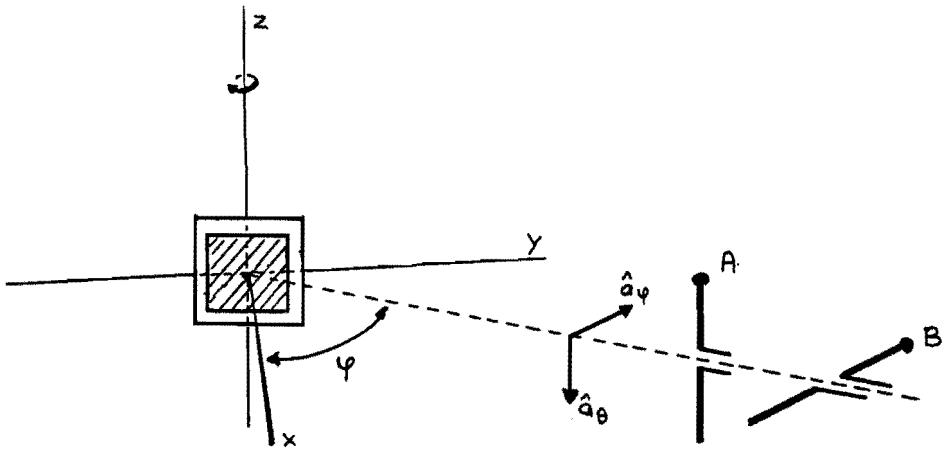

Antenna under test. Linearly polarized antenna.

Fig.2.8 Measuring system obtaining CP-characteristics using the results of two measurements with a linearly polarized antenna.

3. Microstrip antennas

This chapter is intended to give an introduction in the technology of microstrip antennas. The principal operation of the antenna will be briefly summarized and practical design formulas are given.
We only discuss the rectangular patch antenna because this is the type of antenna we shall deal henceforth. For other types of geometry we refer to the literature.
For a first-order approach the antenna operates like a cavity with magnetic conducting sidewalls. This is an accepted approach and will be discussed in the first section.
Other important properties which need attention, are the input impedance, bandwidth and radiation pattern of the antenna. Also some words will be devoted to the losses in the microstrip antenna.

3.1 The cavity model.

Microstrip antennas consist of a very thin metallic strip (patch) placed a small fraction of a wavelength above a ground plane. The strip and the ground plane are separated by a dielectric sheet (referred to as the substrate), as shown in Fig.3.1.
The antenna feed is modelled as a z-directed current probe I_0.

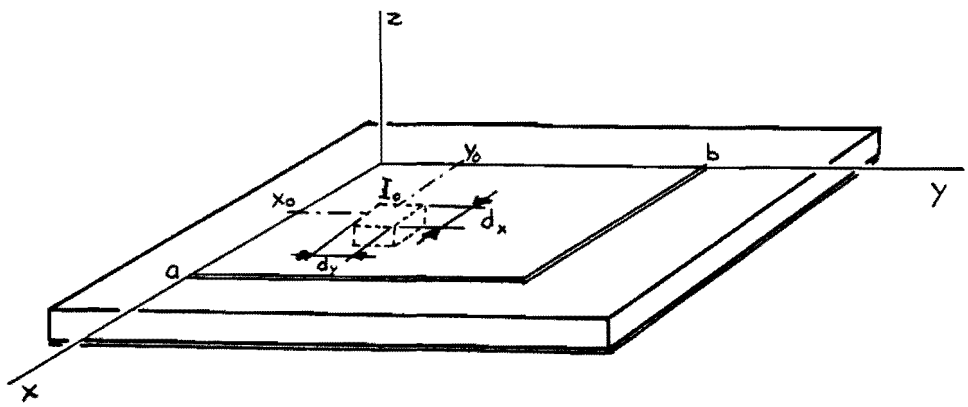

Fig.3.1 Microstrip antenna with inset feed-point.

Because the thickness of the antenna is usually very small, the waves generated within the substrate undergo considerable reflections when they arrive at the edge of the patch. Therefore only a small fraction of the incident energy is radiated. Thus, the antenna behaves more like a cavity instead of a radiator.

Assuming a perfectly magnetic conducting sidewall and perfectly electric conductors at the top and ground plane, we can solve the Helmholtz-equation for the boundary conditions

$$\begin{aligned} \hat{n} \times \bar{H} &= \bar{0} && \text{for the sidewalls} \\ \hat{n} \times \bar{E} &= \bar{0} && \text{for top and ground plane} \end{aligned} \tag{3.1}$$

When the substrate is electrically thin, the electric field will be z-directed and the interior modes will be TM_{mn} to z, so that [3]

$$E_z(x,y) = \sum_m \sum_n A_{mn}\, e_{zmn}(x,y) \tag{3.2}$$

where A_{mn} are the mode amplitude coefficients and $\bar{e}_{mn}$ are the z-directed electric field mode vectors. The orthogonality relationships for the mode vectors are written as [8]

$$\iiint \varepsilon\, \bar{e}_{m_1 n_1} \cdot \bar{e}_{m_2 n_2}\, dV = \begin{cases} 0 & m_1 \neq m_2 \text{ or } n_1 \neq n_2 \\ 1 & m_1 = m_2 \text{ and } n_1 = n_2 \end{cases} \tag{3.3}$$

The mode vectors $\bar{e}_{mn}$, which satisfy the homogeneous scalar Helmholtz wave equation and the boundary conditions (3.1) for the rectangular patch, can be written as

$$e_{zmn}(x,y) = \frac{\chi_{mn}}{\sqrt{\varepsilon_0 \varepsilon_r abh}} \cos k_m x \cos k_n y \tag{3.4}$$

with $$\chi_{mn} = \begin{cases} 1 & m=0 \text{ and } n=0 \\ \sqrt{2} & m=0 \text{ or } n=0 \\ 2 & m\neq 0 \text{ and } n\neq 0 \end{cases}$$

and eigenvalues

$$\begin{aligned} k_m &= \frac{m\pi}{a} \\ k_n &= \frac{n\pi}{b} \end{aligned} \tag{3.5}$$

The eigenvalues k_m and k_n satisfy the separation equation

$$k_{mn}^2 = \omega_{mn}^2 \mu_0 \varepsilon = k_m^2 + k_n^2 \tag{3.6}$$

and so, a first order approximation for the resonant frequency can be written as

$$f_{mn} = \frac{\omega_{mn}}{2\pi} = \frac{1}{2\sqrt{\mu_0 \varepsilon}} \sqrt{\left(\frac{m}{a}\right)^2 + \left(\frac{n}{b}\right)^2} \tag{3.7}$$

The mode amplitude coefficients can be determined by substituting (3.2) and (3.4) into the inhomogeneous wave equation with known current density $\bar{J}$ in the cavity [3].
This results in

$$A_{mn} = \frac{j\sqrt{\mu_o\varepsilon}\,k}{k^2 - k_{mn}^2} \iiint_V \bar{J}\cdot\bar{e}_{mn}^{*}\, dv \tag{3.8}$$

where we integrate over the volume containing the current density $\bar{J}$.
When $\bar{J}$ is a z-directed current probe I_o of small rectangular cross-section $d_x\, d_y$ at (x_o, y_o), eq.3.8 reduces to

$$A_{mn} = j\, I_o \sqrt{\frac{\mu h}{ab}}\; \frac{k\,\chi_{mn}}{k^2 - k_{mn}^2}\; F_{mn}\, \cos k_m x_o \cos k_n y_o \tag{3.9}$$

with $$F_{mn} = \operatorname{sinc}\left(\frac{m\pi d_x}{2a}\right) \operatorname{sinc}\left(\frac{n\pi d_y}{2b}\right) \tag{3.10}$$

$$\operatorname{sinc}(x) = \frac{\sin x}{x} \qquad k = \frac{2\pi}{\lambda} = \omega\sqrt{\mu_o\varepsilon}$$

The voltage at the feed is computed as

$$V_{in} = -h\, E_z(x_o, y_o) \tag{3.11}$$

which leads to the input impedance

$$Z_{in} = \frac{V_{in}}{I_o} = -j\sqrt{\frac{\mu_o}{\varepsilon}}\; kh \sum_{m=0}^{\infty}\sum_{n=0}^{\infty} \frac{\psi_{mn}^2(x_o, y_o)}{k^2 - k_{mn}^2}\; F_{mn} \tag{3.12}$$

with $$\psi_{mn}(x,y) = \frac{\chi_{mn}}{\sqrt{ab}}\, \cos k_m x \cos k_n y \tag{3.13}$$

The input impedance will be considered later on.
To gain some insight in the operation of the antenna, the TM_{01}-mode is closer examined, neglecting the contribution of the other modes.
The TM_{01}-mode is the case of most interest in practical applications.
For the electric field in the cavity holds

$$E_z(x,y) = E_{01} \cos k_n y = E_{01} \cos\left(\frac{\pi y}{b}\right) \tag{3.14}$$

with resonant frequency $$f_{r_0} = \frac{1}{2b\sqrt{\mu_o\varepsilon}} \tag{3.15}$$

Eq.3.15 gives errors up to 20%. A more accurate expression for the resonant frequency is [10]

$$f_{ri} \approx f_{ro} \frac{\varepsilon_r}{\sqrt{\varepsilon_e(a)\,\varepsilon_e(b)}} \cdot \frac{1}{1+\Delta} \qquad (3.16)$$

where

$$\Delta = \frac{h}{b}\left[0.882 + \frac{0.164(\varepsilon_r-1)}{\varepsilon_r^2} + \frac{(\varepsilon_r+1)}{\pi\varepsilon_r}\left\{0.758 + \ln\left(\frac{b}{h}+1.88\right)\right\}\right]$$

$$\varepsilon_e(x) = \frac{\varepsilon_r+1}{2} + \frac{\varepsilon_r-1}{2}\left[1 + \frac{10h}{x}\right]^{-1/2}$$

which gives an error less than 3%.
The field structure of the rectangular patch antenna in the TM_{01}-mode is sketched in Fig.3.2.

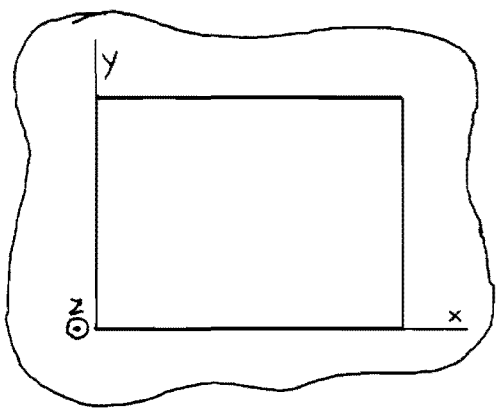

(a) Top view.

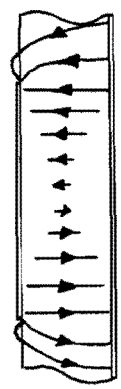

(b) yz-side view.

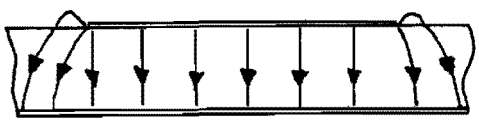

(c) xz-side view.

Fig.3.2 Field structure of rectangular patch in the TM_{01}-mode.

3.2 Input impedance.

The input impedance of a lossless and nonradiating cavity was given by Eq.3.12. This is not a realistic formula because we have neglected the losses under which the radiation 'losses'. This finds expression in the input impedance because it approaches infinity as k is equal to one of the resonant frequencies k_{mn}.
A more reasonable expression is obtained by the introduction of a complex frequency $\bar{k}^2 = \varepsilon_r(1-j\delta_{eff})k_o^2$. The purpose is to lump all the losses in an effective loss tangent δ_{eff} [14].
A discussion of an electric analogon, the RLC-parallel network, will make this acceptable.

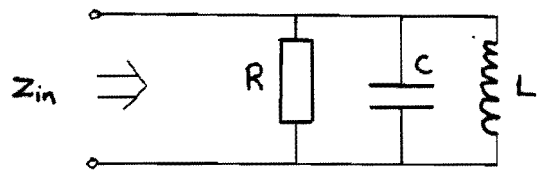

Fig.3.3 Parallel RLC-network.

The input impedance of this network can be written as

$$Z_{in} = \left(\frac{1}{R} + j\omega C + \frac{1}{j\omega L}\right)^{-1} = \frac{R}{1 + jQ\left(\frac{\omega}{\omega_o} - \frac{\omega_o}{\omega}\right)} \qquad (3.17)$$

with resonant frequency $\omega_o = \frac{1}{\sqrt{LC}}$

and quality factor $Q = R\sqrt{\frac{C}{L}} = \omega_o RC$

The bandwidth of this network is defined as that band of frequencies where $|Z_{in}| > R/\sqrt{2}$ and can be calculated as

$$B = \frac{\omega_o}{Q} \qquad (3.18)$$

We can now introduce a complex frequency $\bar{\omega}^2 = \omega^2(1-j/Q)$ by rewriting eq.3.17 as

$$Z_{in} = \frac{j\omega/C}{\frac{1}{LC} - \omega^2\left(1 - \frac{j}{\omega RC}\right)} \overset{(\omega \approx \omega_o)}{\approx} \frac{j\omega/C}{\frac{1}{LC} - \omega^2\left(1 - \frac{j}{\omega_o RC}\right)}$$

$$= \frac{j\omega/C}{\omega_o^2 - \omega^2(1 - j/Q)} = \frac{j\omega/C}{\omega_o^2 - \bar{\omega}^2} \qquad (3.19)$$

Rewriting eq.3.12 with the definitions

$$k^2 = \omega^2 \mu_o \varepsilon$$
$$\bar{k}^2 = \bar{\omega}^2 \mu_o \varepsilon = \omega^2 \mu_o \varepsilon (1 - j\delta_{eff}) = \omega^2 \mu_o \varepsilon (1 - j/Q_{eff}) \qquad (3.20)$$

we obtain, using the antenna in the TM_{01}-mode,

$$Z_{in} = \frac{h}{\varepsilon} \frac{j\omega \psi_{01}^2 F_{01}}{\omega_{01}^2 - \omega^2(1-j\delta_{eff})} + \frac{h}{\varepsilon} \sum_{m=1}^{\infty} \sum_{\substack{n=0 \\ n\neq 1}}^{\infty} \frac{j\omega \psi_{mn}^2 F_{mn}}{\omega_{mn}^2 - \omega^2(1-j\delta_{eff})} \qquad (3.21)$$

An observation of eqs.3.17, 3.19 and 3.21 shows that the antenna, as far as its impedance is concerned, can have a simple network representation. For frequencies near resonance of the TM_{01}-mode, but sufficiently away from all other resonant frequencies ω_{mn}, Z_{in} can be written as

$(\omega \approx \omega_{01})$

$$Z_{in} \approx \frac{1}{j\omega C_{01} + \frac{1}{R_{01}(\omega)} - j\frac{1}{\omega L_{01}}} + j\omega L' \qquad (3.22)$$

where

$$R_{01}(\omega) \approx R_{01}(\omega_{01}) = \frac{h}{\varepsilon \omega_{01} \delta_{eff}} \psi_{01}^2 F_{01} \qquad (3.23.a)$$

$$C_{01} = \frac{\varepsilon}{h \psi_{01}^2 F_{01}} \qquad (3.23.b)$$

$$L_{01} = \frac{h}{\varepsilon \omega_{01}^2} \psi_{01}^2 F_{01} \qquad (3.23.c)$$

$$L' = \frac{h}{\varepsilon} \sum_{m=1}^{\infty} \sum_{\substack{n=0 \\ n\neq 1}}^{\infty} \frac{\psi_{mn}^2 F_{mn}}{\omega_{mn}^2 - \omega^2} \qquad (3.23.d)$$

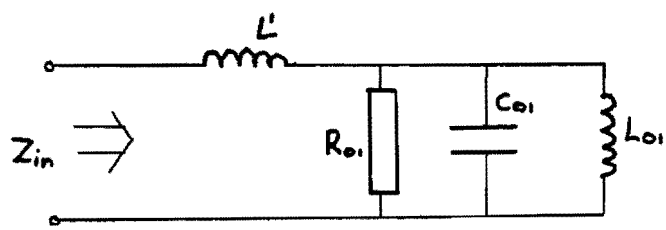

Fig.3.4 Network model for patch antenna operated in frequency band around ω_{01}.

The input impedance at resonance is

$$Z_{in_{res}} = j\omega_{01} L' + R_{01} \tag{3.24}$$

It should be noted, that we have to correct the resonance frequency ω_{01} for the fringing field by edge extension using for instance eq.3.16. The input resistance R_{01} is strongly dependent of the position of the feed point. Writing out eq.3.23.a, we obtain, with the feed centre at $(x_0, y_0) = (a/2, y_0)$. (Fig.3.1)

$$R_{01} = \frac{2h}{\varepsilon ab\, \omega_{01}\, \delta_{eff}} \cos^2\left(\frac{\pi y_0}{b}\right) \mathrm{Sinc}\left(\frac{\pi d_y}{2b}\right) \tag{3.25}$$

We see that, insetting the feed point causes a decrease in resistance. This gives us a method for matching the antenna to a transmission line with characteristic impedance Z_0.
The input impedance at resonance has an inductive part too [15]. This means that the resonant frequency of the antenna is not the frequency, where the absolute magnitude of the reflection coefficient Γ is minimal. An observation of the impedance locus in the Smith-chart will make this clear. If L' were zero, then the impedance 'circle' would be symmetrically disposed about the zero-reactance horizontal.
However, since L' is greater than zero, the impedance locus shifts into the inductive side of the Smith-chart. The resonant frequency must be determined where the right-half portion of the impedance locus crosses the $\omega_{01} L'$ line, as shown in Fig.3.5.

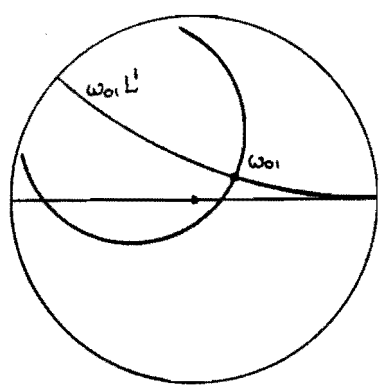

Fig.3.5 Typical Smith-chart display of microstrip antenna impedance locus.

In a practical design, however, the difference between the real resonant frequency and the resonant frequency obtained by determining $|\Gamma_{min}|$ is small, as the antenna is a narrow-band device.
It is found, that the resulting expressions (3.22) and (3.23) for the impedance of the microstrip antenna are in good agreement with measured results [14].

The series inductive reactance $X_{L'}$ may be calculated rigorously from eq.3.23.d, although the series converges slowly. The series reactance depends on the substrate thickness, the probe diameter and the probe inset distance. Measurements indicate, that (3.23.d) predicts the variation of feed inductance with feed location reasonably well, except near the edge of the patch [15]. When the antenna is used in a small band around a resonant mode, the resonant component of the input impedance often strongly dominates the series inductive component. In such cases, a crude estimate of this component is available from the formula of Carver.

$$X_{L'} = \sqrt{\frac{\mu_o}{\varepsilon}} \tan\left(\frac{2\pi h}{\lambda_d}\right) \qquad (3.26)$$

with λ_d the wavelength in the dielectric.
The parameter, that still needs discussion, is the effective loss tangent The loss tangent depends on the losses in the patch antenna.

3.3 Loss parameters in patch antennas.

We have seen that the microstrip antenna behaves like a cavity with losses. The power absorbed by the resonant antenna includes power dissipated in the loss mechanisms as well as the power radiated into the far field.
The quality factor of an ideal cavity and its relation with its loss tangent is defined as

$$Q = \frac{\omega \times \text{energy stored}}{\text{average power dissipated}} = \frac{\omega(W_e + W_m)}{P_d} \qquad (3.27)$$

with W_e: average stored electrical energy $\quad W_e = \frac{\varepsilon}{4}\iiint |\bar{E}|^2 dV$

W_m: average stored magnetic energy $\quad W_m = \frac{\mu}{4}\iiint |\bar{H}|^2 dV$

P_d: average dissipated power.

by analogy to the Q of an RLC-circuit. We know from Harrington [8], that for an ideal cavity, the relation $W_e = W_m$ holds. Hence

$$Q = \frac{2\omega W_e}{P_d} \qquad (3.28)$$

We shall now extend this definition to the microstrip antenna, considering its specific losses.

The average dissipated power can be separated in different parts. The first loss mechanism to be considered is the dielectric loss P_{di} ,which can be taken into account by introducing a complex dielectric constant $\bar{\varepsilon} = \varepsilon(1 - j\delta_{di})$, with δ_{di} the loss tangent of the dielectric.
The dielectric loss can be written as [12]

$$P_{di} = \omega W_e \tan\delta_i \tag{3.29}$$

The second loss mechanism is the conductance loss P_{Cu} . The magnetic field inside the cavity causes a current density in top and ground plane through the relation $\bar{J} = \hat{n} \times \bar{H}$, which results in the ultimate expression [12]

$$P_{Cu} = 2\sqrt{\frac{\omega}{\mu_o \sigma_c}} \cdot \frac{W_e}{h} \tag{3.30}$$

with σ_c the bulk conductivity of the conductor.
Another loss factor is the loss caused by waves, propagating through the substrate. The power carried with these surface waves is found to be less significant in many cases, especially when the antenna thickness is small compared to a wavelength, and will be omitted here for simplicity.
In addition to the loss factors considered until now, the power 'lost' through radiation can be obtained by integrating the radiated power over the upper hemisphere.

$$P_{rad} = \frac{1}{2z_o} \iint_S |\bar{E}(r,\theta,\varphi)|^2 \, dA \tag{3.31}$$

Neglecting the power lost through surface waves, we define the effective loss tangent by

$$Q_{eff} = \frac{1}{\delta_{eff}} = \frac{2\omega W_e}{P_{rad} + P_{Cu} + P_{di}} \tag{3.32}$$

When we have a cavity with a moderate high quality factor, it suffices to consider the dominant mode only, for determining the separate loss factors.

3.4 Radiation pattern of rectangular patch antenna in the TM_{01}-mode.

From antenna theory we know that it is possible to calculate the radiation field of a radiating aperture when the tangential electric field in the aperture is known.
Hammer et al. [7] considered the rectangular patch surrounded by four radiating slots. We may assume that the tangential electric fields in these slots are proportional to the fields inside the cavity. A composition of the radiating slots for an antenna in the TM_{01}-mode is given in Fig.3.5.

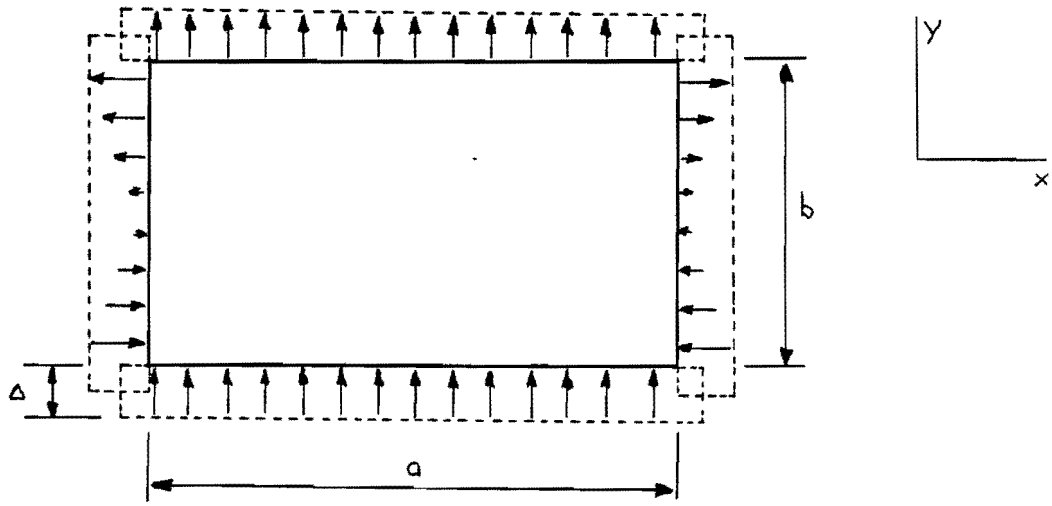

Fig.3.5 Radiating slots for a rectangular patch antenna in the TM_{01}-mode.

The components of the radiation field can be obtained with the help of the aperture distribution method.

$$E_\varphi = \frac{jke^{-jkr}}{4\pi r} 2E_0\Delta(a+\Delta)\cos\left(\frac{k(b+\Delta)}{2}\sin\theta\cos\varphi\right)\mathrm{sinc}\left(\frac{k(a+\Delta)}{2}\sin\theta\sin\varphi\right)\cos\theta\sin\varphi$$

$$\left\{\mathrm{sinc}\left(\frac{k\Delta}{2}\sin\theta\cos\varphi\right)+\frac{k^2\sin^2\theta\cos^2\varphi}{\left(\frac{\pi}{b+\Delta}\right)^2-k^2\sin^2\theta\cos^2\varphi}\,\mathrm{sinc}\left(\frac{k\Delta}{2}\sin\theta\sin\varphi\right)\right\} \qquad (3.33a)$$

$$E_\theta = \frac{jke^{-jkr}}{4\pi r} 2E_0\Delta(a+\Delta)\cos\left(\frac{k(b+\Delta)}{2}\sin\theta\cos\varphi\right)\mathrm{sinc}\left(\frac{k(a+\Delta)}{2}\sin\theta\sin\varphi\right)\cos\varphi$$

$$\left\{\mathrm{sinc}\left(\frac{k\Delta}{2}\sin\theta\cos\varphi\right)\frac{k^2\sin^2\theta\sin^2\varphi}{\left(\frac{\pi}{b+\Delta}\right)^2-k^2\sin^2\theta\cos^2\varphi}-\mathrm{sinc}\left(\frac{k\Delta}{2}\sin\theta\cos\varphi\right)\right\} \qquad (3.33.b)$$

with $\quad \mathrm{Sinc}(x) = \dfrac{\sin x}{x}$

We make now the following approximations.

$$\Delta << \lambda_o \qquad \Delta << a, b \tag{3.34}$$

and from eq.3.15 $$b \approx \frac{\lambda_o}{2\sqrt{\varepsilon_r}} \tag{3.35}$$

with λ_o the wavelength in vacuum.
Substituting these approximations in eqs.3.33 gives

$$E_\varphi = \frac{jke^{-jkr}}{4\pi r} 2E_o \Delta a \cos\left(\frac{\pi}{2\sqrt{\varepsilon_r}} \sin\theta\cos\varphi\right) \operatorname{sinc}\left(\pi \frac{a}{\lambda_o} \sin\theta \sin\varphi\right) \cos\theta \sin\varphi \left\{\frac{\varepsilon_r}{\varepsilon_r - \sin^2\theta\cos^2\varphi}\right\} \tag{3.36.a}$$

$$E_\theta = \frac{jke^{-jkr}}{4\pi r} 2E_o \Delta a \cos\left(\frac{\pi}{2\sqrt{\varepsilon_r}} \sin\theta\cos\varphi\right) \operatorname{sinc}\left(\pi \frac{a}{\lambda_o} \sin\theta \sin\varphi\right) \cos\varphi \left\{\frac{\sin^2\theta - \varepsilon_r}{\varepsilon_r - \sin^2\theta\cos^2\varphi}\right\} \tag{3.36.b}$$

The rectangular patch antenna is linearly polarized. The field components in the principal planes are

E-plane (φ=0) :
$$\begin{cases} E_\varphi = 0 \\ E_\theta = \dfrac{-jke^{-jkr}}{4\pi r} 2E_o \Delta a \cos\left(\dfrac{\pi}{2\sqrt{\varepsilon_r}} \sin\theta\right) \end{cases} \tag{3.37.a}$$

H-plane (φ=$\pi/2$) :
$$\begin{cases} E_\varphi = \dfrac{jke^{-jkr}}{4\pi r} 2E_o \Delta a \operatorname{sinc}\left(\pi \dfrac{a}{\lambda_o} \sin\theta\right)\cos\theta \\ E_\theta = 0 \end{cases} \tag{3.37.b}$$

The factor $\cos\left(\frac{\pi}{2\sqrt{\varepsilon_r}} \sin\theta\cos\varphi\right)$ is the array factor of two radiating slots spaced at a distance $\lambda_o/2\sqrt{\varepsilon_r}$.
We see that the H-plane is strongly dependent of the polar angle θ because of the factor $\cos\theta$, which is not the case for the E-plane. For small polar angles the microstrip antenna behaves like a dipole, as far as the radiation pattern is concerned.

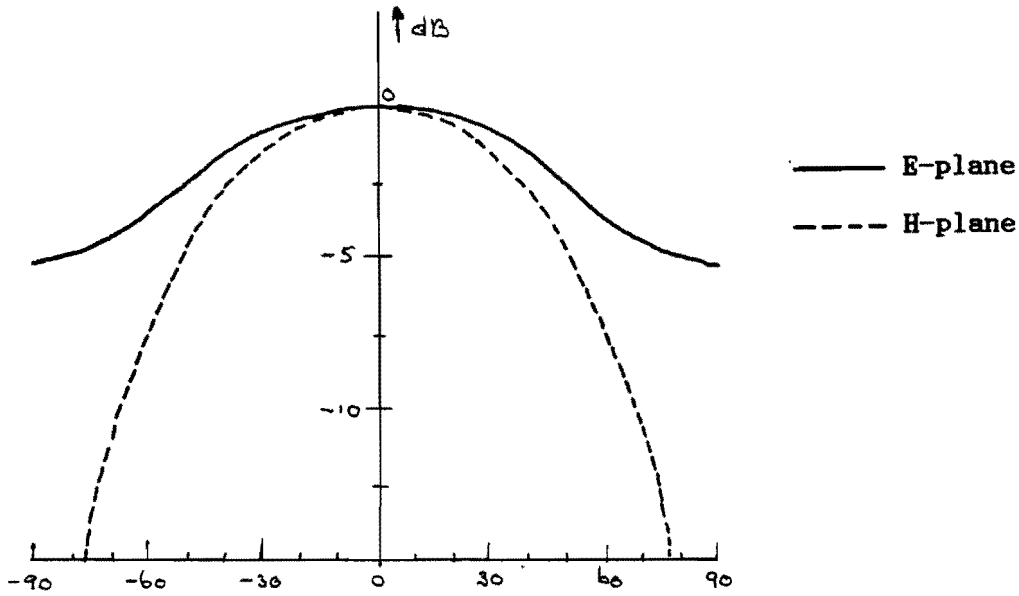

Fig.3.6 Theoretical radiation pattern of square patch antenna in E- and H-plane. (ε_r=2.53)

4. The Wilkinson power splitter.

4.1 Introduction.

The rectangular patch antenna discussed so far is linearly polarized. Generation of circular polarization can only be achieved by combining individual sources with appropriate orientations and phasings. This can be done in a number of ways. Various methods to obtain circular polarization with microstripantennas will be given in Chapter 5.
The use of a power splitting network is necessary, especially for the case of an antenna array. This feeding network should accomodate the required phase shifters too. There are several possibilities to construct such a network. We preferred a feeding network performed in microstrip to maintain the specific advantages of microstrip antenna technology.
A very important part of this network is the power splitter, whose function is to split the incoming power into two equal parts. Therefore, the splitter can be treated as a three-port network.
Manufacturing a power splitter in microstrip can be done in a number of ways [10]. One of them is the reactive T-splitter.(Fig.4.1)

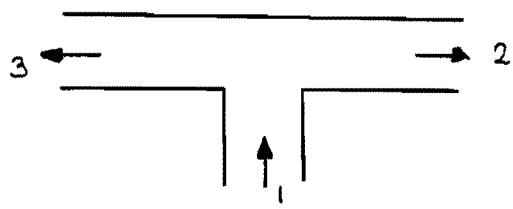

Fig.4.1 Reactive T-splitter.

The main disadvantage of this splitter is the lack of isolation between the output arms, which means that reflected power returning into one of the output ports, will be retransmitted into the other. The advantage of this splitter is its simplicity, and moreover, no absorbing load is required.
To overcome the disadvantage of the reactive T-splitter, we can make use of the so-called 'isolated configurations'. The one, that is chosen for our purpose, is the Wilkinson splitter depicted in Fig.4.2 [4,20]. The choice of this configuration is made because of its relative ease in its design. Other advantages of an isolated configuration compared to a reactive T-splitter will be discussed in Chapter 5. For a treatment of other isolated configurations we refer to the literature [10].

4.2. Fundamental operation.

A sketch of the Wilkinson splitter performed in microstrip is sketched in Fig.4.2.

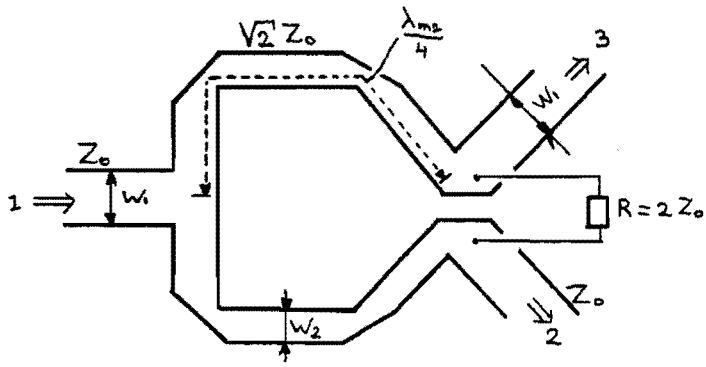

Fig.4.2 Wilkinson splitter in microstrip.
(λ_{m2} is the wavelength in the microstrip line with characteristic impedance $\sqrt{2}\,Z_0$)

The purpose of this configuration is to isolate the output ports 2 and 3, which means that reflected power going into one of these ports will not be retransmitted into the other output port. If a reflection occurs at one of the output ports, part of it will travel to the other port through the resistor R, and the rest of it will travel to the junction, where it will split again. From this junction, part of it will travel to the remaining output port.
Because the total length of the two branches is $\lambda_{m2}/2$, the wave tends to cancel out. This, because the reflected wave arrives 180° out of phase at the other side of the resistor. Complete cancellation occurs, when a proper choice of the resistor and the characteristic impedance of the branches is made.
The matching and isolation properties of the splitter are frequency dependent, because of the frequency dependent electrical branch length. An evaluation of this will be given in the next part of this chapter.
To do this, we will examine the transmission line analogon, shown in Fig.4.3.

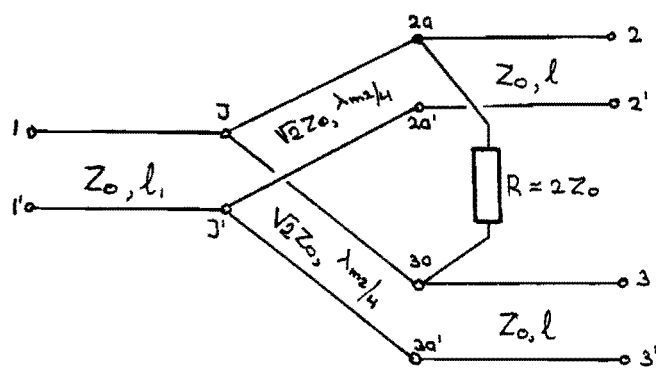

Fig.4.3 Transmission line analogon of the Wilkinson splitter.

A network like this is usually described with its scattering matrix [13,19]. The case of interest is the frequency dependence of the scattering coefficients.
A general three-port is sketched in Fig.4.4.

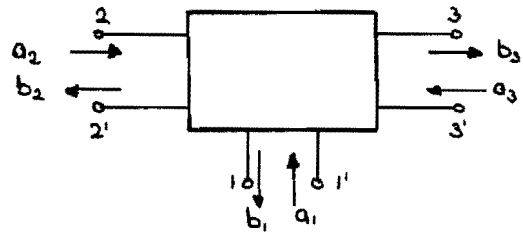

Fig.4.4 Three port network.

Here is : $a_i a_i^*$ the average incoming power on port i.

$b_i b_i^*$ the average outward power on port i.

The scattering matrix for such a three-port is defined as

$$\begin{aligned} b_1 &= S_{11}a_1 + S_{12}a_2 + S_{13}a_3 \\ b_2 &= S_{21}a_1 + S_{22}a_2 + S_{23}a_3 \\ b_3 &= S_{31}a_1 + S_{32}a_2 + S_{33}a_3 \end{aligned} \qquad (4.1)$$

Because of reciprocity and symmetry, the scattering matrix for the Wilkinson splitter can be written as

$$\begin{aligned} b_1 &= S_{11}a_1 + S_{12}a_2 + S_{12}a_3 \\ b_2 &= S_{12}a_1 + S_{22}a_2 + S_{23}a_3 \\ b_3 &= S_{12}a_1 + S_{23}a_2 + S_{22}a_3 \end{aligned} \qquad (4.2)$$

The scattering coefficients will be determined by making use of the even and odd mode excitation method. A brief discussion of this method is given in the next part.

4.3. Frequency dependence of the scattering parameters.

We will start with the determination of S_{11}. From (4.2) follows the definition

$$S_{11} = \left.\frac{b_1}{a_1}\right|_{a_2 = a_3 = 0} \qquad (4.3)$$

We see, that S_{11} is the reflection coefficient of port 1 when ports 2 and 3 are matched. Under these conditions both sides of the resistor have the same potential, and may be omitted (Fig.4.5).

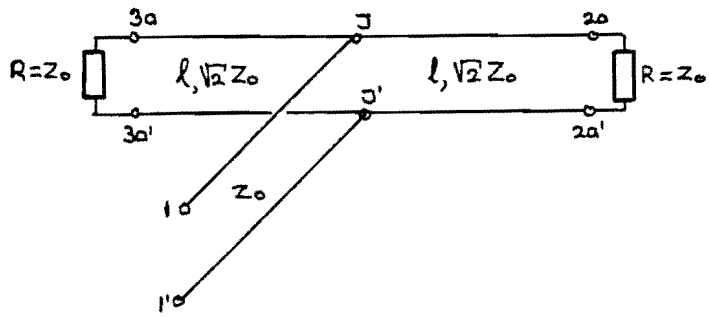

Fig.4.5 Equivalent network representation for determining S_{11} .

As the transmission lines are loss free, the relation holds

$$|S_{11}| = |S_{JJ'}| \tag{4.4}$$

The input impedance at JJ' is the impedance of two parallel equal length transmission lines, both connected to a load Z_o. The ultimate expression for the reflection coefficient S_{11} can be written as

$$|S_{11}| = \left|\frac{Z_{JJ'}-Z_o}{Z_{JJ'}+Z_o}\right| = \left|\frac{-\sqrt{2}}{3\sqrt{2}+4j\tan\left(\frac{2\pi l}{\lambda}\right)}\right| \tag{4.5}$$

with λ the wavelength at the operating frequency.
We want to designate the splitter for a frequency f_r. This means, that $|S_{11}|$ must be zero at this frequency.

$$\frac{2\pi l}{\lambda_r} = \pi/2 \quad \Rightarrow \quad l = \frac{\lambda_r}{4} \tag{4.6}$$

Eq.4.5 can be written as a function of the frequency

$$|S_{11}| = \left|\frac{-\sqrt{2}}{3\sqrt{2}+4j\tan\left(\frac{\pi}{2}\frac{f}{f_r}\right)}\right| \tag{4.7}$$

Because the network is loss free and symmetric, all the incoming power must be delivered to the output ports in equal parts.
The incoming power is obtained by

$$P_1 = P_{in}\left(1-|S_{11}|^2\right) \tag{4.8}$$

Which gives for the outward power

$$P_2 = P_3 = \tfrac{1}{2}P_{in}\left(1-|S_{11}|^2\right) \tag{4.9}$$

From which the transmission coefficients can be determined.

$$|S_{12}| = \sqrt{\tfrac{1}{2}(1-|S_{11}|^2)} \tag{4.10}$$

The scattering coefficients S_{22}, S_{23} are defined as

$$S_{22} = \left.\frac{b_2}{a_2}\right|_{a_1=a_3=0} \tag{4.11.a}$$

$$S_{23} = \left.\frac{b_2}{a_3}\right|_{a_1=a_2=0} \tag{4.11.b}$$

The condition $a_1=0$ is achieved by matching port 1 with a load Z_o. This results in the symmetric network as shown in Fig.4.6.

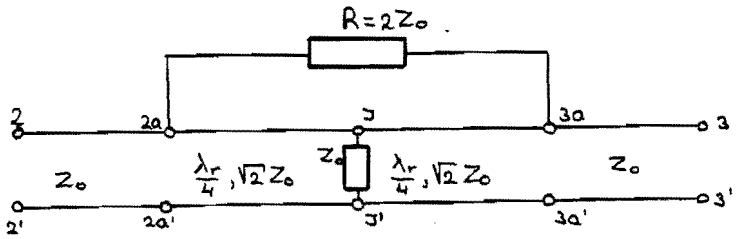

Fig.4.6 Network representation for determining S_{22} and S_{23}.

We are only interested in the absolute magnitude of S_{22} and S_{23}. As the transmission lines are loss free, we can write

$$\begin{aligned} |S_{22}| &= |S_{2a2a}| \\ |S_{23}| &= |S_{2a3a}| \end{aligned} \tag{4.12}$$

A symmetric network is most easily analyzed with the method of even and odd mode excitation. Therefore, we will need the equivalent circuit of Fig.4.7.

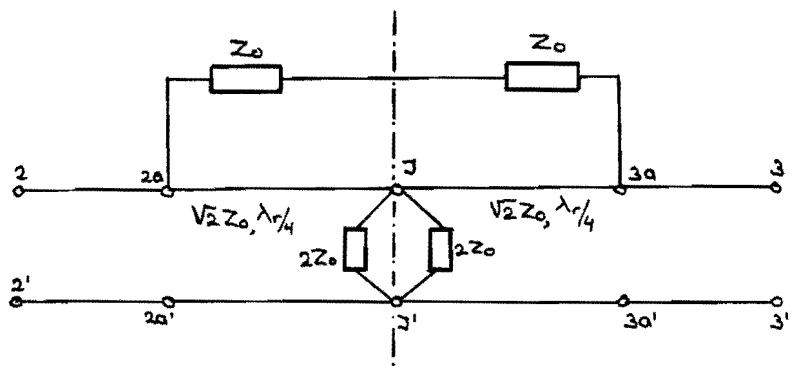

Fig.4.7 Network representation for even and odd mode excitation.

The even and odd mode excitation method can be described as follows. We return to a general symmetric network, described by its impedance matrix.

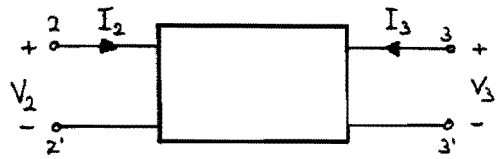

Fig.4.8 Symmetric network.

It's impedance matrix is written as

$$V_2 = Z_{22} I_2 + Z_{23} I_3$$
$$V_3 = Z_{23} I_2 + Z_{22} I_3 \qquad (4.13)$$

Introducing the even and odd mode source currents

$$I_2 = \tfrac{1}{2}(I_2 + I_3) + \tfrac{1}{2}(I_2 - I_3) \triangleq I_{even} + I_{odd}$$
$$I_3 = \tfrac{1}{2}(I_2 + I_3) - \tfrac{1}{2}(I_2 - I_3) \triangleq I_{even} - I_{odd} \qquad (4.14)$$

Writing V_2 and V_3 in the same way, we obtain the source voltages V_{even} and V_{odd}. Substitution in eqs.4.13 yields

$$V_{even} + V_{odd} = Z_{22}(I_{even} + I_{odd}) + Z_{23}(I_{even} - I_{odd})$$
$$V_{even} - V_{odd} = Z_{23}(I_{even} + I_{odd}) + Z_{22}(I_{even} - I_{odd}) \qquad (4.15)$$

Respectively adding and subtracting these relations gives

$$V_{even} = (Z_{22} + Z_{23}) I_{even} \triangleq Z_{even} I_{even}$$
$$V_{odd} = (Z_{22} - Z_{23}) I_{odd} \triangleq Z_{odd} I_{odd} \qquad (4.16)$$

Exciting a symmetric network in both the even and odd mode gives Z_{even} and Z_{odd}, from which Z_{22} and Z_{23} can be extracted with

$$Z_{22} = \tfrac{1}{2}(Z_{even} + Z_{odd})$$
$$Z_{23} = \tfrac{1}{2}(Z_{even} - Z_{odd}) \qquad (4.17)$$

Finally, we obtain the scattering coefficients with the relations [13,19]

$$S_{22} = \frac{(Z_{22}-Z_o)(Z_{22}+Z_o) - Z_{23}^2}{(Z_{22}+Z_o)^2 - Z_{23}^2} \qquad (4.18.a)$$

$$S_{23} = \frac{2 Z_{23} Z_o}{(Z_{22}+Z_o)^2 - Z_{23}^2} \qquad (4.18.b)$$

We will apply this method to the network of Fig.4.5. In the even mode we excite both ports with equal sources as shown in Fig.4.9.

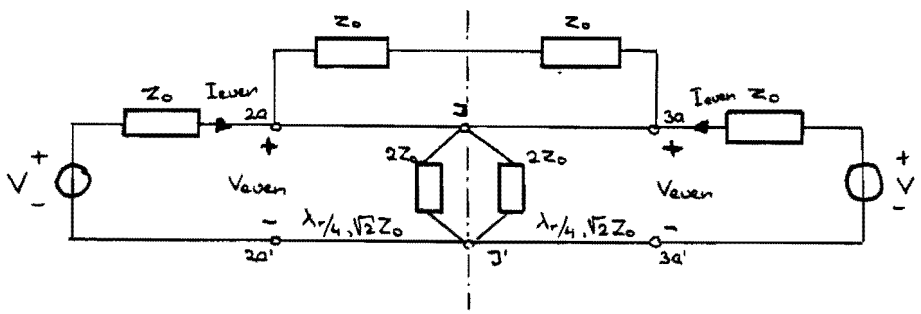

Fig.4.9 Network excited in even mode.

The network can now be bisected symmetrically by a longitudinal non-conducting sidewall. The calculations are simplified considerably because we only have to deal with the bisection shown in Fig.4.10.

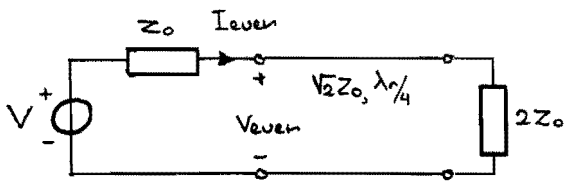

Fig.4.10 Bisection for even mode.

The impedance Z_{even} can be calculated as

$$Z_{even} = Z_o \frac{2 + j\sqrt{2}\tan\left(\frac{\pi}{2}\frac{f}{f_r}\right)}{1 + j\sqrt{2}\tan\left(\frac{\pi}{2}\frac{f}{f_r}\right)} \qquad (4.19)$$

For the odd mode excitation, the configuration is sketched in Fig.4.11.

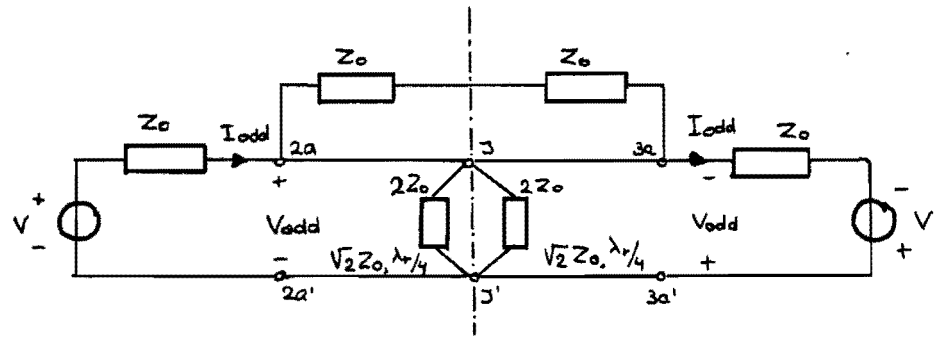

Fig.4.11 Network excited in odd mode.

The network is now bisected symmetrically with a longitudinal conducting sidewall, resulting in the bisection in Fig.4.12.

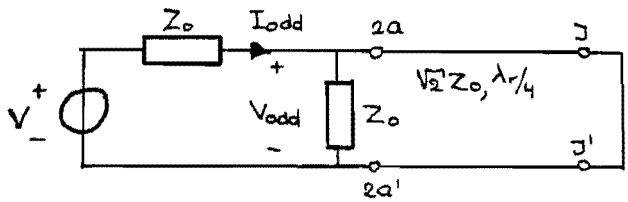

Fig.4.12 Odd mode bisection.

The resulting expression for Z_{odd} can be found as

$$Z_{odd} = Z_o \frac{j\sqrt{2}\tan\left(\frac{\pi}{2}\frac{f}{f_r}\right)}{1+j\sqrt{2}\tan\left(\frac{\pi}{2}\frac{f}{f_r}\right)} \tag{4.20}$$

Applying the relations (4.12), (4.17) and (4.18) results in

$$|S_{22}| = \left| \frac{-1}{3-8\tan^2\left(\frac{\pi}{2}\frac{f}{f_r}\right)+8\sqrt{2}j\tan\left(\frac{\pi}{2}\frac{f}{f_r}\right)} \right| \tag{4.21.a}$$

$$|S_{23}| = \left| \frac{2\left(1+j\sqrt{2}\tan\left(\frac{\pi}{2}\frac{f}{f_r}\right)\right)}{3-8\tan^2\left(\frac{\pi}{2}\frac{f}{f_r}\right)+8\sqrt{2}j\tan\left(\frac{\pi}{2}\frac{f}{f_r}\right)} \right| \tag{4.21.b}$$

A graphical representation of the scattering parameters as a function of frequency is given in Figs.4.13.

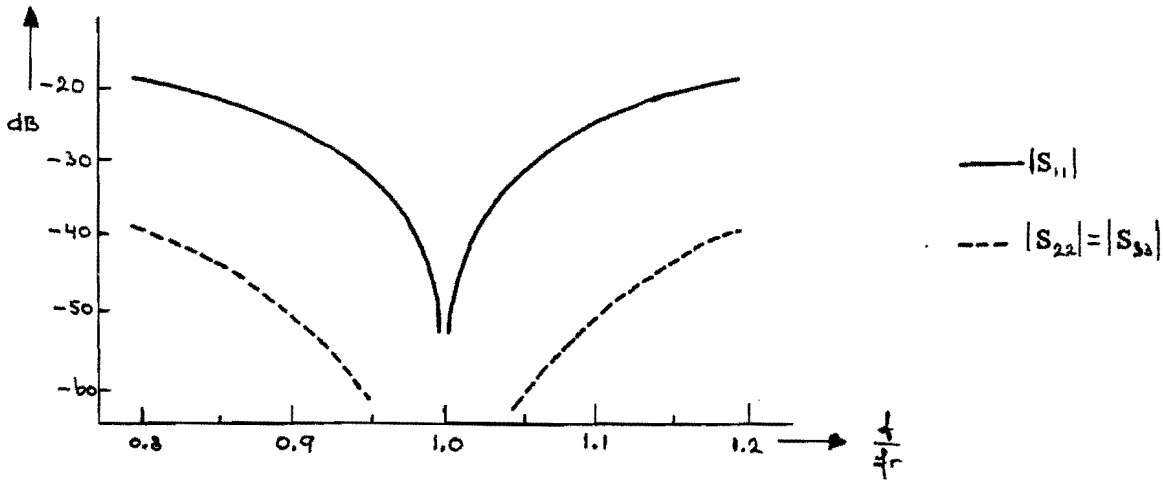

(a) Theoretical reflection coefficients

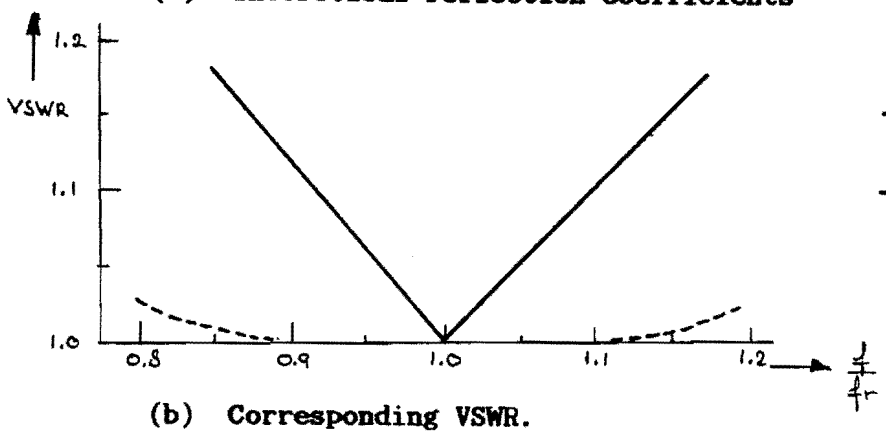

(b) Corresponding VSWR.

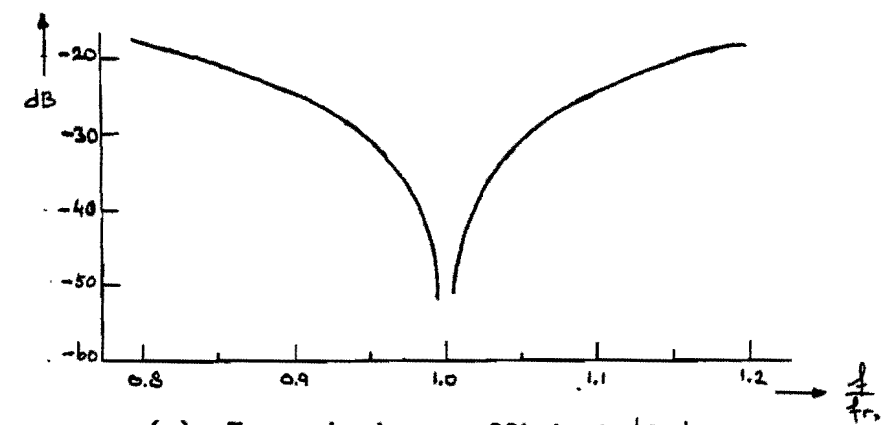

(c) Transmission coefficient $|S_{23}|$.

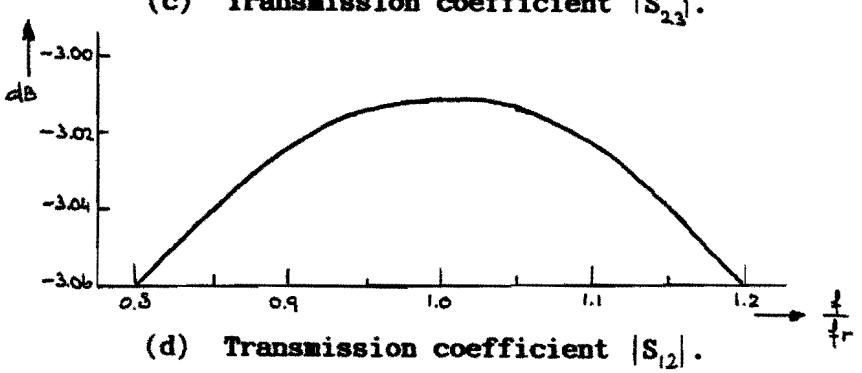

(d) Transmission coefficient $|S_{12}|$.

Fig.4.13 Theoretical scattering coefficients as a function of frequency for the Wilkinson splitter.

We use the Wilkinson splitter in combination with microstrip antennas. The latter have a bandwidth in the order of several percent. From Fig.4.13 we see, that the theoretical bandwidth of the splitter is much greater.
This gives rise to the conclusion that the VSWR bandwidth limitation of the entire antenna configuration is owing to the radiating patches.

As a matter of convenience the scattering coefficients of the reactive T-splitter will be briefly discussed. We will need these results in Chapter 5, where the design of the feeding network is considered.
Using the previous method, the derivation of the coefficients is straightforward. Therefore, the results are simply stated.
The transmission line analogon is shown in Fig.4.14.

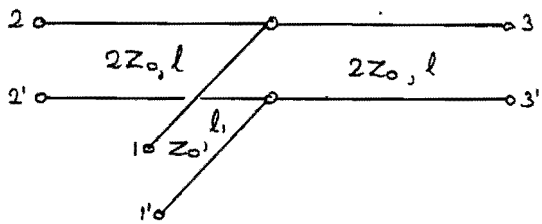

Fig.4.14 Transmission line analogon for the reactive T-splitter.

The scattering coefficients for this configuration are

$$S_{11} = 0 \tag{4.22.a}$$

$$S_{12} = \frac{1}{\sqrt{2}} e^{-j\beta\ell_1} e^{-j\beta\ell} \tag{4.22.b}$$

$$S_{22} = -\frac{1}{2} e^{-2j\beta\ell} \tag{4.22.c}$$

$$S_{23} = \frac{1}{2} e^{-2j\beta\ell} \tag{4.22.d}$$

4.4 Design of a Wilkinson power splitter with phase shifter on Rexolite 1422 substrate.

In this chapter the design of a Wilkinson splitter with a 90° phase shifter in microstrip is discussed.
Application of microstrip requires the calculation of line widths to obtain the desired characteristic impedance and phase velocity in a specific substrate. Practical design formulas can be found in [6] and will be given below.
Suppose, we have a substrate with relative dielectric constant ε_r . The thickness of the substrate is h, and the line width is W. Neglecting the thickness of the metal strip, the characteristic impedance can be well approximated.

For wide strips. (W/h > 1)

$$Z_{om} = \frac{60}{\sqrt{\varepsilon_{re}}} \ln\left(\frac{8h}{W} + 0.25\,\frac{W}{h}\right) \qquad (4.23.a)$$

For narrow strips. (W/h <1)

$$Z_{om} = \frac{120\pi}{\sqrt{\varepsilon_{re}}} \left\{ \frac{W}{h} + 1.393 + 0.667 \ln\left(\frac{W}{h} + 1.444\right) \right\} \qquad (4.23.b)$$

The wavelength in microstrip λ_m is given by the relation

$$\lambda_m = \frac{\lambda_o}{\sqrt{\varepsilon_{re}}} \qquad (4.24)$$

with the effective dielectric constant

$$\varepsilon_{re} = \frac{\varepsilon_r + 1}{2} + \frac{\varepsilon_r - 1}{2} F(W/h) \qquad (4.25)$$

$$F(W/h) = \begin{cases} (1 + 12\,h/W)^{-1/2} & (W/h > 1) \\ (1 + 12\,h/W)^{-1/2} + 0.04(1 - W/h)^2 & (W/h < 1) \end{cases}$$

We note, that the wavelength in the microstrip line is a function of W/h and ε_r ,and thus a function of the characteristic impedance. Measurements have shown that the relations (4.23) and (4.24) have a relative error less than 1 percent.
Making bends in microstrip can be best done by chamfering it as shown in Fig.4.15. Doing this, we reduce the capacitive end effects.

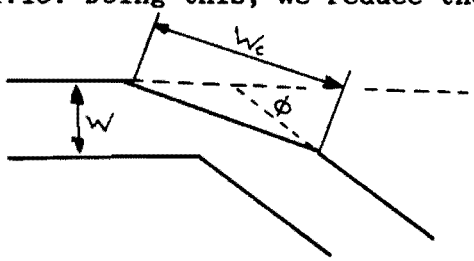

Fig.4.15 A chamfered bend.

Experimental results have shown that a chamfer length W_c = 1.6W gives best results for all angles ϕ .
We have now enough mathematical tools to calculate the physical dimensions of a power splitter.

The splitter must be designed to obtain a good match to 50 Ω for all three ports. We also require an excess quarter wavelength in one output arm to generate a 90° phase difference with the other output arm. The obtained configuration is viewed in Fig.4.16.

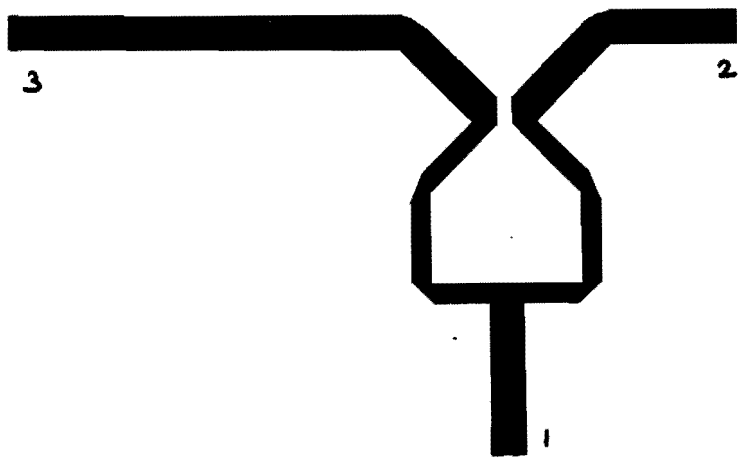

Fig.4.16 View of Wilkinson splitter with 90° phase difference between output arms on Rexolite 1422 substrate. (ε_r=2.53)

The resistor we used was a MSD (Mounted Surface Device) resistor of 100 Ω The design is made on Rexolite 1422 substrate with relative dielectric constant ε_r=2.53. The substrate consists of styrene copolymer and has a thickness of 1/16 inch = 1.59 mm. The splitter is designed for a frequency f = 1.5 GHz. (λ_o = 20 cm)
Substituting these features in eqs.4.23 and 4.24 gives

Z_{o1} = 50 Ω : W =4.50 mm λ_{m1}=138.0 mm $\lambda_{m1/4}$=34.50 mm

Z_{o2}= 70.7 Ω: W =2.55 mm λ_{m2}=140.45 mm $\lambda_{m2/2}$=70.22 mm (4.26)

The scattering coefficients are measured and their results are shown in Figs.4.17 on the next page.

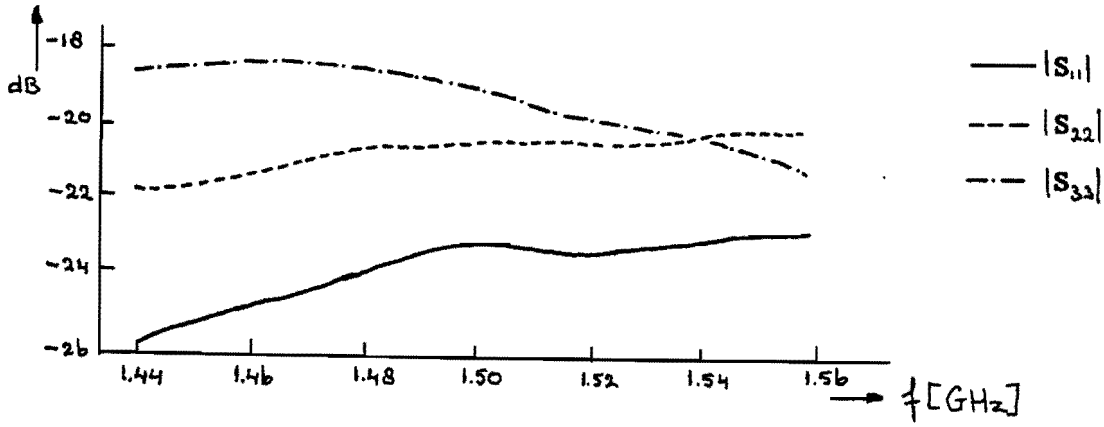

(a) Reflection coefficients.

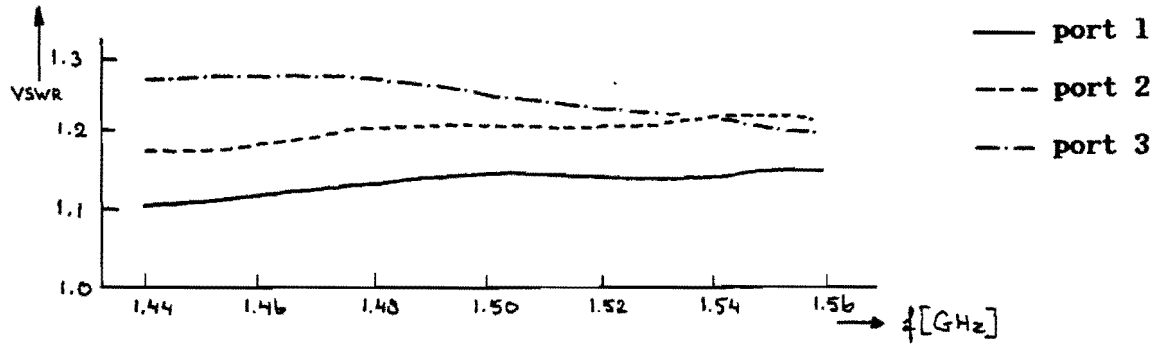

(b) Corresponding VSWR.

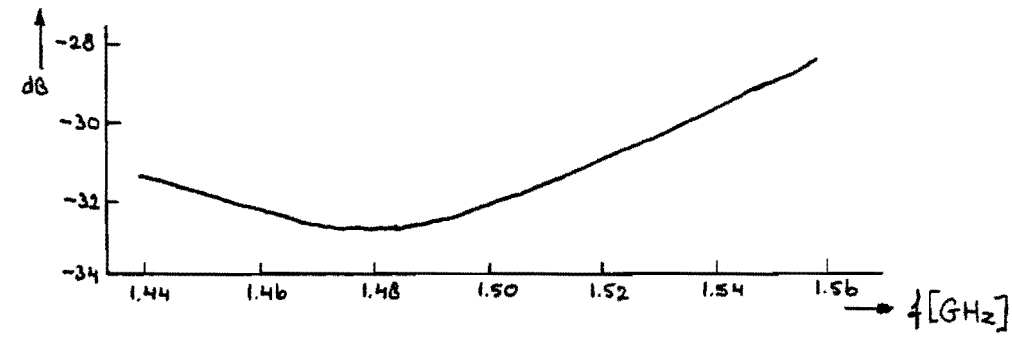

(c) Transmission coefficient $|S_{23}|$.

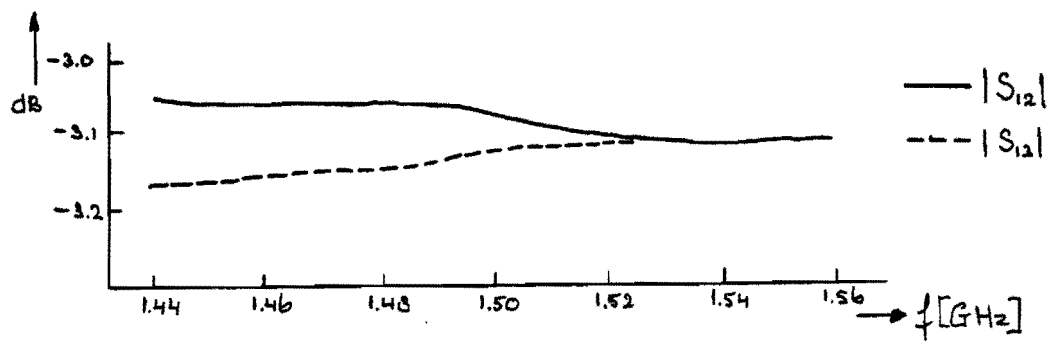

(d) Transmission coefficients.

Fig.4.17 Measured scattering parameters as a function of the frequency of a Wilkinson splitter designed on Rexolite 1422 substrate.

In the relative small frequency band ($0.96 < f/f_r < 1.04$) we have measured it is not well possible to compare the measured with the theoretical results.
Practical difficulties in measuring reflection coefficients smaller than -35 dB are met because of deviations in the matching loads we used to match the unused ports.
An important factor that leads to a deterioriation of the matching properties, is the coaxial to microstrip transition. For this transition we used OSM-connectors mounted as shown in Fig.4.18. Even with the relative low frequencies we used, the occuring reflections appeared to be very sensitive of the spacing d, which must be taken as small as possible.

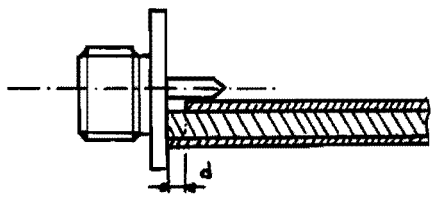

Fig.4.18 Coaxial to microstrip transition.

Another factor leading to mismatch is, that the characteristic impedance is dependent of factors such as strip thickness, dispersion, dielectric constant tolerance etc. (for Rexolite 1422 : $\varepsilon_r = 2.53 \pm 0.05$), in addition to the error in fabrication of the strip width.
So, in general we have to introduce some trial and error stages in the design procedure to achieve optimum performance.
However, our first stage design led to an acceptable performance. Especially, the isolation between the output ports appeared to be rather well (Fig.4.17.c), as well as the power splitting property (Fig.4.17.d). The VSWR is smaller than 1.16 for the output ports and smaller than 1.3 for the input port over the measured frequency band.
The remaining parameter, that needs discussion is the measured phase difference between the output ports. This phase difference $\Delta\phi$ as a function of frequency is shown in Fig.4.19.

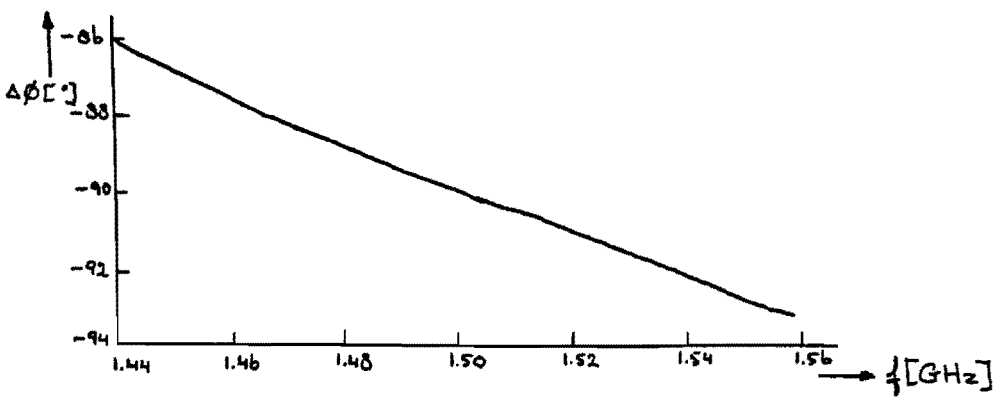

Fig.4.19 Measured phase difference between the output ports of a Wilkinson splitter designed on Rexolite 1422 substrate as a function of the frequency.

The phase difference is almost 90° at f = f_r =1.5GHz, which agrees well with the expected value. $\Delta\phi$ is frequency dependent because of the frequency dependence of the electrical length of the transmission line. Suppose a transmission line with a phase shift of ϕ_r at angular frequency ω_r. The phase change $\Delta\phi$ as a function of the frequency can be written as

$$\Delta\phi = \frac{\phi_r}{\omega_r}\Delta\omega \qquad (4.27)$$

with $\Delta\omega = \omega - \omega_r$

5. Circular polarization with microstrip antennas.

5.1 Introduction.

There are several ways to obtain circularly polarized radiation with microstrip antennas. This can be done with separate elements or with an array of these elements. A brief discussion of these methods with their respective properties is given in the next section.
The goal of our research was to develop a wideband circularly polarized radiator suitable for the frequencyband 1.5 GHz to 1.6 GHz. The bandwidth required is thus 6.5 %. With a patch antenna, a resonant device, it is rather difficult to meet this requirement, because of its high quality factor. However, recent studies [16,17] have shown, that it is possible to improve the bandwidth constraints by placing the elements in a sequential rotated fashion. Especially the axial ratio bandwidth is expected to be considerably improved applying this configuration. A discussion of the sequentially rotated array will be given in this chapter.
Factors, leading to a deterioriation of the axial ratio bandwidth and impedance bandwidth are considered in this chapter too.

5.2 General methods to achieve circular polarization.

We already noted that several methods exist to obtain circular polarization. The most common is to excite two orthogonal modes on the patch surface in phase quadrature from two separate feeds. Both the square and circular patch are able to support circular polarization with this method. An example is shown in Fig.5.1 for a square patch antenna.

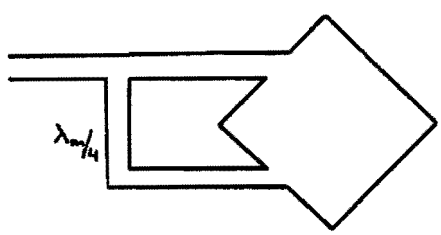

λ_m: wavelength in the microstrip line.

Fig.5.1 Circularly polarized square patch antenna.

It has been demonstrated by [14] that it is possible to obtain circular polarization with a patch element excited in two degenerate modes from a single feed. Examples are the ellipsoidal and pentagonal patch [10], the circular patch with notches [16], as well as the modified square patch. The latter is modified in the sense that the orthogonal patch lengths are slightly different.

More examples of this method can be found in [3], where the square and circular patch with thin diagonal slot are considered. All these methods have the main disadvantage of a very narrow axial ratio bandwidth, in the order of 0.5 percent.
Applying these elements appear to be useful only in a sequentially rotated array. This shall be made plausible in a next part of this chapter.
Another possibility to obtain circular polarization is to combine linear polarized elements with appropriate orientations and phasings [9]. To gain some insight, we shall consider some of these configurations.
In general terms, the field components of an antenna, placed in the origin of the xy-plane as shown in Fig.5.2, can be written as (see eq.2.12)

$$E_\theta = A(r)\, e^{j\psi}\, f_\theta(\theta,\varphi)$$
$$E_\varphi = A(r)\, e^{j\psi}\, g_\varphi(\theta,\varphi) \qquad (5.1)$$

with $A(r) = \dfrac{-jke^{-jkr}}{4\pi r}$ and ψ the element phasing.

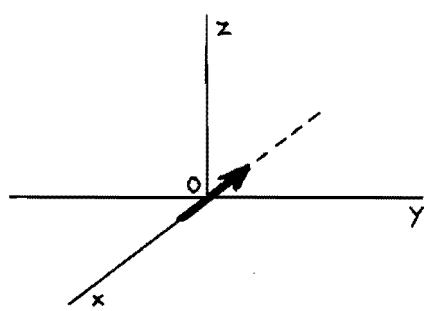

Fig.5.2 Antenna placed in xy-plane.

To facilitate the calculations we will only consider the principal planes $\varphi = 0°$ and $\varphi = 90°$, and the diagonal plane $\varphi = 45°/225°$. For general calculations the computerprogram DIAPOL is available [Appendix A]. The relations $f_\theta(\theta,\varphi)$ and $g_\varphi(\theta,\varphi)$ are taken as a reference. Rotation of the reference antenna over an angle $+\varphi_i$ changes them to $f_\theta(\theta,\varphi-\varphi_i)$ and $g_\varphi(\theta,\varphi-\varphi_i)$. It is assumed, that the antenna in Fig.5.2 has the following symmetry relationships

$$\begin{aligned}
&f_\theta(\theta,\pm\pi/2) = g_\varphi(\theta,0) = g_\varphi(\theta,\pm\pi) = 0\\
&f_\theta(\theta,0) = -f_\theta(\theta,\pm\pi)\\
&g_\varphi(\theta,\pi/2) = -g_\varphi(\theta,-\pi/2)\\
&g_\varphi(\theta,\pi/4) = g_\varphi(\theta,3\pi/4) = -g_\varphi(\theta,-\pi/4) = -g_\varphi(\theta,-3\pi/4)\\
&f_\theta(\theta,\pi/4) = -f_\theta(\theta,3\pi/4) = -f_\theta(\theta,-3\pi/4) = f_\theta(\theta,-\pi/4)
\end{aligned} \qquad (5.2)$$

The arbitrary antenna in Fig.5.2 can be replaced by a rectangular microstrip antenna as shown in Fig.5.3.

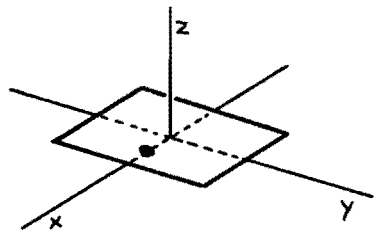

Fig.5.3 Rectangular microstrip antenna in xy-plane.

For the rectangular patch antenna excited in the TM_{01} -mode, we obtain with eqs.3.36.

$$
\begin{aligned}
f_\theta(\theta,0) &= -\cos\left(\frac{\pi}{2\sqrt{\varepsilon_r}}\sin\theta\right) \\
g_\varphi(\theta,\pi/2) &= \operatorname{sinc}\left(\pi\frac{a}{\lambda_0}\sin\theta\right)\cos\theta \\
f_\theta(\theta,\pi/4) &= \frac{1}{\sqrt{2}}\cos\left(\frac{\pi}{2\sqrt{2\varepsilon_r}}\sin\theta\right)\operatorname{sinc}\left(\frac{\pi a}{\sqrt{2}\lambda_0}\sin\theta\right)\left\{\frac{\sin^2\theta-\varepsilon_r}{\varepsilon_r-\frac{1}{2}\sin^2\theta}\right\} \\
g_\varphi(\theta,\pi/4) &= \frac{1}{\sqrt{2}}\cos\left(\frac{\pi}{2\sqrt{2\varepsilon_r}}\sin\theta\right)\operatorname{sinc}\left(\frac{\pi a}{\sqrt{2}\lambda_0}\sin\theta\right)\left\{\frac{\varepsilon_r}{\varepsilon_r-\frac{1}{2}\sin^2\theta}\right\}
\end{aligned}
\qquad (5.3)
$$

Eqs.3.36 can be well approximated for small polar angles θ ,resulting in

$$
\begin{aligned}
f_\theta(\theta,\varphi) &\approx -\cos\varphi \\
g_\varphi(\theta,\varphi) &\approx \sin\varphi\cos\theta
\end{aligned}
\qquad (5.4)
$$

It is well known that circular polarization can be achieved in the broadside direction of an array composed of two identical linearly polarized elements with spatial rotation and phasing arranged in a $0°,90°$ fashion as shown in Fig.5.4.

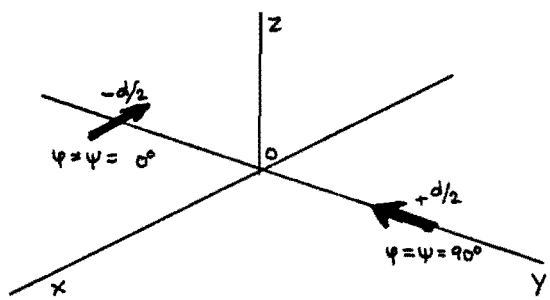

Fig.5.4 Circularly polarized array composed of two linearly polarized elements. ($d = 0.87\lambda_0$)

The polarization quality becomes very poor at angles away from boresight in the plane $\varphi = 90°$. This is caused by the spatial phase delay $\Delta\psi = k_o d \sin\theta$. shown in Fig.5.5, which is due to the spaced radiation centres of the elements, so the condition (2.5.b) is not satisfied anymore.

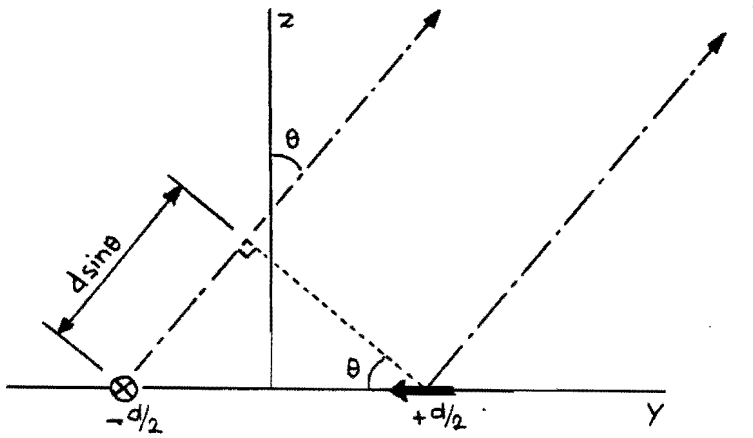

Fig.5.5 Spatial phase delay $\Delta\psi = k_o d \sin\theta$.

The CP-pattern for the array consisting of rectangular microstrip antennas is calculated with the program DIAPOL and depicted in Fig.5.6.

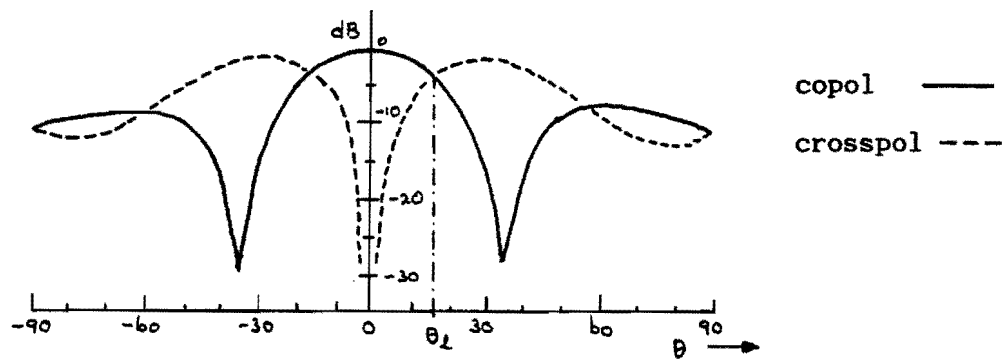

(a) Co- and crosspolarization.

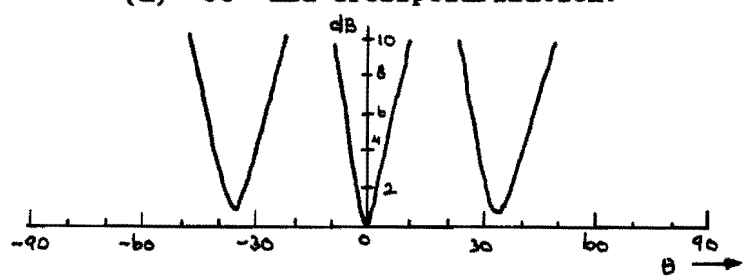

(b) Axial ratio.

Fig.5.6 Calculated CP-characteristics for the two element microstrip antenna array in the principal plane $\varphi = 90°$.
($d = 0.87\lambda_o$, $\varepsilon_r = 2.53$)

We see, that the co- and crosspolarization components cross at the angle θ_ℓ. For this angle exists a linearly polarized wave, ($|E_L| = |E_R|$). It is interesting to note, that this angle is not dependent of the radiation pattern of a single element, but purely of the spacing d and the wavelength λ_o. This can be shown by substitution of (5.1) and (5.2) in (2.19), which results in

$$\begin{aligned} E_\theta^N &= A(r)\left\{ e^{j0^\circ} f_\theta(\theta,\pi/2)\, e^{-jk_o \frac{d}{2}\sin\theta} + e^{j90^\circ} f_\theta(\theta,0)\, e^{jk_o \frac{d}{2}\sin\theta}\right\} \\ &= jA(r)\, f_\theta(\theta,0)\, e^{jk_o \frac{d}{2}\sin\theta} \\ E_\varphi^N &= A(r)\left\{ g_\varphi(\theta,\pi/2)\, e^{-jk_o \frac{d}{2}\sin\theta} + e^{j90^\circ} g_\varphi(\theta,0)\, e^{jk_o \frac{d}{2}\sin\theta}\right\} \\ &= A(r)\, g_\varphi(\theta,\pi/2)\, e^{-jk_o \frac{d}{2}\sin\theta} \end{aligned} \qquad (5.5)$$

Using eqs.2.9 gives

$$E_L^N = \frac{j}{\sqrt{2}} A(r)\left\{ f_\theta(\theta,0)\, e^{jk_o \frac{d}{2}\sin\theta} - g_\varphi(\theta,\pi/2)\, e^{-jk_o \frac{d}{2}\sin\theta}\right\}$$

$$E_R^N = \frac{j}{\sqrt{2}} A(r)\left\{ f_\theta(\theta,0)\, e^{jk_o \frac{d}{2}\sin\theta} + g_\varphi(\theta,\pi/2)\, e^{-jk_o \frac{d}{2}\sin\theta}\right\}$$

Finally, we obtain

$$|E_L^N| = \frac{|A(r)|}{\sqrt{2}}\left\{ f_\theta^2(\theta,0) + g_\varphi^2(\theta,\pi/2) - 2 f_\theta(\theta,0)\, g_\varphi(\theta,\pi/2)\cos(k_o d\sin\theta)\right\}^{1/2} \qquad (5.6.a)$$

$$|E_R^N| = \frac{|A(r)|}{\sqrt{2}}\left\{ f_\theta^2(\theta,0) + g_\varphi^2(\theta,\pi/2) + 2 f_\theta(\theta,0)\, g_\varphi(\theta,\pi/2)\cos(k_o d\sin\theta)\right\}^{1/2} \qquad (5.6.b)$$

Linear polarization occurs as

$$\cos(k_o d\sin\theta) = 0 \qquad (5.7)$$

independent of the radiation pattern. The intersection angle θ_ℓ is thus found from

$$k_o d\sin\theta_\ell = \frac{\pi}{2} \quad \Rightarrow \quad \theta_\ell = \arcsin\left(\frac{\lambda_o}{4d}\right) \qquad (5.8)$$

which is, for the example in Fig.5.4, $\theta_\ell = 16.7^\circ$.
The other principal plane ($\varphi = 0^\circ$) gives a much better performance, because no degradation occurs owing to the spatial phase delay. In this plane, the CP-quality will only be affected by the asymmetric behaviour of the single element radiation pattern.

Because the phase term $(\hat{r}.\bar{r}_i) = 0$ in (2.19) for both elements, we can write

$$E_\theta^N = A(r)\, f_\theta(\theta,0)$$
$$E_\varphi^N = jA(r)\, g_\varphi(\theta,-\pi/2) = -jA(r)\, g_\varphi(\theta,\pi/2) \qquad (5.9)$$

Using eqs.2.9 and 2.10 we obtain

$$|E_L^N| = \frac{|A(r)|}{\sqrt{2}} \left| f_\theta(\theta,0) - g_\varphi(\theta,\pi/2) \right| \qquad (5.10.a)$$

$$|E_R^N| = \frac{|A(r)|}{\sqrt{2}} \left| f_\theta(\theta,0) + g_\varphi(\theta,\pi/2) \right| \qquad (5.10.b)$$

$$AR = \begin{cases} \left| \dfrac{f_\theta(\theta,0)}{g_\varphi(\theta,\pi/2)} \right| & f_\theta(\theta,0) > g_\varphi(\theta,\pi/2) \\ \left| \dfrac{g_\varphi(\theta,\pi/2)}{f_\theta(\theta,0)} \right| & f_\theta(\theta,0) < g_\varphi(\theta,\pi/2) \end{cases} \qquad (5.10.c)$$

The calculated CP-patterns and axial ratio in the plane $\varphi = 0°$ are shown in Fig.5.7.

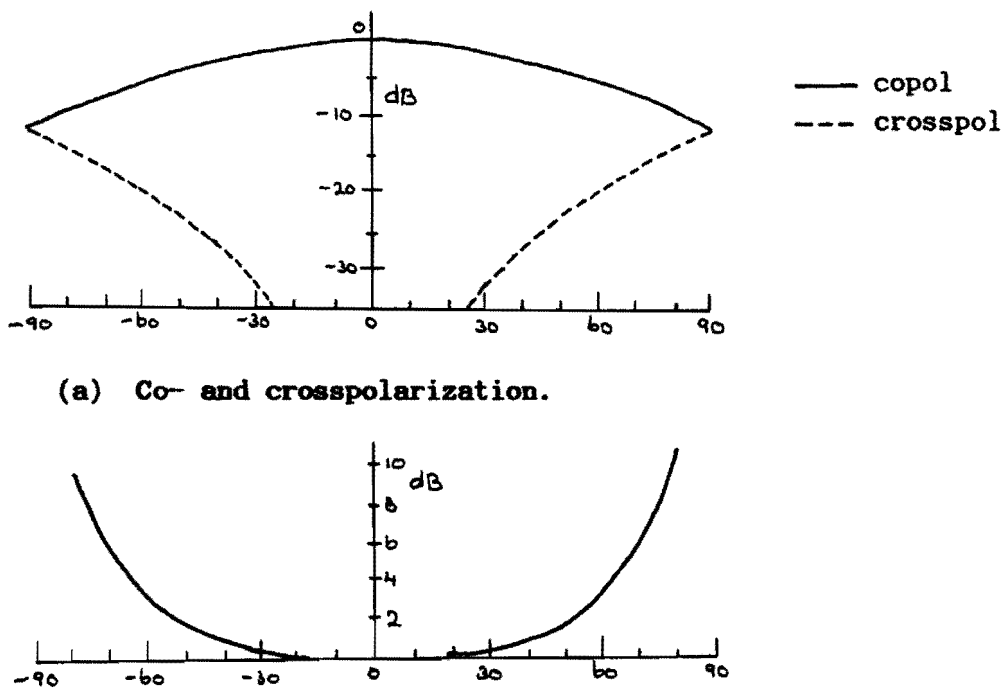

(a) Co- and crosspolarization.

(b) Axial ratio.

Fig.5.6 Calculated CP-characteristics for the two element microstrip antenna array in the plane $\varphi = 0°$. ($d = 0.87\lambda_0$, $\varepsilon_r = 2.53$)

Using (5.4), we can approximate (5.10) by

$$|E_L^N| = \frac{|A(r)|}{\sqrt{2}}(1+\cos\theta) \qquad (5.11.a)$$

$$|E_R^N| = \frac{|A(r)|}{\sqrt{2}}(1-\cos\theta) \qquad (5.11.b)$$

$$AR = \frac{1}{\cos\theta} \qquad (5.11.c)$$

for small polar angles θ .
We see, that the two element array has good CP-quality in the plane $\varphi = 0°$ and very poor quality in the plane $\varphi = 90°$.
Huang [9] considered a four element patch antenna array, as sketched in Fig.5.8, which gives good performance in both principal planes.

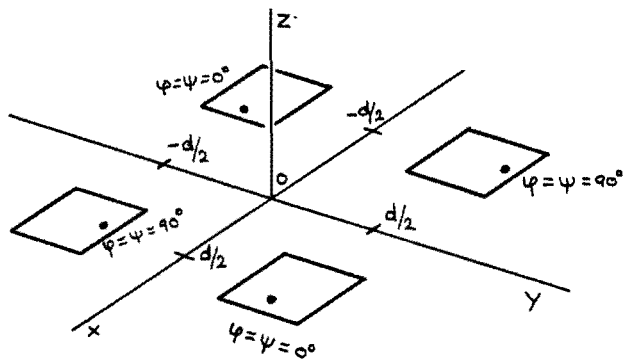

Fig.5.8 Four element circularly polarized microstrip antenna array.

As the array is uniformly excited, it will show the same behaviour in both principal planes, thus only one plane has to be considered.
The total far field components of the array in the plane $\varphi = 90°$ can be written as

$$E_\theta^N = A(r)\, e^{j90°} f_\theta(\theta,0)\left\{ e^{jk_0 \frac{d}{2}\sin\theta} + e^{-jk_0 d\sin\theta} \right\} \qquad (5.12.a)$$

$$E_\varphi^N = A(r)\, e^{j0°} g_\varphi(\theta,\pi/2)\left\{ e^{jk_0 \frac{d}{2}\sin\theta} + e^{-jk_0 \frac{d}{2}\sin\theta} \right\} \qquad (5.12.b)$$

The co- and crosspolarization are found as

$$|E_L^N| = 2\,|A(r)|\cdot\left| f_\theta(\theta,0) - g_\varphi(\theta,\pi/2)\right| \cos\left(k_0 \frac{d}{2}\sin\theta\right) \qquad (5.13.a)$$

$$|E_R^N| = 2\,|A(r)|\cdot\left| f_\theta(\theta,0) + g_\varphi(\theta,\pi/2)\right| \cos\left(k_0 \frac{d}{2}\sin\theta\right) \qquad (5.13.b)$$

and its axial ratio

$$AR = \begin{cases} \left| \dfrac{f_\theta(\theta,0)}{g_\varphi(\theta,\pi/2)} \right| & f_\theta(\theta,0) > g_\varphi(\theta,\pi/2) \\ \left| \dfrac{g_\varphi(\theta,\pi/2)}{f_\theta(\theta,0)} \right| & f_\theta(\theta,0) < g_\varphi(\theta,\pi/2) \end{cases} \qquad (5.14)$$

with $f_\theta(\theta,0)$ and $g_\varphi(\theta,\pi/2)$ given by (5.3).
We see, that the circular polarization quality, determined by the axial ratio, is the same as for the previous two element array.
The factor $\cos(k_0 d \sin\theta)$ is a two element array factor. The total field is thus equivalent to that generated from two circularly polarized elements. The calculated polarization patterns and axial ratio for the principal planes are shown in Fig.5.9.

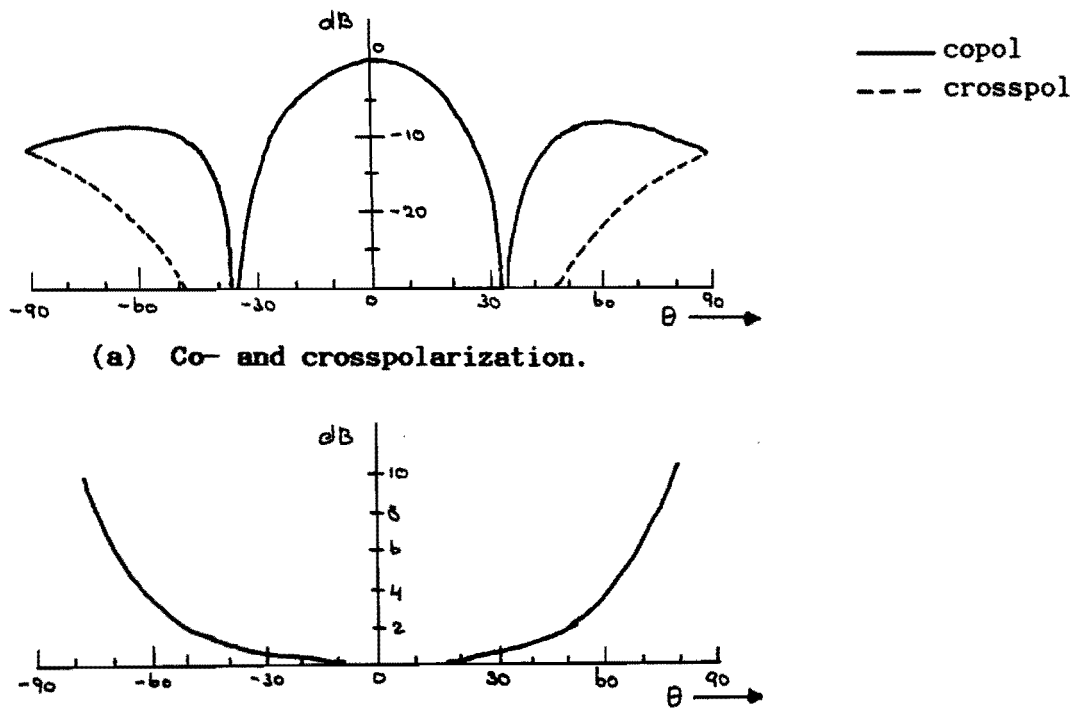

(a) Co- and crosspolarization.

(b) Axial ratio.

Fig.5.8 Calculated CP-characteristics for the four element array in the principal planes. ($d = 0.87\lambda_0$, $\varepsilon_r = 2.53$)

With the four element array we obtain good CP-quality in both principal planes, which is an improvement compared to the two element array. Hence, the diagonal plane remains to be considered and it will be shown that it gives poor CP-quality at angles off broadside. This can be best explained by referring to Fig.5.10.

The field generated in the diagonal plane can be seen as that generated from a non-uniformly excited three element linear array. The center element thus delivers a greater contribution to the radiation field as the end elements.

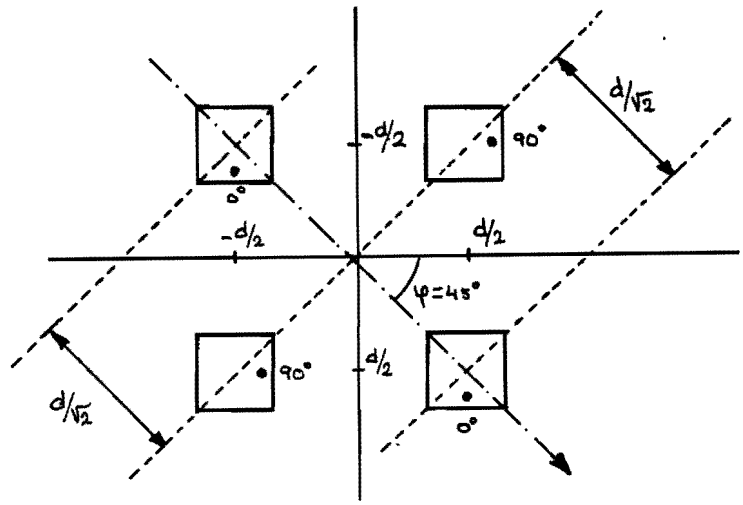

Fig.5.10 Diagonal plane configuration. (φ = 45°, d = 0.87λ_o)

Using (2.19), (5.1) and (5.2) we write for the array field components

$$E_\theta^N = A(r)e^{j0^\circ} f_\theta(\theta,\pi/4)\, e^{jk_o\frac{d}{\sqrt{2}}\sin\theta} + 2A(r)e^{j90^\circ} f_\theta(\theta,-\pi/4) + A(r)e^{j0^\circ} f_\theta(\theta,\pi/4)\, e^{-jk_o\frac{d}{\sqrt{2}}\sin\theta}$$

$$= 2A(r) f_\theta(\theta,\pi/4)\left\{ j + \cos\left(k_o \frac{d}{\sqrt{2}}\sin\theta\right)\right\} \qquad (5.15.a)$$

and

$$E_\varphi^N = A(r)e^{j0^\circ} g_\varphi(\theta,\pi/4)\, e^{jk_o\frac{d}{\sqrt{2}}\sin\theta} + 2A(r)e^{j90^\circ} g_\varphi(\theta,-\pi/4) + A(r)e^{j0^\circ} g_\varphi(\theta,\pi/4)\, e^{-jk_o\frac{d}{\sqrt{2}}\sin\theta}$$

$$= 2A(r) g_\varphi(\theta,\pi/4)\left\{\cos\left(k_o \frac{d}{\sqrt{2}}\sin\theta\right) - j\right\} \qquad (5.15.b)$$

which results with (2.9) in, writing $f_\theta(\theta,\pi/4)$ as f_θ and $g_\varphi(\theta,\pi/4)$ as g_φ

$$|E_L^N| = \sqrt{2}\,|A(r)|\left\{ (f_\theta^2+g_\varphi^2)\left(1+\cos^2\left(k_o \frac{d}{\sqrt{2}}\sin\theta\right)\right) - 4 f_\theta g_\varphi \cos\left(k_o \frac{d}{\sqrt{2}}\sin\theta\right)\right\}^{1/2} \qquad (5.16.a)$$

$$|E_R^N| = \sqrt{2}\,|A(r)|\left\{ (f_\theta^2+g_\varphi^2)\left(1+\cos^2\left(k_o \frac{d}{\sqrt{2}}\sin\theta\right)\right) + 4 f_\theta g_\varphi \cos\left(k_o \frac{d}{\sqrt{2}}\sin\theta\right)\right\}^{1/2} \qquad (5.16.b)$$

Linear polarization arises as $|E_L| = |E_R|$, thus

$$\cos\left(k_o \frac{d}{\sqrt{2}}\sin\theta_\ell\right) = 0 \qquad (5.17)$$

which is independent of f_θ and g_φ.

The first zero can be found with

$$\theta_\ell = \arcsin\left(\frac{\lambda_0}{2\sqrt{2}\,d}\right) \qquad (5.18)$$

In our example, $d = 0.87\lambda_0$, we find $\theta_\ell = 24°$, which is not far from broadside direction.
The calculated CP-characteristics for the diagonal plane are shown in Fig.5.11.

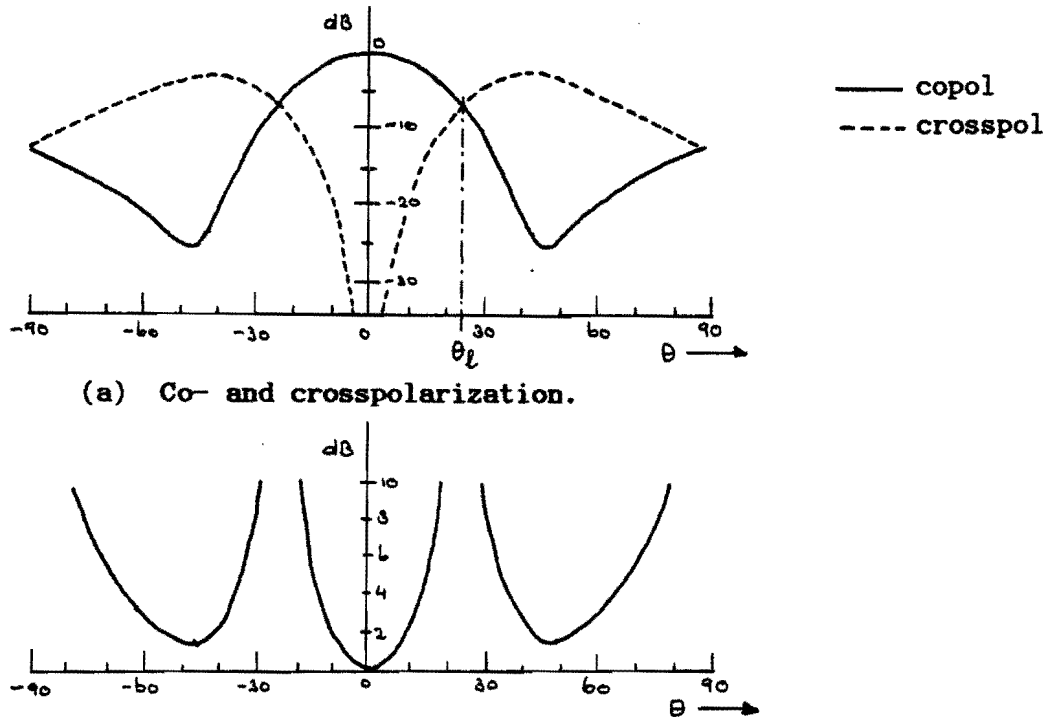

(a) Co- and crosspolarization.

(b) Axial ratio.

Fig.5.11 Calculated CP-characteristics in the diagonal plane for the four element microstrip antenna array in Fig.5.8. ($\varphi = 45°/225°$)

Summarizing, we have seen that the two element array gives good performance in one principal plane. The other principal plane gives poor CP-quality.
The four element array performs well in both principal principal planes, but its CP-quality remains bad in the diagonal plane.
Huang [9] has shown, that increasing the number of elements leads to an improvement in all planes. His calculations are based on the multimode cavity model, which leads to slightly other results as the results obtained with the program DIAPOL.
The poor CP behaviour for the arrays, discussed so far, is primarily due to the spacing of the orthogonally polarized radiation centres.
The relative ease in the design of the feeding network is the main advantage for such arrays, especially when they consist of a large number of elements.

To overcome the mentioned disadvantage for small arrays, we will have to resort to circularly polarized elements as building blocks.
The formulas, we have used until now, where based on the use of linearly polarized elements. A circularly polarized element can be treated as two linearly polarized elements, located orthogonally on the same place, and excited with 90° phase difference and equal amplitude.
Let us now consider a circularly polarized microstrip antenna, placed in the origin of the co-ordinate system as sketched in Fig.5.12.

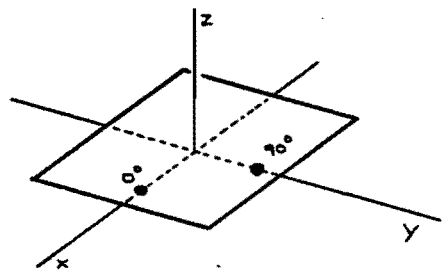

Fig.5.12 Circularly polarized square patch antenna.

Its calculated polarization characteristics are shown in Fig.5.13.

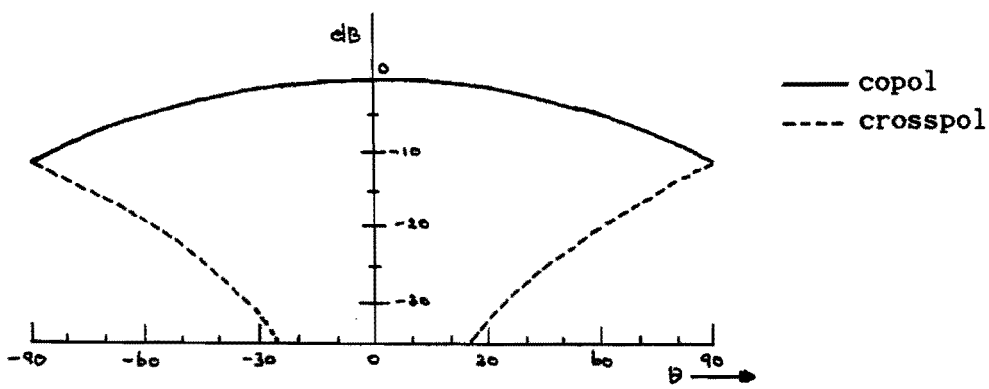

Fig.5.12 Calculated CP-characteristics for the square patch dual feed antenna in Fig.5.11. Principal plane. ($\varepsilon_r = 2.53$)

The field components of this antenna are written as

$$E_{\theta c} = e^{j0^\circ} A(r)\, f_\theta(\theta,\varphi) + e^{j90^\circ} A(r)\, f_\theta(\theta,\varphi-\pi/2)$$
$$= A(r)\left\{ f_\theta(\theta,\varphi) + j\, f_\theta(\theta,\varphi-\pi/2)\right\} \qquad (5.19.a)$$

$$E_{\varphi c} = e^{j0^\circ} A(r)\, g_\varphi(\theta,\varphi) + e^{j90^\circ} A(r)\, g_\varphi(\theta,\varphi-\pi/2)$$
$$= A(r)\left\{ g_\varphi(\theta,\varphi) + j\, g_\varphi(\theta,\varphi-\pi/2)\right\} \qquad (5.19.b)$$

The copolarization, crosspolarization and axial ratio can be found from eqs.2.9 and 2.10, resulting in

$$E_{LC} = \frac{A(r)}{\sqrt{2}} \left\{ f_\theta(\theta,\varphi) + g_\varphi(\theta,\varphi-\pi/2) + j\left(f_\theta(\theta,\varphi-\pi/2) - g_\varphi(\theta,\varphi)\right)\right\} \qquad (5.20.a)$$

$$E_{RC} = \frac{A(r)}{\sqrt{2}} \left\{ f_\theta(\theta,\varphi) - g_\varphi(\theta,\varphi-\pi/2) + j\left(f_\theta(\theta,\varphi-\pi/2) + g_\varphi(\theta,\varphi)\right)\right\} \qquad (5.20.b)$$

$$AR_c = \left| \frac{|E_{LC}| + |E_{RC}|}{|E_{LC}| - |E_{RC}|} \right| \qquad (5.20.c)$$

We make up an array consisting of N of these elements with equal orientation and phasing in the xy-plane. Its field components given by

$$E^N_{\theta c} = A(r) \left\{ f_\theta(\theta,\varphi) + j\, f_\theta(\theta,\varphi-\pi/2)\right\} \sum_{i=1}^{N} e^{jk(\hat{r}\cdot\bar{r}_i)} \qquad (5.21.a)$$

$$E^N_{\varphi c} = A(r) \left\{ g_\varphi(\theta,\varphi) + j\, g_\varphi(\theta,\varphi-\pi/2)\right\} \sum_{i=1}^{N} e^{jk(\hat{r}\cdot\bar{r}_i)} \qquad (5.21.b)$$

resulting in the co-, crosspolarization and axial ratio

$$E^N_{LC} = E_{LC} \sum_{i=1}^{N} e^{jk(\hat{r}\cdot\bar{r}_i)} \qquad (5.22.a)$$

$$E^N_{RC} = E_{RC} \sum_{i=1}^{N} e^{jk(\hat{r}\cdot\bar{r}_i)} \qquad (5.22.b)$$

$$AR^N_c = AR_c \qquad (5.22.c)$$

With $|E_{LC}|$, $|E_{RC}|$, AR_c the co-, crosspolarization and axial ratio for a single element. In this ideal case, we may conclude that the CP-quality, described by the axial ratio, will not be improved. The quality is thus determined by the axial ratio of a single element, and only the directivity is increased by placing these elements in an array structure. In practical situations the orientation will be important in optimizing the behaviour of the antenna, especially as the axial ratio bandwidth is considered.
Eqs.5.22 do not hold true either, as the elements have arbitrarily spatial rotations and phasings. In this case we have to resort to numerical methods, for example the program DIAPOL in appendix A.
To see, if the polarization properties are improved, we will calculate the polarization characteristics of the four element array in Fig.5.8, but now consisting of circularly polarized elements as in Fig.5.13.

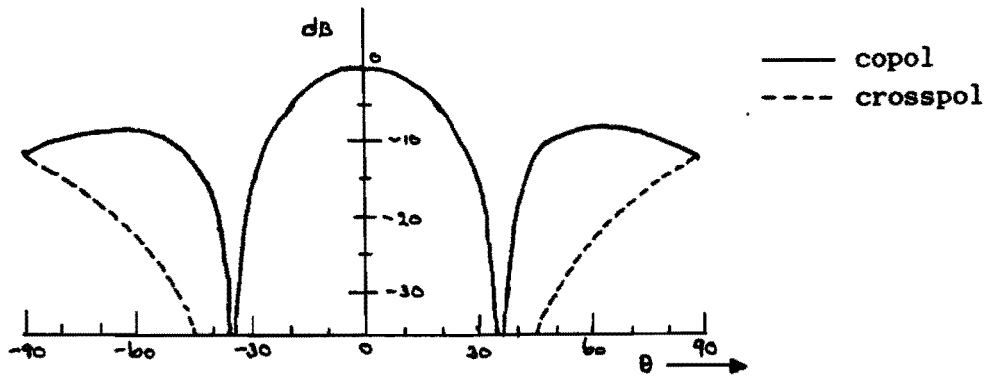

Fig.5.14 Calculated polarization characteristics of a four element array as in Fig.5.8, consisting of circularly polarized square patch elements. (Principal plane)

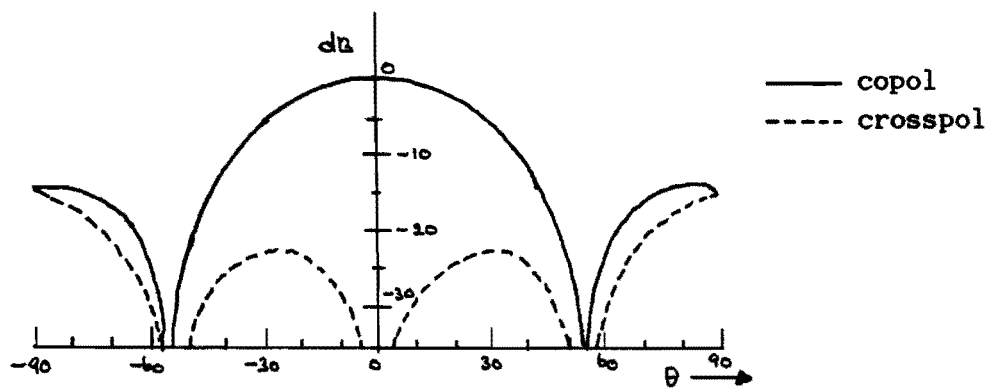

Fig.5.15 Calculated polarization characteristics of a four element array as in Fig.5.8, consisting of circularly polarized square patch elements. (Diagonal plane)

From these figures we can conclude that the latter array structure gives a much better performance in all planes. For small arrays, use of circularly polarized elements seems to be the proper way.

5.3 Bandwidth restrictions and design considerations.

Until now, we were primarily concerned with ideal radiating elements, phase shifters and other components to achieve the desired circular polarization. In practical situations however, there are a number of factors degrading the performance. In the case of microstrip antennas, the bandwidth appears to be an important limiting factor.

We will consider the axial ratio bandwidth and the impedance bandwidth.
The first and most important factor is the narrow band behaviour of the resonant patch antenna. This means that, when the antenna operates away from its resonant frequency, a considerable part of the incoming power will be reflected, resulting in a poor impedance match and loss of antenna gain.
The occuring standing wave pattern in the feeding network is an inherent consequence of the reflected power. As this network is performed in microstrip coplanar with the radiating elements, spurious radiation occurs, which strongly affects the required radiation pattern. This is why it is preferable to attach the feeding network at the rear of the antenna ground plane. The power is then coupled to the antenna elements using feed-throughs, which behaves well as the wavelength used is large compared to the length of the feed-through. A second advantage using this network is, that more space is available for the feeding network.
As the resonant patch has a rather high Q-factor, we have to put strict demands to deviations in their resonant frequencies. To make this clear, consider the circularly polarized square patch antenna. As its two orthogonal modes are not equally tuned, the contribution to the radiation field are not the same for both modes, which is a requirement for good circular polarization.
The resonant frequency is strongly dependent of the patch size, so there is an inherent demand to high manufacturing tolerances.
Other factors, leading to degradation of the axial ratio are the mutual coupling effects between the orthogonal modes of a single patch and those between the different patch antennas.
In practical situations, the TM_{01}-mode is not the only excited mode. Other higher order modes will be excited, dependent of the excitation place and substrate thickness. These modes will affect the radiation pattern and thus worsen the axial ratio. A thin substrate will strongly suppress these modes.
Until now, we were primarily concerned with the radiating elements. The feeding network delivers also a contribution in altering the radiation characteristics as a function of the frequency. We can distinguish two main causes for these alterations.
The first is due to the fact, that the power splitters will only split the incoming power in equal parts, as the output ports are equally matched. This is hard to realize as the output ports are cascaded with different phase shifters. The output ports will 'see' an equal impedance only in the case of a perfect match. This will be worked out in a later section of this chapter.
The other cause resulting in a frequency dependent axial ratio, is the frequency dependent behaviour of the phase shifters. The individual output phase is linearly proportional to the frequency as can be seen in eq.4.27. The influence of this can be optimized by minimizing the relative phase difference between the antenna input ports. Relative phase differences however, are inherent to generating circularly polarized radiation with acceptable bandwidth.

Improving the bandwidth of a patch antenna can be done by lowering its Q-factor, hence a thicker substrate with low dielectric loss should be used. This gives rise to the introduction of higher order modes which are amenable of a less controllable axial ratio. Increasing the substrate thickness alone, thus seems to be of less importance.
We can increase the axial ratio bandwidth of a single element considerably by feeding it with four different probes, as is shown in Fig.5.16. [2]

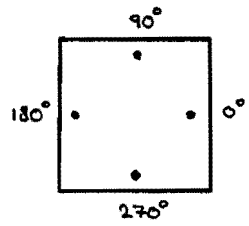

Fig.5.16 Four-probe fed patch. (Balanced excitation)

Using this method suppresses the higher order modes strongly, hence a much more symmetric radiation pattern is obtained.
The obvious disadvantage of the four-probe fed patch is its complicated feeding network, especially when it is used in an array.
Another case of interest for our purpose is the control of the radiation pattern. Control of the half power beamwidth for example, cannot sufficiently be done with a single element, so we are constrained to an array structure.
This, and because of the results in the previous section we have chosen for a square dual feed patch antenna as the building block of an antenna array. The array structure consists of four elements in a 2X2-structure, aimed at a particular project requirement [18] and bears no special significance.
The ultimate array structure is diagrammed in Fig.5.17.

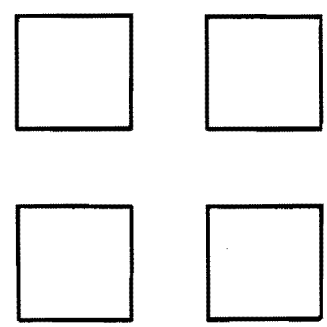

Fig.5.17 Four element circularly polarized antenna array consisting of four dual feed square patch antennas.

5.3.1 Sequential rotation as an improvement of the axial ratio bandwidth.

The matter of interest is how to place and excite the separate elements. Usually the elements are equally oriented and excited. Recent developments [9,16,17] have shown that a special array configuration leads to a much better performance. This configuration is referred to as a sequentially rotated antenna array and its principal operation can be described as follows.
Suppose, the array consists of N identical elements with arbitrary polarization. A sequentially rotated array is obtained as the i^{th}-element is provided with a spatial rotation φ_i and feeding phase shift ψ_i.

$$(N \geq 3) \qquad \psi_i = \varphi_i = \pm \frac{2\pi i}{N} \qquad 0 \leq i \leq N-1 \qquad (5.23)$$

The advantage of this configuration is, that circular polarization in broadside direction is obtained independent of the polarization of the element. Occuring asymmetrical behaviour in the radiation pattern of a single element will be cancelled out as long as the asymmetry is identical to each element.
Examples of effects leading to this kind of asymmetry are the occuring higher order modes in a patch antenna, and the asymmetry due to the unbalanced excitation (e.g. the dual feed square patch antenna).
This kind of array appears to be quite successful when single feed circularly polarized patch antennas are used [16]. The axial ratio bandwidth using these elements in a sequentially rotated fashion is significantly improved compared to the axial ratio bandwidth of a single element, due to the effect mentioned above. Using elements as the four-probe fed patch (Fig.5.15) in a sequentially rotated fashion seems to be less advantageous, due to the increased feed complexity.
We already stated that circular polarization is obtained in broadside direction. The proof of this goes as follows.
We know from Chapter 2 (eq.2.2), that the electric field vector for an arbitrarily polarized antenna in broadside direction can be written as

$$\bar{E} = E_\theta(0,0)\,\hat{a}_\theta + E_\varphi(0,0)\,\hat{a}_\varphi \qquad (5.24)$$

Rotating the antenna over an angle φ_i , the vector components will alter as shown in Fig.5.18. ($E_\theta(0,0) = E_\theta$, $E_\varphi(0,0) = E_\varphi$)

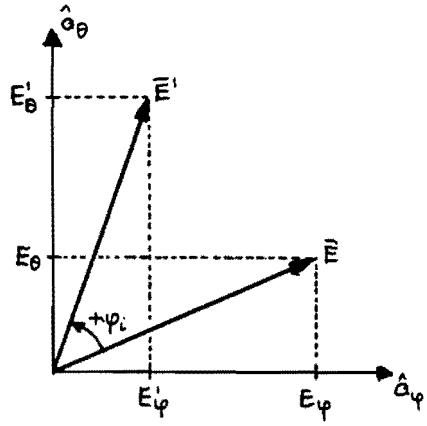

Fig.5.18 Rotation of E-vector over an angle $+\varphi_i$.

The rotated vector components can be found from

$$E'_\theta = E_\theta \cos\varphi_i - E_\varphi \sin\varphi_i \tag{5.25.a}$$

$$E'_\varphi = E_\theta \sin\varphi_i + E_\varphi \cos\varphi_i \tag{5.25.b}$$

The total field for the sequentially rotated array can be written as

$$E'^N_\theta = \sum_{i=0}^{N-1} \left\{ E_\theta \cos\phi_i - E_\varphi \sin\phi_i \right\} e^{j\phi_i} \tag{5.26.a}$$

$$E'^N_\varphi = \sum_{i=0}^{N-1} \left\{ E_\theta \sin\phi_i + E_\varphi \cos\phi_i \right\} e^{j\phi_i} \tag{5.26.b}$$

with $\phi_i = \varphi_i = \psi_i = \frac{2\pi i}{N}$ $\qquad (i = 0, \ldots, N-1)$

With the help of (2.9) and the geometric series

$$\sum_{i=0}^{N-1} e^{j2\phi_i} = 0$$

we obtain

$$E_L = \frac{1}{\sqrt{2}} \left(E'^N_\theta - jE'^N_\varphi \right) = \frac{N}{\sqrt{2}} \left(E_\theta + jE_\varphi \right) \tag{5.27.a}$$

$$E_R = 0 \tag{5.27.b}$$

which is a perfect left-hand circularly polarized wave in broadside direction.

We already mentioned that the ultimate antenna array must consist of four circularly polarized square patch elements in a 2X2-fashion. To obtain a higher axial ratio bandwidth, we have chosen for a sequentially rotated array as diagrammed in Fig.5.19.
The structure of the feeding network and its impedance bandwidth will be discussed later on.

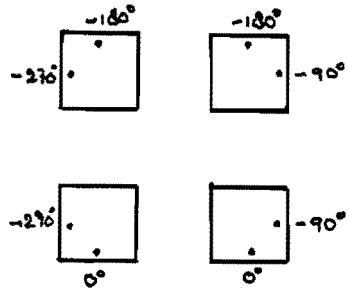

Fig.5.19 Four element sequentially rotated array consisting of circularly polarized elements.

5.4 Matching and power splitting properties of the feeding network.

The purpose of the feeding network is to deliver an equal amount of power to the radiating elements with appropriate phasings.
The network impedance is highly dependent of the frequency dependent impedance of the patch elements. The latter impedance was described in Chapter 3.
We already noted that the axial ratio relies on well defined output phasings of the phase shifters, and the equal power splitting facility of the power splitters.
Before the performance of the total feeding network is discussed, the following questions have to be answered for the power splitters. The first question is, under what conditions does equal power splitting occur, and the second is how the input match of the splitter behaves as a function of the output matches.
To answer these questions we will consider a general symmetric three-port network and we will apply the results to the reactive T-splitter and the Wilkinson splitter.
The network is shown in Fig.5.20. We assume that the input and output ports are connected to arbitrary impedances, in general causing a mismatch to all ports.

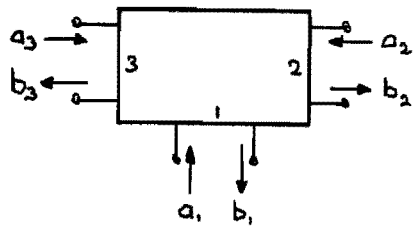

Fig.5.20 Symmetric three-port network.

We consider port 1 as the input port. The input reflection coefficient of this port is defined as

$$\rho_1 \triangleq \frac{b_1}{a_1} \tag{5.28}$$

Note, that this definition of the reflection coefficient is not the same as the definition in (4.3), because the output ports do not have to be matched.
The output reflection coefficients ρ_2 and ρ_3 are related to the outward going power. They are defined as

$$\rho_2 \triangleq \frac{a_2}{b_2} \tag{5.29.a}$$

$$\rho_3 \triangleq \frac{a_3}{b_3} \tag{5.29.b}$$

The incoming power at port 1 can be written as

$$P_1 = |a_1|^2 - |b_1|^2 = |a_1|^2(1-|\rho_1|^2) \tag{5.30}$$

and the outward going power at port 2 and 3 are found from

$$P_2 = |b_2|^2 - |a_2|^2 = |b_2|^2(1-|\rho_2|^2) \tag{5.31.a}$$

$$P_3 = |b_3|^2 - |a_3|^2 = |b_3|^2(1-|\rho_3|^2) \tag{5.31.b}$$

We will need the scattering matrix for a symmetrical three-port, which is given by (4.2). Substitution of (5.28) and (5.29) in (4.2) results in

$$\begin{aligned} b_1 &= S_{11}\,a_1 + S_{12}\,\rho_2\,b_2 + S_{12}\,\rho_3\,b_3 \\ b_2 &= S_{12}\,a_1 + S_{22}\,\rho_2\,b_2 + S_{23}\,\rho_3\,b_3 \\ b_3 &= S_{12}\,a_1 + S_{23}\,\rho_2\,b_2 + S_{22}\,\rho_3\,b_3 \end{aligned} \tag{5.32}$$

The purpose is to express the outgoing waves b_1, b_2, and b_3 in terms of a_1, the scattering coefficients and the output reflection coefficients. Working out (5.32), we obtain

$$b_1 = \left(S_{11} + S_{12}^2 \frac{\rho_2 + \rho_3 - 2\rho_2\rho_3(S_{22} - S_{23})}{1 - S_{22}(\rho_2+\rho_3) + \rho_2\rho_3(S_{22}^2 - S_{23}^2)} \right) a_1 \qquad (5.33.a)$$

$$b_2 = \left(\frac{1 - (S_{22} - S_{23})\rho_3}{1 - S_{22}(\rho_2 + \rho_3) + \rho_2\rho_3(S_{22}^2 - S_{23}^2)} \right) S_{12}\, a_1 \qquad (5.33.b)$$

$$b_3 = \left(\frac{1 - (S_{22} - S_{23})\rho_2}{1 - S_{22}(\rho_2 + \rho_3) + \rho_2\rho_3(S_{22}^2 - S_{23}^2)} \right) S_{12}\, a_1 \qquad (5.33.c)$$

The input reflection coefficient is found from (5.33.a) as

$$\rho_1 = S_{11} + S_{12}^2 \frac{\rho_2 + \rho_3 - 2\rho_2\rho_3(S_{22} - S_{23})}{1 - S_{22}(\rho_2+\rho_3) + \rho_2\rho_3(S_{22}^2 - S_{23}^2)} \qquad (5.34)$$

The ratio between the output power P_2 and P_3 with (5.31) as

$$\frac{P_2}{P_3} = \frac{(1-|\rho_2|^2)}{(1-|\rho_3|^2)} \frac{|1-(S_{22}-S_{23})\rho_3|^2}{|1-(S_{22}-S_{23})\rho_2|^2} \qquad (5.35)$$

From (5.35) we see, that equal power splitting only occurs in the case $\rho_2 = \rho_3$, which means that the ports 2 and 3 must 'see' equal impedances.
Let's now consider a dual feed circularly polarized microstrip antenna (Fig.5.1) with an arbitrary power splitter.
We assume, that the antenna input reflection coefficients are equal ρ_a. The transmissionlines between antenna and power splitter are supposed to be loss free.
The equivalent network is sketched in Fig.5.21.

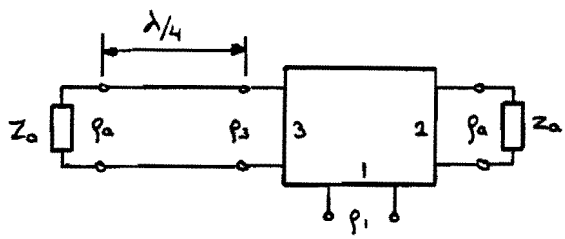

Z_a: antenna impedance

Fig.5.21 Equivalent feeding network for circularly polarized dual feed microstrip antenna.

The output reflection coefficient ρ_3 can be found with

$$\rho_3 = \rho_a e^{-2j\beta\lambda/4} = -\rho_a \tag{5.36}$$

Substitution in (5.34) and (5.35) gives

$$\rho_1 = S_{11} + S_{12}^2 \frac{2\rho_a^2(S_{22}-S_{23})}{1-\rho_a^2(S_{22}^2-S_{23}^2)} \tag{5.37}$$

$$\frac{P_2}{P_3} = \left| \frac{1+(S_{22}-S_{23})\rho_a}{1-(S_{22}-S_{23})\rho_a} \right|^2 \tag{5.38}$$

It is worthwhile to compare the matching and power splitting properties of a reactive T-splitter and a Wilkinson splitter. For the reactive T-splitter we obtain with (4.22)

$$|\rho_1| = |\rho_a|^2 \tag{5.39}$$

$$\frac{P_2}{P_3} = \left| \frac{1-e^{-2j\beta\ell}\rho_a}{1+e^{-2j\beta\ell}\rho_a} \right|^2 \tag{5.40}$$

We see, that the input reflection coefficient ρ_1 is improved with respect to the antenna input reflection coefficient ρ_a , because $|\rho_a| < 1$.
If $|\rho_a| = 1$, all the power must be reflected to the input port, because the network is assumed to be loss free.
The problem using the reactive T-splitter originates in the unequal power splitting, as can be seen in (5.40). The power is only divided equally as $\rho_a = 0$, i.e. the antenna must be well matched.

The Wilkinson splitter gives a considerable improvement with respect to the T-splitter, when it operates in the vicinity of the frequency f_r. The theoretical values for the scattering coefficients can be found with (4.7), (4.10) and (4.21), resulting in $S_{11} = S_{22} = S_{23} = 0$ as $f = f_r$.
We obtain

$$\rho_1 = 0 \tag{5.41}$$

$$\frac{P_2}{P_3} = 1 \tag{5.42}$$

for all output reflection coefficients ρ_a .
The relation $\rho_1 = 0$ means, that all the power reflected from the antenna input ports must be dissipated in the internal resistor.

As the operating frequency f deviates from f_r, the relations (5.41) and (5.42) are not valid anymore. This is due to the fact that the scattering parameters $S_{11} = S_{22} = S_{21} \neq 0$ in this case. Note, that although the argument of ρ_2 and ρ_3 will alter as a function of the frequency, the relation $|\rho_2| = |\rho_3|$ remains valid.
From Fig.4.13 we see, that the considered scattering parameters remain small numbers over a relative wide frequency band. Within this band (5.42) can still be used, only (5.41) will be slightly altered.
The Wilkinson splitter does not split its power equally, as $|\rho_2| \neq |\rho_3|$, this is as the antenna impedances are not equal. However, in general the Wilkinson splitter is expected to give a much better performance compared to the reactive T-splitter. The Wilkinson splitter provides a good impedance match independent of the antenna input reflection coefficient as it operates in the neighbourhood of the frequency f_r, in contrast with the reactive T-splitter.

Another interesting case we will analyze is the input matching property of a network consisting of N parallel transmissionlines (e.g. microstrip). In certain circumstances the reflected waves will be partly cancelled out.
The general network we will consider is sketched in Fig.5.22.

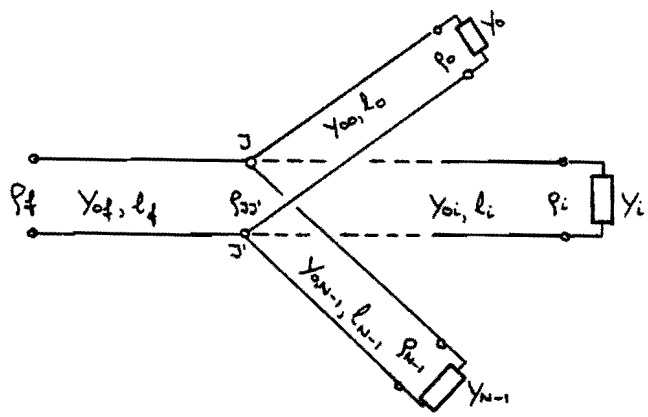

Fig.5.22 N transmissionlines in parallel configuration.

This network can be considered as the feeding network for an N-element antenna array. The admittance Y_i represents the input admittance of antenna i. The input reflection coefficient of the total network can be obtained with the following method.
First we write the input admittance of a transmissionline in terms of its output reflection coefficient (Fig.5.23).

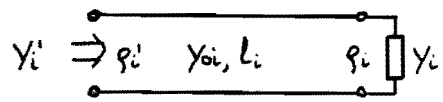

Fig.5.23 Transmissionline and its characteristics.

The input admittance Y_i' can be written as [19]

$$Y_i' = Y_{oi} \frac{1 - \rho_i e^{-2j\beta l_i}}{1 + \rho_i e^{-2j\beta l_i}} \tag{5.43}$$

If we connect N of these lines in parallel, we obtain for the total input admittance at the junction JJ'

$$Y_{JJ'} = \sum_{i=0}^{N-1} Y_i' = \sum_{i=0}^{N-1} Y_{oi} \frac{1 - \rho_i e^{-2j\beta l_i}}{1 + \rho_i e^{-2j\beta l_i}} \tag{5.44}$$

from which the reflection coefficient at the junction JJ' can be obtained with

$$\rho_{JJ'} = \frac{Y_{of} - Y_{JJ'}}{Y_{of} + Y_{JJ'}} \tag{5.45}$$

and the reflection coefficient at the feeding point with

$$\rho_f = \rho_{JJ'} e^{-2j\beta l_f} \tag{5.46}$$

We will now make some assumptions. First is assumed that each antenna must dissipate an equal amount of power as it is perfectly matched, i.e. $\rho_i = 0$, (i = 0,..,N-1). This implies, that $Y_{oi} = Y_o$, (i = 0,..,N-1) as can be obtained with the help of Fig.5.24.

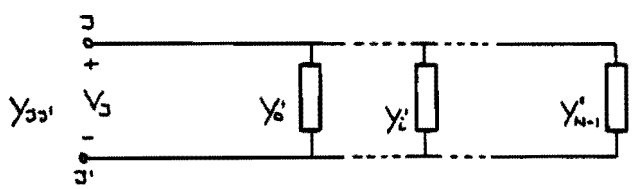

Fig.5.24 Network analogon for the input admittance at the junction JJ'.

The power dissipated in Y' is

$$P_{Y_i'} = \tfrac{1}{2}|V_J|^2 R_e\, Y_i' \tag{5.47}$$

and can be written as ($\rho_i = 0$)

$$P_{Y_i'} = \tfrac{1}{2}|V_J|^2 Y_{oi} \tag{5.48}$$

because the characteristic admittance is real. We can conclude, that for equal amounts of power in the antennas, the characteristic admittances have to be equal.
With (5.45) we find the required value for Y_{oj}.

$$Y_{oj} = N Y_o \tag{5.49}$$

Further on, we assume that the antenna admittances Y_i are equal to all antennas. This gives

$$\rho_a = \rho_i \qquad (i = 0,..,N-1) \tag{5.50}$$

Eqs.5.44 and 5.45 can now be written as

$$Y_{JJ'} = Y_o \sum_{i=0}^{N-1} \frac{1-\rho_a e^{-2j\beta l_i}}{1+\rho_a e^{-2j\beta l_i}} \tag{5.51}$$

$$\rho_{JJ'} = \frac{NY_o - Y_{JJ'}}{NY_o + Y_{JJ'}} \tag{5.52}$$

Let's first consider the special case of equal line lengts. Working this out we see that the input reflection coefficient at the junction becomes

$$\rho_{JJ'} = \rho_a e^{-2j\beta l} \tag{5.53}$$

and we see that the reflection coefficient remains the same compared to the reflection coefficient of a single transmissionline.
We have already considered a circularly polarized patch antenna fed in phase quadrature, the resulting reflection coefficient given by (5.39). This improvement is due to the fact that the reflected waves will partly cancel out as they return at the junction. This was to be expected as there is a half wavelength difference in electrical length for these waves.
We are now ready to consider the feeding network for a sequentially rotated array. The antennas are excited with a phase difference given by (5.23).

The physical lengths of the consecutive transmissionlines are given by

$$l_i = l_o + \frac{\lambda}{N} i \tag{5.54}$$

The junction impedance (5.51) can be written as

$$Y_{JJ'} = Y_o \sum_{i=0}^{N-1} \frac{1 - z e^{-j\frac{4\pi i}{N}}}{1 + z e^{-j\frac{4\pi i}{N}}} \tag{5.55}$$

with $$z = \rho_a e^{-2j\beta l_o} \tag{5.56}$$

The input matching properties for the case N = 3 are considered for example. We obtain for the input admittance

(N = 3)

$$Y_{JJ'} = Y_o \left\{ \frac{1-z}{1+z} + \frac{1 - z e^{-j\frac{4\pi i}{3}}}{1 + z e^{-j\frac{4\pi i}{3}}} + \frac{1 - z e^{-j\frac{8\pi i}{3}}}{1 + z e^{-j\frac{8\pi i}{3}}} \right\} = 3Y_o \left\{ \frac{1-z^3}{1+z^3} \right\} \tag{5.57}$$

which results in the input reflection coefficient

$$\rho_{JJ'} = z^3 = \rho_a^3 e^{-j6\beta l} \quad \Longrightarrow \quad |\rho_{JJ'}| = |\rho_a|^3 \tag{5.58}$$

The calculations for other N are given in Table 5.1.

N	$Y_{JJ'}$	$\rho_{JJ'}$
4	$4Y_o\left(\frac{1+z^2}{1-z^2}\right)$	$-\rho_a^2 e^{-4j\beta l}$
5	$5Y_o\left(\frac{1-z^5}{1+z^5}\right)$	$\rho_a^5 e^{-10j\beta l}$
8	$8Y_o\left(\frac{1+z^4}{1-z^4}\right)$	$-\rho_a^4 e^{-8j\beta l}$

Table 5.1 Junction input admittance and reflection coefficient for the sequentially rotated array fed by N transmission lines (Fig.5.22).

The proof for the general case is given in appendix C, from which we observe

N even:
$$Y_{jj'} = N Y_0 \left\{ \frac{1+(-z)^{N/2}}{1-(-z)^{N/2}} \right\} \qquad (5.61.a)$$

$$\rho_{jj'} = -\rho_a^{N/2} e^{-jN\beta\ell} \qquad (5.61.b)$$

N odd :
$$Y_{jj'} = N Y_0 \left\{ \frac{1-z^N}{1+z^N} \right\} \qquad (5.61.c)$$

$$\rho_{jj'} = \rho_a^N e^{-j2N\beta\ell} \qquad (5.61.d)$$

We see, that increasing N gives an improved performance as far as the input reflection coefficient is considered, because $|\rho_a| < 1$. The reduction of the input reflection coefficient appears to be more sensitive for the number of transmissionlines in the case of an odd number compared to the case of an even number.
In practical situations however, there are many other factors that disturb the input reflection coefficient, degrading the value of the foregoing theory. One of these factors is, that in general the antenna input admittances are not equal.
Increasing the number of transmissionlines does not include a decisive answer to the power splitting quality and thus no answer can be given for the behaviour of the axial ratio. The axial ratio will undoubtedly alter as $\rho_a \neq 0$, because this results in unequal real parts of the input admittances .
Teshirogi [16] stated, that the input reflection coefficient of a sequentially rotated array would be zero independent of the input reflection coefficient of the antenna. This is definitely not the case as we have seen. If the reflection coefficient $\rho_a = 1$ for instance, the output admittance would dissipate no power, and still the input would be perfectly matched. This is in contradiction with the energy conservation law, as the transmissionlines are loss free. The mistake he made was the assumption of equally divided power to the output admittances.
This is only true when we use isolated configurations, as the Wilkinson splitter is for example. The Wilkinson splitter has a very good input match of its own, because the reflected power is dissipated in the internal resistor.

6. Experimental results.

6.1 Introduction.

In this chapter, we will discuss the practical results of our investigation. The objective of this research was to compare the bandwidth characteristics of a sequentially rotated four element array with the bandwidth characteristics of a single element. The design steps can be summarized as follows.

a) Determination of patch size and location of the inset feed point of the square patch to obtain a good impedance match at the resonant frequency.
b) Using the results of a), a circularly polarized square patch was made together with its feeding network.
c) Design of the four element sequentially rotated array and its feeding network.

These design steps will be discussed in the next sections, together with the measured results.

6.2 Determination of patch size and place of the inset feed point.

The material used for the printed circuit antennas and feeding network was Rexolite 1422. This material has a polystyrene substrate with nominal dielectric constant $\varepsilon_r = 2.53$, and substrate thickness h = 0.1588 cm. Antenna designers have found that the dielectric constant of the substrate is the most sensitive parameter in microstrip antenna performance estimation. The manufacturer quotes an absolute dielectric constant tolerance of 0.05 for Rexolite 1422.
We know from (3.15), that the first order approximation for the resonant frequency can be written as

$$f_{r_0} = \frac{1}{2b\sqrt{\mu_0 \varepsilon_0 \varepsilon_r}} \tag{6.1}$$

The change in resonant frequency, due to a slight variation $\Delta\varepsilon_r$ can be written as

$$\Delta f_{r_0} = \frac{\partial f_{r_0}}{\partial \varepsilon_r} \Delta \varepsilon_r = -\frac{1}{2} f_{r_0} \frac{\Delta \varepsilon_r}{\varepsilon_r}$$

$$\frac{\Delta f_{r_0}}{f_{r_0}} = -\frac{1}{2} \frac{\Delta \varepsilon_r}{\varepsilon_r} \tag{6.2}$$

so the tolerance in the resonant frequency for Rexolite 1422 is to be expected in the order of one percent. In our measurements however, this effect appeared to be less significant than was expected.

The patch size tolerance Δb is taken into account with

$$\frac{\Delta f_r}{f_r} \simeq \frac{-\Delta b}{b} \qquad (6.3)$$

The resonant frequency of a square patch antenna in the TM_{01} -mode is found from (3.16), and is the same for the resonant frequency in the TM_{10} -mode.
The required resonant frequency for the circularly polarized antenna is 1.5 GHz. The patch sizes for this frequency are thus calculated as a = b = 6.04 cm.
The antenna impedance on both input ports is required to give a good impedance match to a 50 Ω transmissionline. From Chapter 3 we know that the antenna impedance is strongly dependent of the location of the feed point. A trial and error approach was used to find the place that gives optimum performance. Therefore, two samples were made with each of them three possible feed points. The lay-out was made four times enlarged and reduced by a photographic process. This was done to minimize the imperfect size tolerances in the design lay-out. This process did not give quite acceptable results, because the ultimate patch sizes were 6.02 cm instead of the required 6.04 cm. The resultant patches are sketched in Fig.6.1.

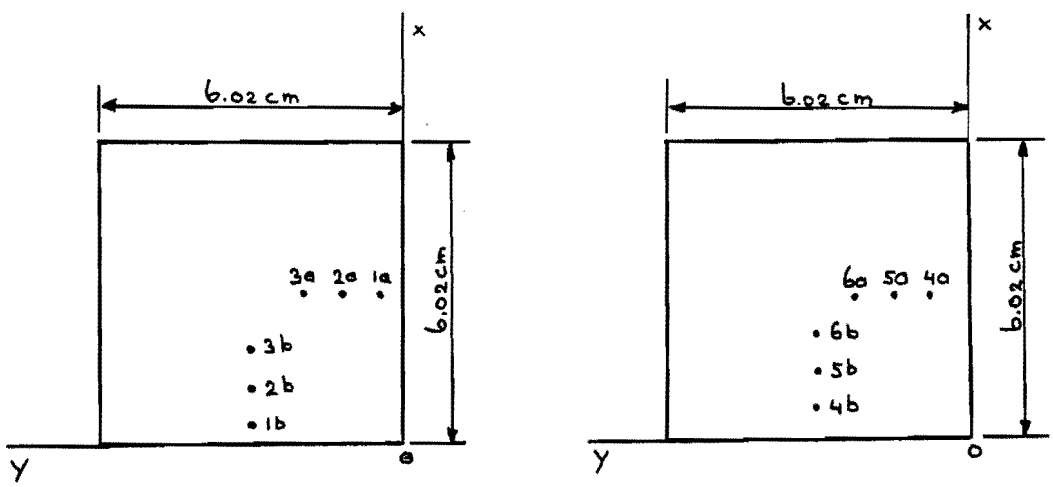

Fig.6.1 Samples on Rexolite 1422 substrate (ε_r = 2.53, h = 0.1588 cm) to determine the input impedance as a function of the place of the inset feed point.

The locations of the input ports can be found in Table 6.1.

Port	x [cm]	y [cm]	Port	x [cm]	y [cm]
1a	3.01	0.47	1b	0.47	3.01
2a	3.01	1.10	2b	1.10	3.01
3a	3.01	1.74	3b	1.74	3.01
4a	3.01	0.79	4b	0.79	3.01
5a	3.01	1.42	5b	1.42	3.01
6a	3.01	2.06	6b	2.06	3.01

Table 6.1 Feed point locations of the samples in Fig.6.1.

The variations in the input resistance, given by (3.25), appears to be quite sensitive to variations in feed location, especially as the antenna is fed in the neighbourhood of the patch centre. To see this, we write (3.25) as

$$R_{01} \simeq C \cos^2\left(\frac{\pi y_0}{b}\right) \tag{6.4}$$

Variations in the location of the feed point Δy_0 can be taken into account with

$$\Delta R_{01} = \frac{\partial R_{01}}{\partial y_0} \Delta y_0 = \frac{2\pi}{b} C \cos\left(\frac{\pi y_0}{b}\right) \sin\left(\frac{\pi y_0}{b}\right) \Delta y_0$$

We obtain

$$\frac{\Delta R_{01}}{R_{01}} \simeq 2\pi \tan\left(\frac{\pi y_0}{b}\right) \frac{\Delta y_0}{b} \tag{6.5}$$

The relative variations in the input variations for some ports are compared. Assuming $\Delta y_0 = 0.02$ cm gives for

port 2a $\quad \frac{\Delta R_{01}}{R_{01}} \approx 0.014$

port 3a $\quad \frac{\Delta R_{01}}{R_{01}} \approx 0.039$

As $y_0 \simeq b/2$, the relative error $\Delta R_0/R_0$ will become very high, so we have to put strict demands in manufacturing tolerance as the antenna is to be excited in the vicinity of the patch centre.
The reflection coefficient of the input ports was measured as a function of the frequency, with the corresponding other input port matched with a load R = 50Ω.

The results are shown in Figs.D.1-6 in appendix D. From these figures we see, that the antenna input impedance is indeed strongly dependent of the feed point location. The reflection coefficient appeared to be very sensitive to reflections in the room, especially in the neighbourhood of the resonant frequency. Rotation of the antenna showed variations in the order of 3 dB in the minimum value of the reflection coefficient at ports 3 and 6.
Port 6 gives a good impedance match to 50Ω at resonance. The antennas to be discussed later on, are therefore excited with an inset feed point localized at this place.
From Fig.D.6 we see, that the antenna excited at port 6 has a small input impedance bandwidth. For both input ports 6, the impedance bandwidths are given as

$$\begin{aligned} &\text{(port 6)} \qquad \text{VSWR} < 1.5 \qquad B \approx 9.2 \text{ MHz} \\ &\qquad\qquad\qquad\quad \text{VSWR} < 2 \qquad B \approx 16 \text{ MHz} \end{aligned} \tag{6.6}$$

In Chapter 3 we derived the input impedance of a rectangular patch antenna as a function of the frequency. From (3.22) we know that the antenna, operating around its resonant frequency, behaves as a parallel RLC-circuit with a series inductance L'. We will now compare the measured results with this theory.
First we will consider the input resistance R_{01}, denoted as R_r, as a function of the feed point location. To facilitate our calculations the effect of the series reactance $X_{L'}$ is neglected, so we assume that the antenna input impedance behaves as the input impedance of a parallel RLC-circuit. From the formula of Carver (3.26), we obtain in our case

$$X_{L'} = 18\Omega \tag{6.7}$$

The approximation we made is thus only valid as the impedance of the resonant RLC-circuit is large compared to $X_{L'}$.
The input resistance R_r is given by (3.23.a). The missing parameter in this equation is the loss tangent $\delta_{eff} = 1/Q_{eff}$. We can obtain this parameter from the previous measurements with the following method.
The qualitative behaviour of the input reflection coefficient $|\rho_i|$ of a parallel RLC-circuit is depicted in Fig.6.2.

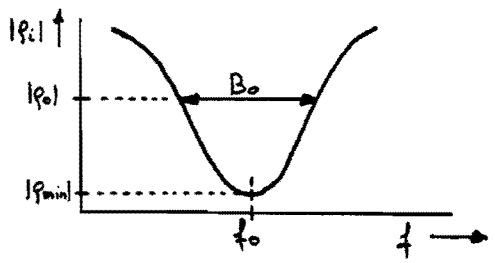

Fig.6.2 Qualitative behaviour of the input reflection coefficient of a parallel RLC-circuit.

The input impedance of the parallel RLC-circuit is described as

$$Z_{in} = \frac{R_r}{1 + j Q_{eff} \nu} \tag{6.7}$$

with $\nu = \left(\frac{\omega}{\omega_o} - \frac{\omega_o}{\omega}\right)$

We will try to find a relation for Q_{eff}, expressed in the parameters B_o, $|\rho_o|$ and $|\rho_{min}|$, as the circuit is connected to a transmissionline with characteristic impedance R_o. The value for $|\rho_{min}|$ can be found with

($\nu = 0$)

$$|\rho_{min}| = \left|\frac{R_r - R_o}{R_r + R_o}\right| \tag{6.8}$$

We obtain

($R_r > R_o$)
$$R_r = \frac{1 + |\rho_{min}|}{1 - |\rho_{min}|} R_o = VSWR_{min} \cdot R_o \tag{6.9.a}$$

($R_r < R_o$)
$$R_r = \frac{1 - |\rho_{min}|}{1 + |\rho_{min}|} R_o = \frac{1}{VSWR_{min}} \cdot R_o \tag{6.9.b}$$

The input reflection coefficient $|\rho_o|$ can be written as

$$|\rho_o|^2 = \left|\frac{Z_{in} - R_o}{Z_{in} + R_o}\right|^2 = \frac{(R_r - R_o)^2 + Q_{eff}^2 \nu^2 R_o^2}{(R_r + R_o)^2 + Q_{eff}^2 \nu^2 R_o^2} \tag{6.10}$$

Substitution of (6.9) in (6.10) gives

$$Q_{eff}^2 \nu^2 = 4 \frac{|\rho_o|^2 - |\rho_{min}|^2}{1 - |\rho_o|^2} \tag{6.11}$$

Solving this equation in the same way as is done for the bandwidth of the parallel RLC-circuit in Chapter 3 (eq.3.18), we obtain

$$B_o = \frac{2}{Q_{eff}} \sqrt{\frac{|\rho_o|^2 - |\rho_{min}|^2}{1 - |\rho_o|^2}} \tag{6.12}$$

With (6.12) it is possible to obtain Q_{eff} from the measurements in appendix D. We have extracted Q_{eff} from the reflection measurement of port 5a because the measured R_r in this case is approximately 110 Ω and is thus rather large compared to X_L.

The measured parameters are (Fig.D.5)

$|\rho_{min}| = -8.8$ dB $= 0.363$, $|\rho_0| = -5.7$ dB $= 0.519$, $B_0 = 32$ MHz, $f_r = 1.513$ MHz

which result in $Q_{eff} = 41$, which is a reasonable value.
Following the same operation for ports 3 and 4 we find for

port 3 $\quad Q_{eff} \approx 50$

port 4 $\quad Q_{eff} \approx 35$

We see an increasing effective quality factor as the feed point is more inset. This is in contrast with our expectations. For some Q_{eff} we have compared the calculated values with (3.25) and the measured values of the input resistance. This is shown in Fig.6.3. The measured values for R_r are found with (6.9).

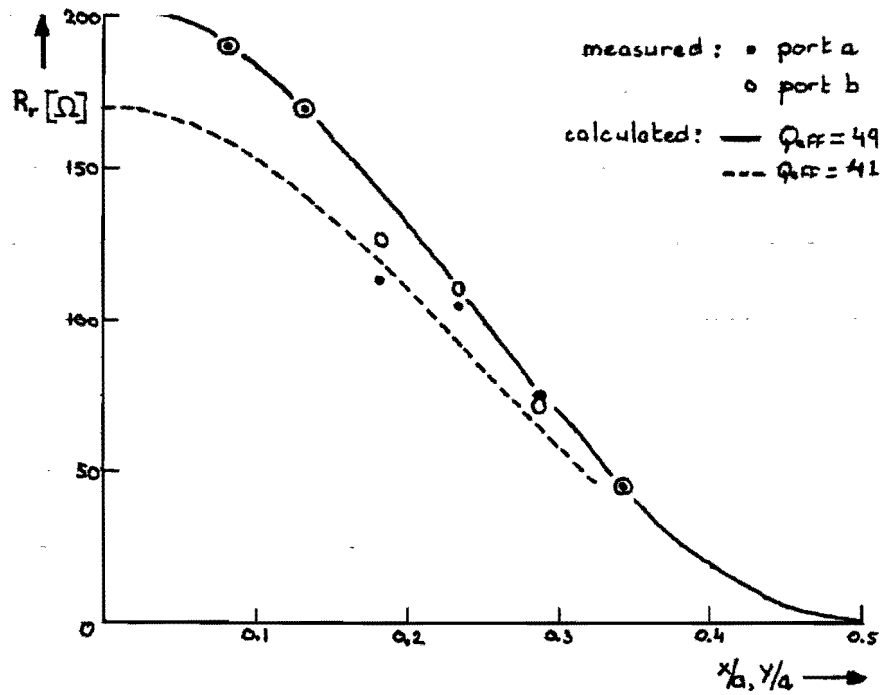

Fig.6.3 Measured and calculated input resistance versus feed location.

We see, that a quality factor $Q_{eff} = 49$ agrees well with the measured values, in contradiction with the expected value. The foregoing theory is thus only valid to obtain an estimate of the effective quality factor. From Fig.6.3 we see, that the measured input resistance obtained with the previous method appears to be larger as the expected value.

The difference can be explained by the effect of the series inductance. To obtain a more accurate theory, which gives a better description of the input impedance, we have to calculate the series inductance with (3.23.d) The disadvantage of this method is, that numerical methods are required. Our purpose was however, to match the antenna to a 50Ω transmissionline The previous method suffices to obtain a good match in an acceptable amount of time.
The transmission coefficients between the corresponding input ports a and b are measured too. They appeared to be smaller than -35 dB in the vicinity of the resonant frequency. The mutual coupling effects between the input ports are thus of less importance.

6.3 A dual feed circularly polarized square patch antenna.

A single dual feed patch antenna was made on Rexolite 1422 substrate. The lay-out was made with a computer controlled cutting-machine, resulting in a much better design accuracy.
The feeding network, consisting of a Wilkinson power splitter and a 90° phase shifter, was attached at the rear of the patch antenna using feed-throughs with diameter 0.9 mm. The feeding network was enclosed by a metal box, to eliminate spurious radiation of this network.
The design of this network was discussed in Chapter 4, resulting in a practical design shown in Fig.4.26. The obtained feeding network for the antenna is viewed in Fig.6.4.
The antenna is shown in Fig.6.5.
The measured input reflection coefficient as a function of the frequency can be found in appendix D (Fig.D.7). From this figure the resonant frequency can be found as 1.508 GHz, with a minimum reflection coefficient of -21.2 dB. This corresponds with an input VSWR of 1.19.
The bandwidth for which VSWR < 1.5, $|\rho_a|$ < -14 dB, is very large, namely from 1.26 GHz to 1.73 GHz. This does not mean however, that all the ingoing power will be radiated. Only the dip around 1.5 GHz appeared to be sensitive for a metal plate at different distances in front of the antenna. The reflection coefficient at other frequencies was not affected. We concluded, that no power was radiated at these frequencies, which means that the power has to be dissipated in the antenna configuration.
We see, that a very strong decrease in the reflection coefficient is apparent at the frequency 1.36 GHz. We first thought, that this was due to the metal box at the rear, acting like a cavity around its resonant frequency, and excited by the network radiation. Removing the metal box gave no change at all in the measured characteristic. The only possibility left is that the ingoing power must be dissipated into the resistor. However, a theoretical explanation was not found.

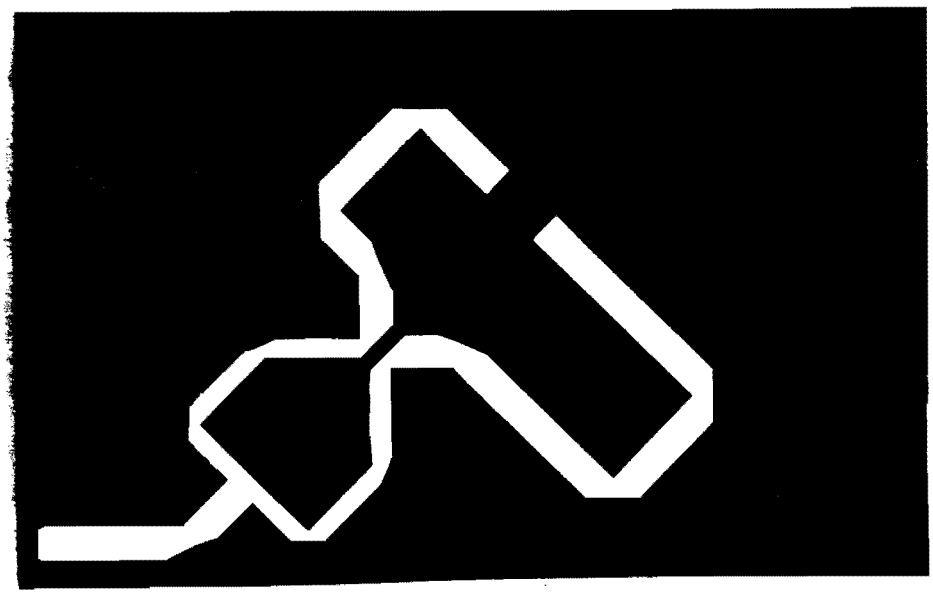

Fig.6.4.a Feeding network lay-out for the circularly polarized square patch antenna.

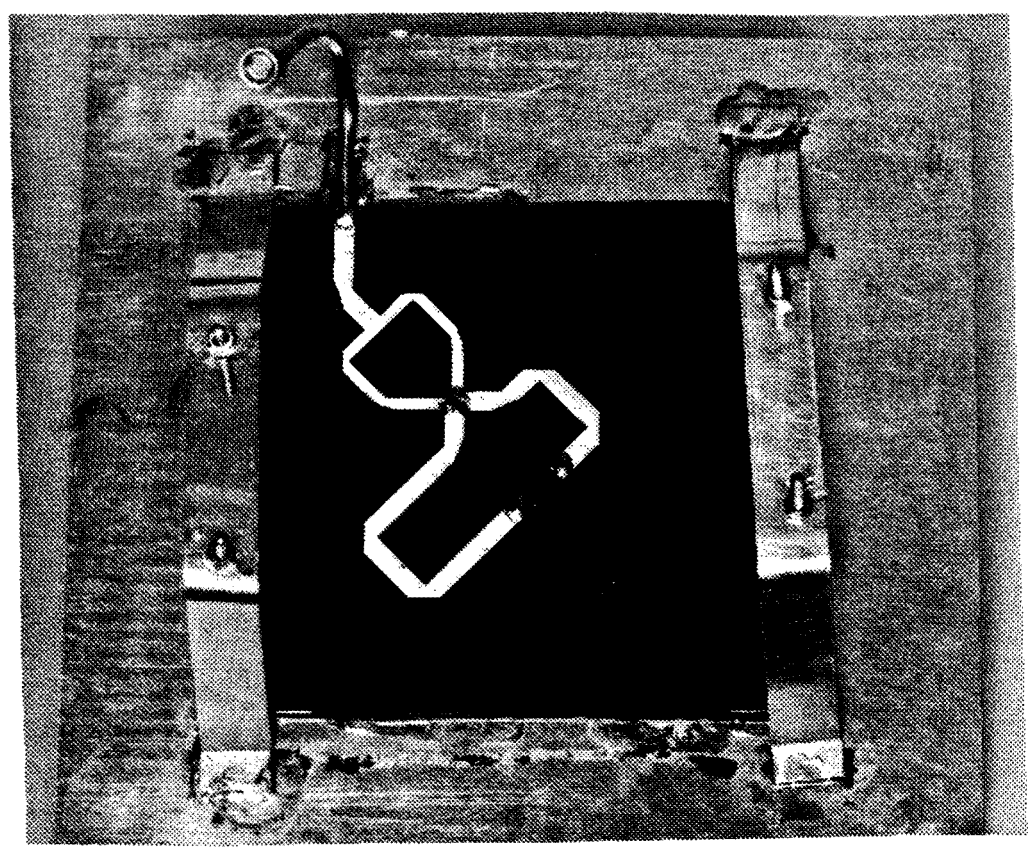

Fig.6.4.b Photo of the feeding network for the circularly polarized square patch antenna.

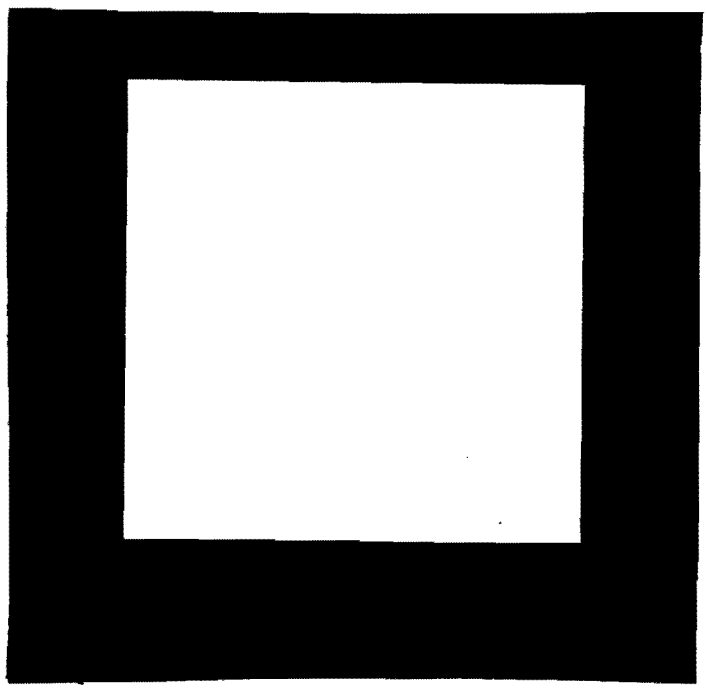

Fig.6.5.a Lay-out of circularly polarized square patch antenna.

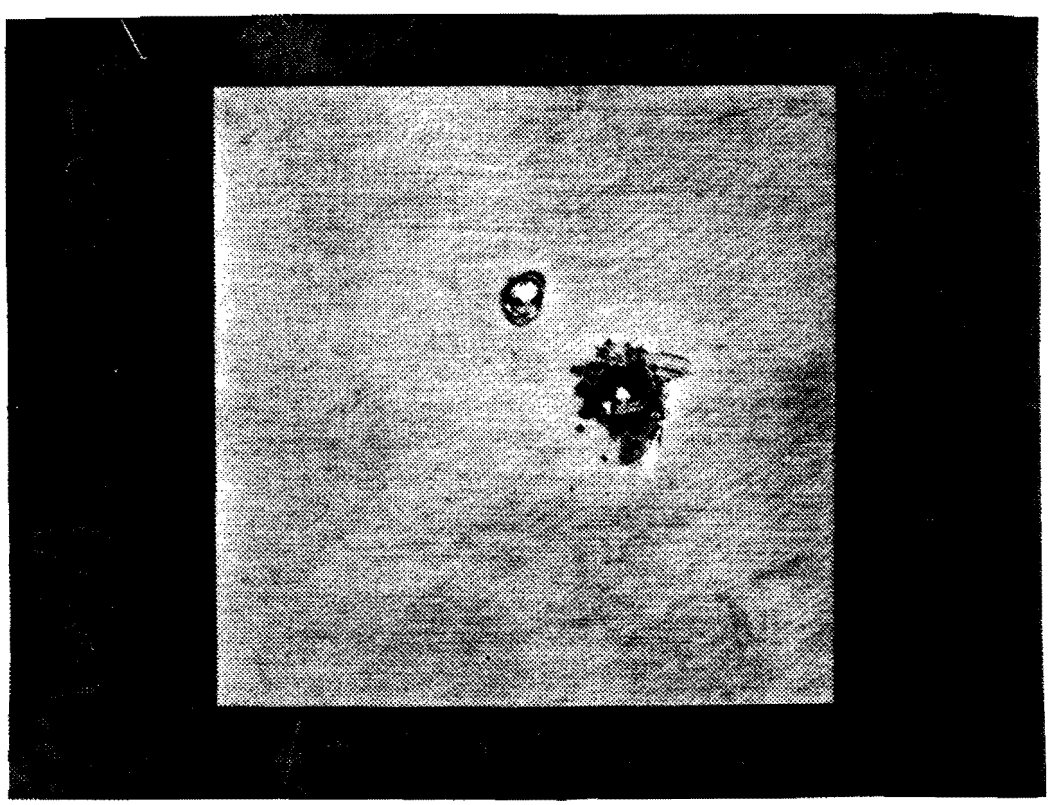

Fig.6.5.b Photo of circularly polarized square patch antenna.

From the previous section we know, that the feed points are localized at the input ports 6. In Fig.D.7 we see, that the impedance bandwidth where $|\rho_a| < -18$ dB is 6.5 MHz. The corresponding input impedance bandwidth for this antenna with feeding network is approximately 21 MHz, thus a considerable improvement is obtained.
Measurement of the radiation pattern was done at the antenna test range located at the Technical University. The compact range was not used in this case. A gating technique was used to distinguish the direct radiation from the indirect radiation caused by reflections.
This gating technique, which requires a computer system is described as follows.
The amplitude and phase of the received signal are measured over a wide frequency band. An inverse Fourier-transformation of these data delivers the time domain response. The direct received radiation component can be extracted by placing a suitable time gate. Transformation of this time gate to the frequency domain provides a calibration set, needed to adjust the data obtained during the measurement of the antenna radiation pattern.

We know from Chapter 2, that the far field relations may be used as the distance r between source and test antenna satisfies the condition

$$r > \frac{2D^2}{\lambda} \tag{6.13}$$

With the smallest used wavelength $\lambda = 0.12$ m and $D \approx 0.3$ m for the four element array, we obtain

$$r > 1.5 \text{ m} \tag{6.14}$$

This distance satisfies the far field condition for all antenna measurements.
The source antenna we used was a logarithmic-periodic antenna with broadband facilities.
The polarization measurements were done with the method shown in Fig.2.8 and the results that are of most interest can be found in appendix E.
The case f = 1.5 GHz is compared with the theoretical results. The copolarization, crosspolarization and axial ratio as a function of the polar angle θ (azimuth), are shown in respectively Figs.E.1-2 and E.7-8.
The measured copolarization agrees very well with the calculated values for angles $\theta < 0°$. The difference between calculated values and measured values for $\theta > 0°$ is partly caused by interference with a reflected radiation component. A three-dimensional plot, with along the x- and y-axis respectively frequency and azimuth shows this quite clearly. This means that the gate setting was not optimum. We were not able to repeat the measurements, because a frequency synthesizer was not available anymore. This does not mean however, that the measurements are useless. Especially the case $\theta < 0°$ is useful.

Other factors leading to degradation of the polarization quality are the mutual coupling effects between the radiating elements, and the existence of higher order modes in the patches. The latter are expected to be less significant, as the substrate thickness is rather small.
The crosspolarization is completely different compared with the calculated values and so is the axial ratio pattern. A possible cause is, that the crosspolarization is very sensitive to deviations in its parameters. We will show this with a discussion of eqs.2.9.

$$E_L = \frac{1}{\sqrt{2}}(E_\theta - jE_\varphi)$$
$$E_R = \frac{1}{\sqrt{2}}(E_\theta + jE_\varphi) \qquad (6.14)$$

With $E_\theta = |E_\theta| e^{j\phi_\theta}$
$E_\varphi = |E_\varphi| e^{j\phi_\varphi}$

we obtain

$$|E_L| = \frac{1}{\sqrt{2}}\left\{|E_\theta|^2 + |E_\varphi|^2 + 2|E_\theta||E_\varphi| \sin(\phi_\varphi - \phi_\theta)\right\}^{1/2}$$
$$|E_R| = \frac{1}{\sqrt{2}}\left\{|E_\theta|^2 + |E_\varphi|^2 - 2|E_\theta||E_\varphi| \sin(\phi_\varphi - \phi_\theta)\right\}^{1/2} \qquad (6.15)$$

The crosspolarization originates from the subtraction of two nearly equal values, resulting in large relative errors if its parameters slightly alter.
The co- and crosspolarization for other frequencies are shown in Figs.E.3-6. We see, that the crosspolarization strongly variates as a function of the frequency, in contrast with the copolarization.
The axial ratio measurement for the frequency f = 1.6 GHz is not completely reliable. This can be concluded if we compare these measurements for the polar angle $\theta = 0^\circ$ for the principal plane and diagonal plane (Figs.E.7-8). In theory these values have to be the same but a rather large difference is measured.

Another limiting factor in antenna performance is the antenna gain. It was not possible to measure this feature with the available facilities.
We expect however, that although the impedance bandwidth and axial ratio bandwidth are relatively large, this will not be the case for the gain bandwidth.
In the previous section we have measured, that the antenna input reflection coefficient is considerably worsened away from its resonant frequency. An inherent consequence is the gain loss.

6.4 A sequentially rotated array consisting of four dual feed circularly polarized square patch antennas.

A configuration of four square patch antennas in a sequentially rotated fashion was made. The antenna configuration and its feeding network are shown in Fig.6.6 (scale 2:1), and Fig.6.7. This feeding network is quite complex because the goal was to obtain an optimum axial ratio bandwidth. That is why each power splitter is performed as a Wilkinson splitter, to prevent that reflected power going into one output port, is not retransmitted in the other.
The phase shifters were designed to minimize the relative phase differences between the antenna phasings. These phasings can be found in Fig.5.18.
The input reflection coefficient as a function of the frequency was measured and the result is shown in Fig.D.8. Comparison with the response of the single element in Fig.D.7, we see that a degradation of the input impedance is obtained. No explicit resonant dip around 1.5 GHz can be found. Interesting is however, that the dip around 1.36 GHz in Fig.D.7 has disappeared.
An explanation for the relative poor quality of the input impedance bandwidth can be found in the design procedure. First of all too little design steps were made, so the output phasings were not optimized. Also the effects of cascaded Wilkinson splitters were not evaluated.
Another possibility is, that the feeding network during the manufacture was slightly damaged. Making a new feeding network was not possible due to lack of Rexolite 1422 material.

The polarization characteristics of this antenna were measured and the results can be found in appendix E.
In Figs.E.9-14 the co- and crosspolarization as a function of the polar angle θ are plotted for different frequencies. The calculated values for the frequency f= 1.5 GHz are added in Fig.E.9.
We see, that the dip, caused by the array factor does not correspond with the theoretical value. The array factor is only dependent of the wavelength and of the element spacing. This difference is probably attributed to the fact that the calculation is performed on an infinite ground plane while the measurement is carried out on a finite ground plane.
The axial ratio is very good over the polar angle $|\theta| < 40^\circ$ at the frequency 1.5 GHz (Figs.E.15-16).
The contourplots in Figs.E.17-20 show that a considerable improvement in axial ratio bandwidth is obtained as a sequentially rotated configuration is used. Moreover, the axial ratio as a function of the frequency is plotted in Fig.E.21 for both configurations in broadside direction. The improvement is quite clearly. A good axial ratio bandwidth over the frequency band 1.5 GHz to 1.6 GHz appears to be realizable, especially when a careful design procedure is used.

The gain loss however, is expected to limit the overall system bandwidth in this case, because a thin substrate is used. To overcome this problem a thicker substrate is required.

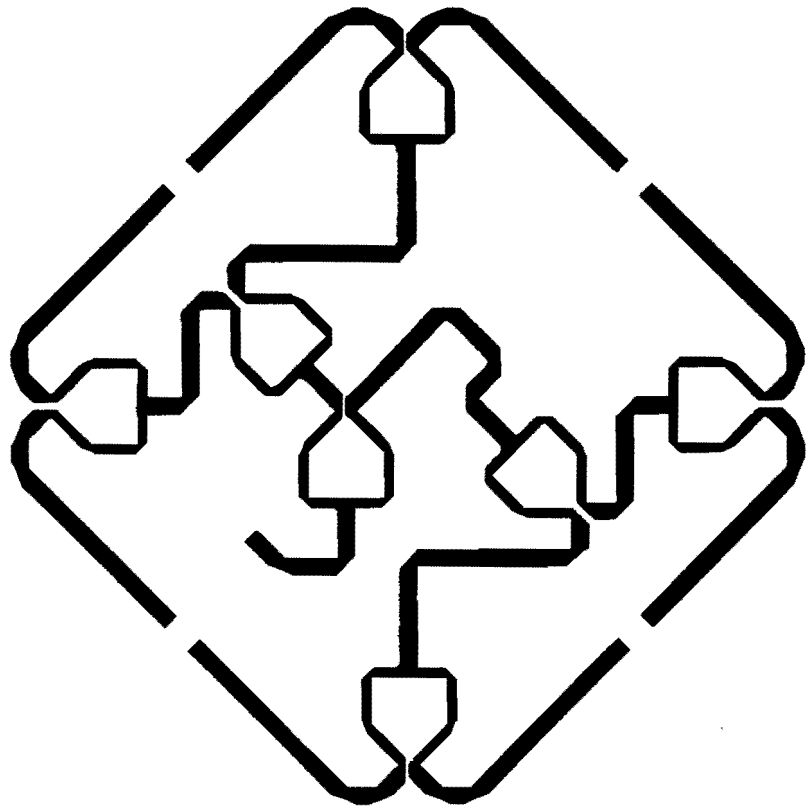

Fig.6.6.a Lay-out of the feeding network for the four element circularly polarized microstrip antenna array. (scale 2:1)

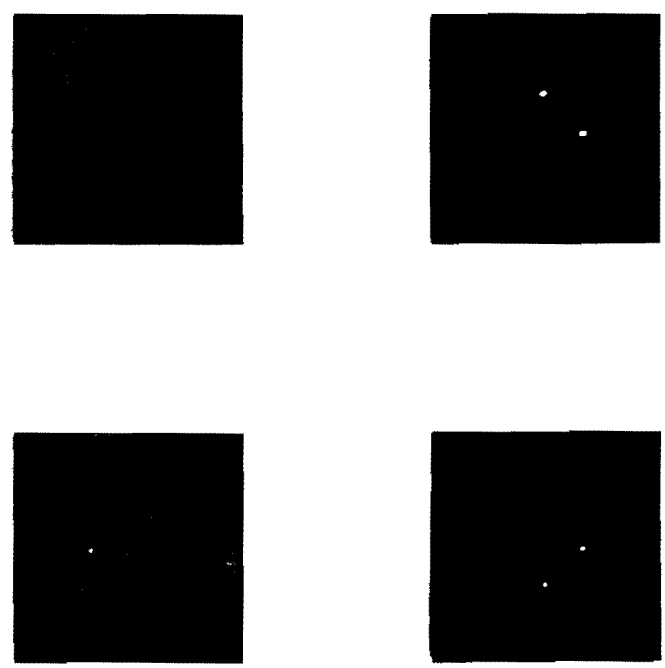

Fig.6.6.b Layout of the circularly polarized microstrip antenna array. (scale 2:1)

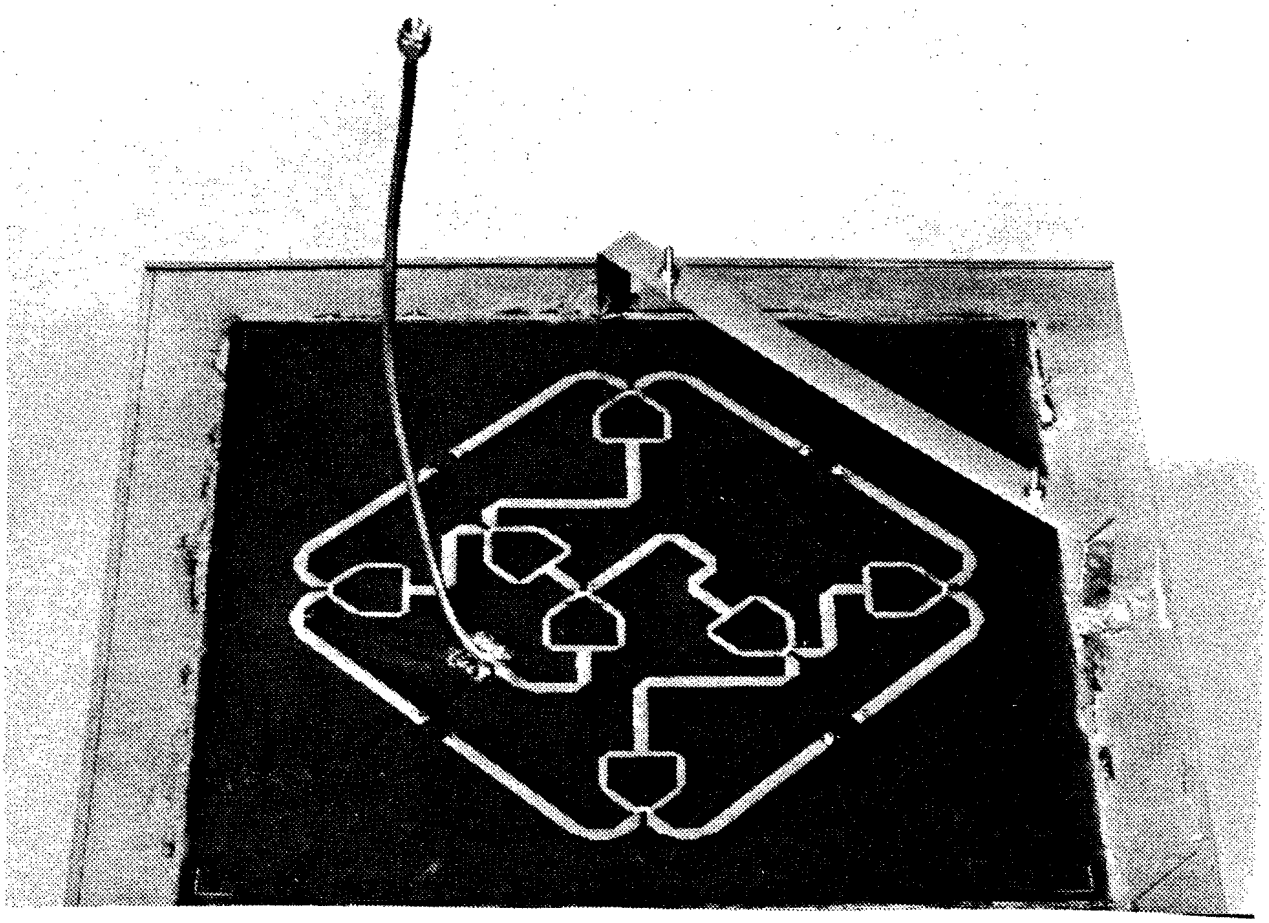

Fig.6.7.a Photo of the feeding network for the circularly polarized four element microstrip antenna array.

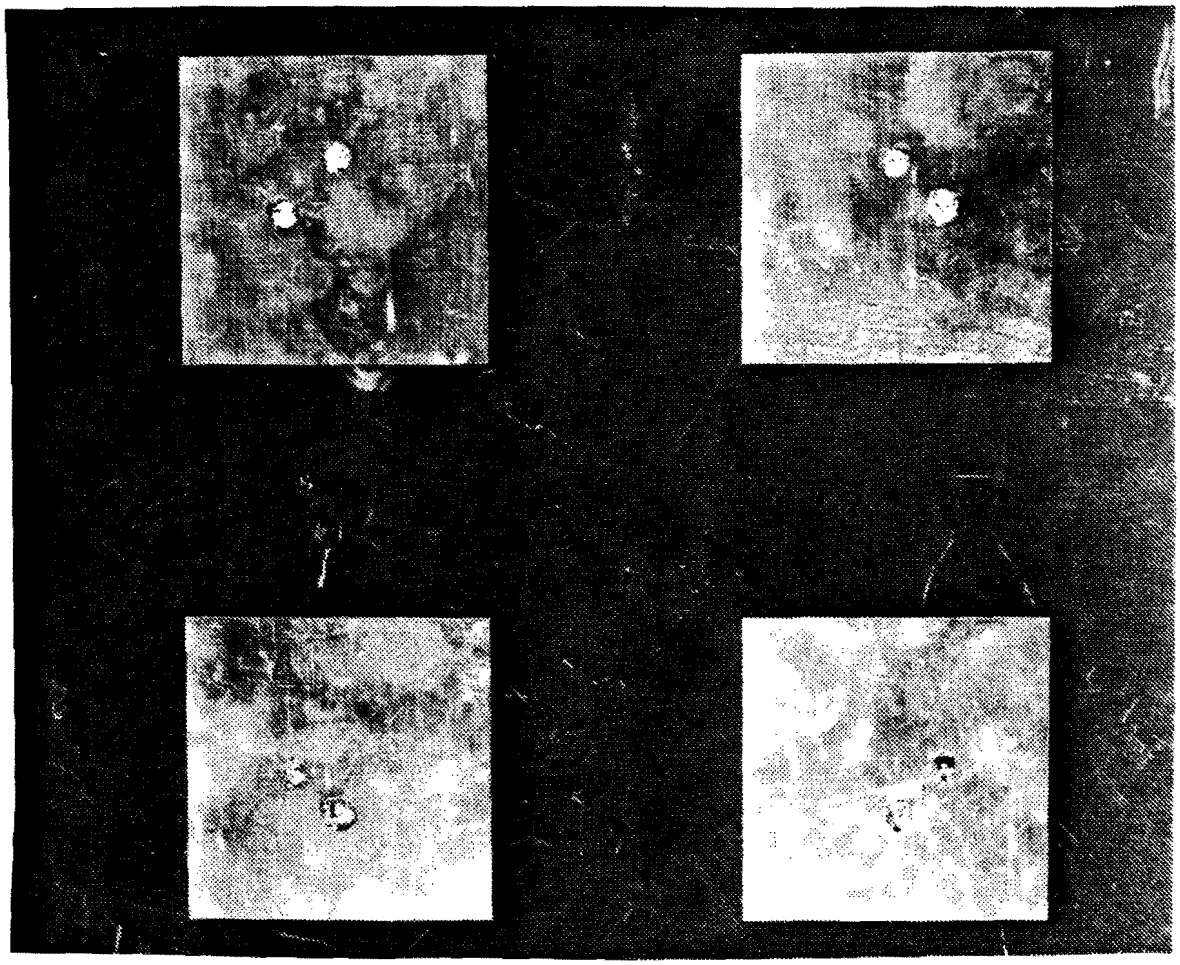

Fig.6.7.b Photo of the circularly polarized four element antenna array.

7. Conclusions.

A large improvement in axial ratio bandwidth is obtained by placing four microstrip elements in a sequentially rotated fashion. In broadside direction an axial ratio better than 1 dB was measured for the frequency band 1.42 GHz to 1.54 GHz, which is a relative bandwidth of 8 %.
Because the antenna was developed for the frequency 1.5 GHz, the requirement 1.5 GHz to 1.6 GHz could not be met. It is likely however, that a good axial ratio is possible in this frequency band, if the antenna is dimensioned around a frequency 1.55 GHz.
The impedance bandwidth of the four element array is worsened compared to the impedance bandwidth of a single element, which is in contrast with our expectations. This is probably due to an imperfect design of the feeding network. In future designs it is therefore recommended to optimize this network with respect to its output phasings and its power splitting property.
Another possible cause for the poor impedance match is, that a small damage in the feeding network has more effect as expected.
The feeding network is designed with Wilkinson splitters as power dividers. The only reason for this choice is the ease in its design. Each network power divider is performed as a Wilkinson splitter, resulting in a quite complex network. In how far a configuration like this is better as a network with reactive T-splitters or other types of isolated configurations could not be analyzed, due to practical limitations. Numerical methods are required to analyze microstrip networks in general. If the research to microstrip antennas and feeding networks is to be continued, we strongly recommend that such computerprograms are available in the future.

Another important factor that needs consideration is the antenna gain bandwidth. Although it was not possible to measure this property, we may expect that this will be the overall limiting factor of the four element array. This is based on the reflection measurement of the patch input port. The impedance bandwidth of this port is very small, even compared to the axial ratio bandwidth. An inherent consequence of the increasing input reflection coefficient is the occuring gain loss.
The gain bandwidth can be considerably enlarged if a larger substrate thickness is used. Introduction of higher order modes, increasing surface waves and mutual coupling effects will severely degrade the axial ratio performance in this case, if no special provisions are made.
Balanced feeding of the patch is a possibility to eliminate this degradation, but the feed complexity is greatly increased. The other solution, the sequentially rotated array is the best compromise in this situation.
To obtain the overall system bandwidth, we thus have to measure the gain. A facility to measure this property is therefore recommended.

References.

[1] **Balanis C.A.**, 'Antenna theory : Analysis and design'.
New York: Harper & Row, 1982, The Harper & Row series in Electrical Engineering.

[2] **Bauer R.L., J.J. Schuss**, 'Axial ratio of balanced and unbalanced fed circularly polarized patch radiator arrays'.
AP-S International Symposium 1986, 1986 International Symposium Digest Antennas and Propagation (Cat. no. 86 CH2325-9), Philadelphia, PA, USA, 8-13 June 1987, Vol.1, p.286-289.
IEEE, New York, 1987.

[3] **Carver K.R., J.W. Mink**, 'Microstrip antenna technology'.
IEEE Trans. on Antennas and Propagation, Vol.AP-29, 1981, no.1, p.2-24.

[4] **Cohn S.B.**, 'A class of broadband three port TEM-mode hybrids'.
IEEE Trans. on Microwave Theory and Design, Vol.MTT-16, 1968, p.110-116.

[5] **Griffin J.M., M.J. Alexander, G.E.D. Swann**, 'Development of low gain radiating elements; Final Report'.
Marconi Research Centre, General Electric Co., Ltd, May 1987.
ESTEC Contract no. 6180/86/NL/JG(SC).

[6] **Gupta K.C., Ramesh Garg, I.J. Bahl**, 'Microstrip lines and slotlines'.
Dedham, MA: Artech House, 1979.

[7] **Hammer P., D. Van Bouchaute, D. Verschraeven, A. Van de Capelle**, 'A model for calculating the radiation field of microstrip antennas'.
IEEE Trans. on Antennas and Propagation, Vol.AP-27, 1979, no.2, p.267-270.

[8] **Harrington R.F.**, 'Time-harmonic electromagnetic fields'.
New York: McGraw-Hill, 1961,
McGraw-Hill Texts in Electrical Engineering.

[9] **Huang J.**, 'A technique for an array to generate circularly polarization with linearly polarized elements'.
IEEE Trans. on Antennas and Propagation, Vol.AP-34, 1986, no.9, p.1113-1124.

[10] **James J.R., P.S. Hall, J.W. Mink,** 'Microstrip antenna: Theory and design'.
Stevenage, UK: Peter Peregrinus, 1981,
IEE Electromagnetic series, Vol.12.

[11] **Jeuken M.E.J.,** 'Elektromagnetische golven en antennes 1'.
Vakgroep Theoretische Elektrotechniek, Faculteit der Elektrotechniek, Technische Universiteit Eindhoven, 1983, Collegediktaat.

[12] **Lo Y.T., D. Solomon, W.F. Richards,** 'Theory and experiment on microstrip antennas'.
IEEE Trans. on Antennas and Propagation, Vol.AP-27, 1979, no.2, p.137-145.

[13] **Ramo S., J.R. Whinnery, T. Van Duzer,** 'Fields and waves in communication electronics', 2nd edition.
New York: John Wiley & Sons, 1984.

[14] **Richards W.F., Y.T. Lo, D.D. Harrison,** 'An improved theory for microstrip antennas and applications'.
IEEE Trans. on Antennas and Propagation, Vol.AP-29, 1981, no.1, p.38-46.

[15] **Richards W.F., J.R. Zinecker, R.D. Clark, S.A. Long,** 'Experimental and theoretical investigation of the inductance associated with a microstrip antenna feed'.
Electromagnetics, Vol.3, 1983, p.327-346.

[16] **Teshirogi T., M. Tanaka, W. Chujo,** 'Wideband circularly polarized array antenna with sequential rotation and phase shift of elements'.
Proc. of the 1985 Int. Symp. on Antennas and propagation, Kyoto, 20-22 August 1985, Vol.1, p.117-120.
IECEC, Tokyo, Japan.

[17] **Teshirogi T., M. Tanaka, S. Ohmori,** 'Airborne phased array antenna for mobile satellite communications'.
AP-S International Symposium 1986, 1986 International Symposium Digest Antennas and Propagation (Cat. no.86 CH2325-9),
Philadelphia, PA, USA, 8-13 June 1986, Vol.2, p.719-722.
IEEE, New York, USA, 1986.

[18] **Van Hezewijk J.G.**, 'A multiple-beam antenna system with microstrip feeds'.
Professional Group Electromagnetism and Circuit Theory, Department of electrical engineering, Eindhoven, University of Technology, Netherlands, 1988, Report ET-5-88.

[19] **Versnel W.**, 'Microgolftechniek'.
Vakgroep Theoretische Elektrotechniek, Faculteit der Elektrotechniek, Technische Universiteit Eindhoven, 1985, Collegediktaat no.5.528.1.

[20] **Wilkinson E.J.**, 'An N-way hybrid power divider'.
IRE Trans. on Microwave Theory and Design, Vol.MTT-8, 1960, p.116-118.

Acknowledgements.

This work has been performed in fulfilment of the requirements for the degree of Master of Science (Ir.) at the Eindhoven University of Technology. At this place I want to acknowledge Ing. M. Knoben for his support in antenna design and measurements, and I. Ongers for his help in the development of the software.

M.L.A. Vrinten Eindhoven, 12 April 1988

Program **DIAPOL**

This program calculates the co- ,crosspolarization and axial ratio as a function of the polar angle θ for an N-element two dimensional microstrip antenna array. The program also provides a facility to calculate the directivity of the array.
The radiation pattern of the rectangular patch antenna is calculated with eqs.3.36.
The computerprogram omits the r-dependency, because this is of no use in calculating the polarization characteristics.
The program uses the antenna, placed in the origin as a reference (Fig.A.1).

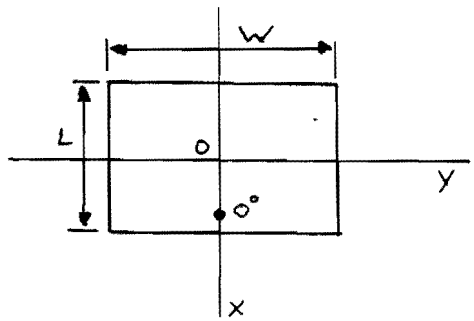

Fig.A.1 Reference antenna placed in the origin.

A two dimensional array is obtained by arbitrarily placing N antennas in the xy-plane, with specific spatial rotation and phasing. The total field components of the array are computed with (2.19). The computerprogram needs the parameters defined in Fig.A.2.

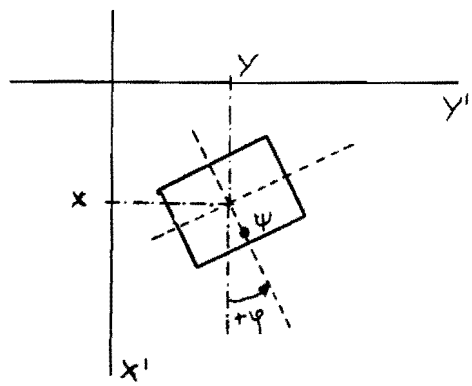

Fig.A.2 Antenna, arbitrarily placed in xy-plane.

Here is: ψ (PSI), the antenna phasing relative to the reference antenna.

φ (PHI), the spatial rotation of the element relative to the reference antenna.

The co-, crosspolarization and axial ratio are now calculated with (2.9) and (2.10).
Until now, the concerned antennas are linearly polarized. A circularly polarized square patch antenna can be easily obtained by orthogonally localizing two antennas at the same place, with 90° phase difference between the input ports. (Fig.A.3)

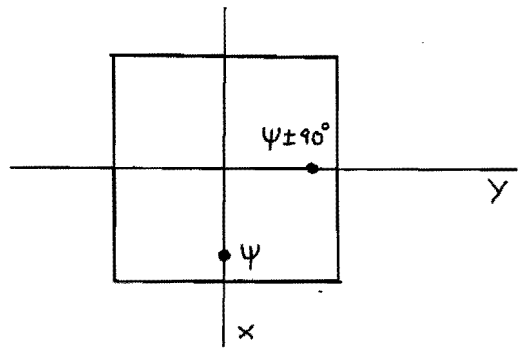

Fig.A.3 Circularly polarized square patch antenna. (W/L = 1)

Another facility, provided by this computerprogram is the directivity. The directivity is calculated as follows. From [1] the definition for the directivity D can be found as

$$D = 4\pi \frac{\frac{1}{2Z_o}|\bar{E}(\theta,\varphi)|^2_{max}}{P_{rad}} \qquad (A.1)$$

with $\frac{1}{2Z_o}|E(\theta,\varphi)|^2_{max}$ the maximum radiation intensity and P_{rad} the total radiated power, defined as

$$P_{rad} = \frac{1}{2Z_o}\int_0^{\pi}\int_0^{2\pi}|\bar{E}(\theta,\varphi)|^2 \sin\theta \, d\varphi \, d\theta \qquad (A.2)$$

In most situations, the integration cannot be performed analytically, so we have to resort to numerical methods.
In theory, the considered microstrip antennas do not radiate at polar angles $\theta > \pi/2$. This is why we define a maximum angle θ_{max}, and (A.2) becomes

$$P_{rad} = \frac{1}{2Z_o}\int_0^{\theta_{max}}\int_0^{2\pi}|\bar{E}(\theta,\varphi)|^2 \sin\theta \, d\varphi \, d\theta \qquad (A.3)$$

A series approximation for the integration can be written as follows

$$\int_0^{\theta_{max}} d\theta \int_0^{2\pi} |\bar{E}(\theta,\varphi)|^2 \sin\theta \, d\varphi \approx \frac{\theta_{max}}{N} \frac{2\pi}{M} \sum_{j=1}^{N} \sum_{i=1}^{M} |\bar{E}(\theta_j, \varphi_i)|^2 \sin\theta_j \qquad (A.4)$$

with $$\theta_j = \frac{\theta_{max}}{N} \cdot j$$

$$\varphi_i = \frac{2\pi}{M} \cdot i$$

In our case, the step size is chosen to be one degree, which gives quite accurate results.

The program does not only send its information to the screen. The output data is also stored in datafiles, needed to make a plot with the plotprogram IA2DPLOT. The data files are

PCOPOL.DAT for the copolarization.

PCRPOL.DAT for the crosspolarization.

PAXRAT.DAT for the axial ratio.

The program IA2DPLOT needs frame files to obtain a graphical representation of the polarization patterns and axial ratio pattern. These frame files are available under the names

PPOL.FRM for a plot of the polarization patterns.

PAX.FRM for a plot of the axial ratio pattern.

```
****************** Program DIAPOL.FOR ***************************
*****************************************************************

 This program calculates the copolarization, crosspolarization,
 axial ratio and directivity for an N-element two dimensional
 microstrip antenna array.

*****************************************************************

      INTEGER NEWFIL,N,K,J,CHANGE,WHAT,NUM,BACK
      INTEGER L,TETA,TETEND,TETSTP,TYPCIR,TET,NPT
      INTEGER TU,I
      REAL EPSR,X(50),Y(50),WL(50),LAMBDA,PSI(50),PHI(50),M
      REAL PHI0,RPHI0,XA(50),EMAX,IMARG,RTET
      REAL RPHI(50),RPSI(50),RPHIA(50),PRAD,THETA
      REAL FI,F,UMAX,UA,DIR,DIRDB,XB,RPHIJ,RTETI
      REAL ELABS,ERABS,ELDB,ERDB,LENGT,W
      COMPLEX ELFAC,FACMIN,FACPLU,EL0,ER0,EL,ER
      COMPLEX EPHIK,ETETK
      CHARACTER*10 FNAME
      DATA PI/3.141592654/
      WRITE(*,10)
 10   FORMAT(' FILENAME ?:')
      READ(*,20) FNAME
 20   FORMAT(A10)
      WRITE(*,30)
 30   FORMAT(' NEW FILE ? ENTER 1 :')
      READ(*,*) NEWFIL
      IF (NEWFIL.EQ.1) THEN
          WRITE(*,50)
 50       FORMAT(' NUMBER OF ANTENNAS ?:')
          READ(*,*) N
          WRITE(*,70)
 70       FORMAT(' DIELECTRIC CONSTANT OF THE SUBSTRATE ?:')
          READ(*,*) EPSR
          WRITE(*,90)
 90       FORMAT(' WAVELENGTH VACUUM IN CM ?:')
          READ(*,*) LAMBDA
          WRITE(*,110)
110       FORMAT(' ENTER :')
          WRITE(*,111)
111       FORMAT(' (X,Y) IN CM,(PSI,PHI) IN DEGREES, W/L ?:')
          DO 1,K=1,N
          WRITE(*,115) K
115       FORMAT(' ANTENNA :',I2,'  X,Y,PSI,PHI,W/L ?:')
          READ(*,*) X(K),Y(K),PSI(K),PHI(K),WL(K)
  1       CONTINUE
```

```
          OPEN(UNIT=1,FILE=FNAME,STATUS='NEW')
          WRITE(1,*) N,EPSR,LAMBDA,(X(J),J=1,N),(Y(J),J=1,N),
     *                (PSI(J),J=1,N),(PHI(J),J=1,N),(WL(J),J=1,N)
          CLOSE(UNIT=1)
        ELSE
          OPEN(UNIT=1,FILE=FNAME,STATUS='OLD')
          READ(1,*) N,EPSR,LAMBDA,(X(J),J=1,N),(Y(J),J=1,N),
     *               (PSI(J),J=1,N),(PHI(J),J=1,N),(WL(J),J=1,N)
          CLOSE(UNIT=1)
        END IF
        WRITE(*,400)
400     FORMAT (' ANTENNA PARAMETERS')
        WRITE(*,405)
        WRITE(*,410)
405     FORMAT(' ------------------')
410     FORMAT(' NO.',9X,'X(CM)',5X,'Y(CM)',5X,'PSI',9X,'PHI',
     *          5X,'W(CM)',7X,'L(CM)')
        WRITE(*,421)
        LENGT=LAMBDA/(2*SQRT(EPSR))
        DO 7,K=1,N
        W=WL(K)*LENGT
        WRITE(*,420) K,X(K),Y(K),PSI(K),PHI(K),W,LENGT
420     FORMAT(I3,7X,F7.2,3X,F7.2,4X,F5.0,7X,F5.0,4X,F7.2,5X,F7.2)
  7     CONTINUE
        WRITE(*,421)
421     FORMAT(' ------------------------------------------------------
     *-------------')
        WRITE(*,422) EPSR,LAMBDA
422     FORMAT(3X,' EPSR=',F6.2,' ****LAMBDA=',F6.2,1X,'CM. *****')
        WRITE(*,421)
        WRITE(*,800)
800     FORMAT(' CHANGE PARAMETERS ? ENTER 1 :')
        READ(*,*) CHANGE
        IF (CHANGE.EQ.1) THEN
         WRITE(*,805)
         WRITE(*,810)
         WRITE(*,815)
805      FORMAT(' ANTENNA PARAMETERS ?, ENTER 0')
810      FORMAT(' EPSR ?,               ENTER 1')
815      FORMAT(' LAMBDA ?,             ENTER 2****CHOICE : ')
         READ(*,*) WHAT
         IF (WHAT.EQ.0) THEN
  12      WRITE(*,820)
820       FORMAT(' ANTENNA NO. ?:')
          READ (*,*) NUM
```

```
        WRITE(*,825)
825     FORMAT(' (X,Y) IN CM ,(PSI,PHI) IN DEGREES ,W/L ?:')
        READ(*,*) X(NUM),Y(NUM),PSI(NUM),PHI(NUM),WL(NUM)
        WRITE(*,830)
830     FORMAT (' NEXT ? ENTER 1 :')
        READ(*,*) BACK
        IF (BACK.EQ.1) THEN
          GOTO 12
        ENDIF
       ENDIF
       IF (WHAT.EQ.1) THEN
         WRITE(*,850)
850      FORMAT(' EPSR ?:')
         READ(*,*) EPSR
       ENDIF
       IF (WHAT.EQ.2) THEN
         WRITE(*,860)
860      FORMAT(' WAVELENGTH IN CM (VACUUM) ?: ')
         READ(*,*) LAMBDA
       ENDIF
       WRITE(*,870)
       WRITE(*,875)
870    FORMAT(' TO NEW FILE     : ENTER 0')
875    FORMAT(' TO PRESENT FILE : ENTER 1   ***CHOICE ?:')
       READ (*,*) NEWFIL
       IF (NEWFIL.EQ.0) THEN
        WRITE(*,880)
880     FORMAT(' FILENAME ?: ')
        READ(*,20) FNAME
        OPEN(UNIT=1,FILE=FNAME,STATUS='NEW')
        WRITE(1,*) N,EPSR,LAMBDA,(X(J),J=1,N),(Y(J),J=1,N)
    *          ,(PSI(J),J=1,N),(PHI(J),J=1,N),(WL(J),J=1,N)
        CLOSE (UNIT=1)
       ENDIF
       IF (NEWFIL.EQ.1) THEN
         OPEN(UNIT=1,FILE=FNAME,STATUS='UNKNOWN')
         WRITE(1,*) N,EPSR,LAMBDA,(X(J),J=1,N),(Y(J),J=1,N)
    *           ,(PSI(J),J=1,N),(PHI(J),J=1,N),(WL(J),J=1,N)
         CLOSE(UNIT=1)
       ENDIF
       GOTO 199
      ENDIF
```

```
199     WRITE(*,200)
200     FORMAT(' PLANE PHI IN DEGREES ?:')
        READ(*,*) PHI0
        RPHI0=(2*PI*PHI0)/360
        DO 2,L=1,N
        XA(L)=(X(L)*COS(RPHI0))+(Y(L)*SIN(RPHI0))
  2     CONTINUE
        WRITE(*,300)
300     FORMAT(' THETA: START, END, STEP IN DEGREES ?:')
        READ(*,*) TETA,TETEND,TETSTP
        EL0=(0.,0.)
        ER0=(0.,0.)
        DO 3,K=1,N
         RPSI(K)=(PI*PSI(K))/180
         ELFAC=CMPLX(0.,RPSI(K))
         RPHI(K)=(PI*PHI(K))/180
         RPHIA(K)=RPHI0-RPHI(K)
         FACMIN=CMPLX(ETETA(0.,RPHIA(K),EPSR,WL(K)),
     *                -EPHI(0.,RPHIA(K),EPSR,WL(K)))
         FACPLU=CONJG(FACMIN)
         EL0=EL0+(FACMIN*CEXP(ELFAC))
         ER0=ER0+(FACPLU*CEXP(ELFAC))
  3     CONTINUE
        IF (CABS(EL0).GT.CABS(ER0)) THEN
                EMAX=CABS(EL0)
                TYPCIR=1
            ELSE
                 EMAX=CABS(ER0)
                 TYPCIR=0
        ENDIF
            WRITE(*,552)
552         FORMAT(' THETA',5X,'COPOL (DB)',5X,'CROSSPOL (DB)',5X,
     *              'AXIAL RATIO (DB)')
            WRITE(*,553)
553         FORMAT(' ------------------------------------------------')
         OPEN(UNIT=2,FILE='PCOPOL.DAT',STATUS='UNKNOWN')
         OPEN(UNIT=3,FILE='PCRPOL.DAT',STATUS='UNKNOWN')
         OPEN(UNIT=4,FILE='PAXRAT.DAT',STATUS='UNKNOWN')
         NPT=(TETEND-TETA)/TETSTP
         WRITE(2,*) NPT,1,2,1,2
         WRITE(3,*) NPT,1,1,2,2
         WRITE(4,*) NPT,1,2,1,2
```

```
      TET=TETA
      DO 4,L=TETA,TETEND,TETSTP
       EL=(0.,0.)
       ER=(0.,0.)
       RTET=(2*PI*FLOAT(TET))/360
        DO 5,K=1,N
         IMARG=RPSI(K)+((2*PI*XA(K)*SIN(RTET))/LAMBDA)
         ELFAC=CMPLX(0.,IMARG)
     FACMIN=CMPLX(ETETA(RTET,RPHIA(K),EPSR,WL(K)),
    *              -EPHI(RTET,RPHIA(K),EPSR,WL(K)))
      FACPLU=CONJG(FACMIN)
         EL=EL+(FACMIN*CEXP(ELFAC))
         ER=ER+(FACPLU*CEXP(ELFAC))
5      CONTINUE
       ELABS=CABS(EL)/EMAX
       ERABS=CABS(ER)/EMAX
       ELDB=20*ALOG10(ELABS)
       ERDB=20*ALOG10(ERABS)
           AXRAT=ABS((ELABS-ERABS)/(ELABS+ERABS))
           AXDB=-20*ALOG10(AXRAT)
          IF (TYPCIR.EQ.1) THEN
              WRITE(*,555) TET,ELDB,ERDB,AXDB
              WRITE(2,*) TET,ELDB
              WRITE(3,*) TET,ERDB
              WRITE(4,*) TET,AXDB
           ELSE
              WRITE(*,555) TET,ERDB,ELDB,AXDB
              WRITE(2,*) TET,ERDB
              WRITE(3,*) TET,ELDB
              WRITE(4,*) TET,AXDB
555           FORMAT(I3,9X,F7.2,7X,F7.2,8X,F7.2)
          ENDIF
        TET=TET+TETSTP
   4  CONTINUE
          IF (TYPCIR.EQ.1) THEN
              WRITE(*,900)
900           FORMAT(' LEFT-HAND CIRCULAR POLARIZATION')
            ELSE
              WRITE(*,901)
901           FORMAT(' RIGHT-HAND CIRCULAR POLARIZATION')
          ENDIF
          CLOSE(UNIT=2)
          CLOSE(UNIT=3)
          CLOSE(UNIT=4)
```

```
      WRITE(*,700)
700    FORMAT(' DIRECTIVITY ?  ENTER 1 :')
       READ (*,*) K
       IF (K.EQ.1) THEN
       PRAD=0.
       UMAX=0.
      WRITE(*,705)
705    FORMAT(' MAX. ANGLE THETA IN DEGREES ?:')
       READ(*,*) TU
      THETA=PI/180
      FI=PI/180
      DO 710,J=1,360
        WRITE(*,*) J
       RPHIJ=(FLOAT(J)*PI)/180
        DO 710,I=1,TU
         RTETI=(FLOAT(I)*PI)/180
         EPHIK=(0.,0.)
         ETETK=(0.,0.)
         DO 750,K=1,N
          RPHI0=RPHIJ-RPHI(K)
          XB=(X(K)*COS(RPHI0))+(Y(K)*SIN(RPHI0))
       IMARG=RPSI(K)+((2*PI*XB*SIN(RTETI))/LAMBDA)
        ELFAC=CMPLX(0.,IMARG)
     EPHIK=EPHIK+(EPHI(RTETI,RPHI0,EPSR,WL(K))*CEXP(ELFAC))
     ETETK=ETETK+(ETETA(RTETI,RPHI0,EPSR,WL(K))*CEXP(ELFAC))
750      CONTINUE
        F=(CABS(EPHIK)**2)+(CABS(ETETK)**2)
      IF (F.GT.UMAX) THEN
              UMAX=F
      ENDIF
      UA=THETA*FI*F*SIN(RTETI)
      PRAD=PRAD+UA
710    CONTINUE
      DIR=(4*PI*UMAX)/PRAD
      DIRDB=10*ALOG10(DIR)
      WRITE(*,715)
      WRITE(*,720) TU
      WRITE(*,725) DIR
      WRITE(*,730) DIRDB
715   FORMAT(' DIRECTIVITY COMPUTED  0<PHI<360 GRAD.')
720   FORMAT('                       0<THETA<',I3,'GRAD.')
725   FORMAT(' DIRECTIVITY :',F7.3)
730   FORMAT('             :',F6.2,' dB')
      ENDIF
      STOP
      END
```

```
 REAL FUNCTION ETETA(FT,FP,FEP,FWL)
 FPI=3.141592654
 IF (FT.NE.0.) THEN
    ARG=(FPI*SIN(FT))/(2*SQRT(FEP))
    A=ARG*COS(FP)
    IF (FP.NE.0.) THEN
        T=ARG*FWL*SIN(FP)
        SINC=SIN(T)/T
      ELSE
        SINC=1
     ENDIF
    C=SIN(FT)*SIN(FT)
    D=COS(FP)*COS(FP)
    FAC=(C-FEP)/(FEP-(D*C))
    ETETA=COS(A)*SINC*COS(FP)*FAC*FWL
 ELSE
    ETETA=-COS(FP)*FWL
 ENDIF
RETURN
END

 REAL FUNCTION EPHI(FT,FP,FEP,FWL)
 FPI=3.141592654
 IF (FT.NE.0.) THEN
    ARG=(FPI*SIN(FT))/(2*SQRT(FEP))
    A=ARG*COS(FP)
    IF (FP.NE.0.) THEN
        T=ARG*FWL*SIN(FP)
        SINC=SIN(T)/T
      ELSE
        SINC=1
     ENDIF
    C=SIN(FT)*SIN(FT)
    D=COS(FP)*COS(FP)
    FAC=FEP/(FEP-(C*D))
   EPHI=COS(A)*SINC*COS(FT)*SIN(FP)*FAC*FWL
 ELSE
   EPHI=SIN(FP)*FWL
 ENDIF
RETURN
END
```

```
****************** Program CIRPOL.FOR ***************************
*****************************************************************

This program computes the copolarization, crosspolarization and
axial ratio from two separate antenna measurements with a linearly
polarized source antenna.

*****************************************************************

      CHARACTER*40 ETMS,EPMS
      CHARACTER*1  VAR
      CHARACTER*40 BINET,BINEP
      CHARACTER*9  DATET,DATEP
      CHARACTER*8  TIMET,TIMEP
      CHARACTER*80 COMNTT,COMNTP
      CHARACTER*80 COMSTR
      CHARACTER*15 AZTXTT,FTXTT,AZTXTP,FTXTP
      CHARACTER*4  AZDIMT,AZYT,FDIMT,FYT
      CHARACTER*5  AZXT,FXT
      INTEGER      ARANGT,FRANGT,ARANGP,FRANGP
      DOUBLE PRECISION AZFRMT,AZTOT,FFRMT,FTOT
      DOUBLE PRECISION AZFRMP,AZTOP,FFRMP,FTOP
      CHARACTER*4  AZDIMP,AZYP,FDIMP,FYP
      CHARACTER*5  AZXP,FXP
      CHARACTER*40 RFILEL,RFILER,RFILAX
      CHARACTER*40 BFILEL,BFILER,BFILAX
      COMPLEX      ETHETA(1000),EPHI(1000),EL(1000)
      COMPLEX      ER(1000),CAXRAT(1000)
      COMPLEX      j
C
C
      WRITE (*,25)
25    FORMAT(//,' Enter name reportfile containing data of',/,
     *      ' H-plane measurements  : ')
      READ(*,80) ETMS
      WRITE(*,26)
26    FORMAT(//,' Enter name reportfile containing data of',/,
     *       ' E-plane measurements  : ')
      READ(*,80) EPMS
80    FORMAT(A)
      NET=2
      NEP=3
      OPEN(NET,STATUS='UNKNOWN',FILE=ETMS)
```

```
C  Read page 1-3 of reportfile containing H-plane measurements
        IPAGE=1
10      VAR='L'
        READ(NET,20) VAR
20      FORMAT(A)
        IF(ICHAR(VAR).EQ.12) IPAGE=IPAGE+1
        IF(IPAGE.EQ.4) GOTO 40
        GOTO 10
40      CONTINUE
C  Read page 4 of reportfile containing H-plane measurements.
        CALL RPHEAD(NET,.TRUE.,BINET,DATET,TIMET,COMNTT,ILEVT,
     *              INTT1,INTT2)
C  Level has to be zero. Number of functions and sequences must be one
        IF((ILEVT.EQ.0).AND.(INTT1.EQ.1).AND.(INTT2.EQ.1)) GOTO 130
        WRITE(*,41)
41      FORMAT(/,' File organization not correct ! ')
        CLOSE(NET)
        STOP
130     CONTINUE
        DO 141,I=1,6
        READ(NET,150)
141     CONTINUE
150     FORMAT()
        CALL RPAXIS(NET,.TRUE.,AZTXTT,AZFRMT,AZTOT,AZDIMT,
     *              ARANGT,AZXT,AZYT)
        READ(NET,150)
        CALL RPAXIS(NET,.TRUE.,FTXTT,FFRMT,FTOT,FDIMT,
     *              FRANGT,FXT,FYT)
        CLOSE(NET)
C
C  Read page 1-3 of reportfile containing E-plane measurements.
        OPEN(NEP,STATUS='UNKNOWN',FILE=EPMS)
        IPAGE=1
15      VAR='L'
        READ(NEP,27) VAR
27      FORMAT(A)
        IF(ICHAR(VAR).EQ.12) IPAGE=IPAGE+1
        IF (IPAGE.EQ.4) GOTO 45
        GOTO 15
45      CONTINUE
```

```
C  Read page 4 of reportfile containing E-plane measurements.
        CALL RPHEAD(NEP,.TRUE.,BINEP,DATEP,TIMEP,COMNTP,
     *              ILEVP,INTP1,INTP2)
C  Level has to be zero. Number of sequences and functions must be one.
        IF((ILEVP.EQ.0).AND.(INTP1.EQ.1).AND.(INTP2.EQ.1)) GOTO 135
        WRITE(*,41)
        CLOSE(NEP)
        STOP
135     CONTINUE
        DO 146,I=1,6
        READ(NEP,150)
146     CONTINUE
        CALL RPAXIS(NEP,.TRUE.,AZTXTP,AZFRMP,AZTOP,AZDIMP,
     *              ARANGP,AZXP,AZYP)
        READ(NEP,150)
        CALL RPAXIS(NEP,.TRUE.,FTXTP,FFRMP,FTOP,FDIMP,
     *              FRANGP,FXP,FYP)
        CLOSE(NEP)
C
C  Are the input reportfiles compatible ?
        IF((AZFRMP.EQ.AZFRMT).AND.(AZTOP.EQ.AZTOT).AND.
     *     (FFRMP.EQ.FFRMT).AND.(FTOP.EQ.FTOT).AND.
     *     (ARANGP.EQ.ARANGT).AND.(FRANGP.EQ.FRANGT)) GOTO 699
        WRITE(*,180)
180     FORMAT(/,' INPUT FILES ARE NOT COMPATIBLE !')
        STOP
C
C Creation output files, containing EL,ER,Axial ratio.
699     WRITE(*,700)
700     FORMAT(/,' ENTER NAME OUTPUTFILE, THAT MUST CONTAIN',/,
     *      ' LEFT-HAND CIRCULAR POLARIZATION PATTERN : ')
        READ(*,705) RFILEL
        IND=INDEX(RFILEL,'.')
        IF (IND.EQ.0) THEN
        WRITE(*,715)
715     FORMAT(/,' Extension !')
        GOTO 699
        ENDIF
        BFILEL=RFILEL
        DO 710,I=1,40
710     IF(BFILEL(I:I).EQ.'.') GOTO 711
711     BFILEL(I+1:I+3)='RCS'
```

```
698     WRITE(*,702)
702     FORMAT(/,' ENTER NAME OUTPUTFILE, THAT MUST CONTAIN',/,
     *          ' RIGHT-HAND CIRCULAR POLARIZATION PATTERN : ')
        READ(*,705) RFILER
        IND=INDEX(RFILER,'.')
        IF (IND.EQ.0) THEN
        WRITE(*,715)
        GOTO 698
        ENDIF
        BFILER=RFILER
        DO 720,I=1,40
720     IF (BFILER(I:I).EQ.'.') GOTO 721
721     BFILER(I+1:I+3)='RCS'
697     WRITE(*,703)
703     FORMAT(/,' ENTER NAME OUTPUTFILE, THAT MUST CONTAIN',/,
     *          ' AXIAL RATIO PATTERN : ')
        READ(*,705) RFILAX
        IND=INDEX(RFILAX,'.')
        IF (IND.EQ.0) THEN
        WRITE(*,715)
        GOTO 697
        ENDIF
        BFILAX=RFILAX
        DO 730,I=1,40
730     IF (BFILAX(I:I).EQ.'.') GOTO 731
731     BFILAX(I+1:I+3)='RCS'
705     FORMAT(A)
C
C  Write page 1-3 output reportfiles.
        COMSTR=' '
        OPEN(2,STATUS='UNKNOWN',FILE=RFILEL)
        WRITE(2,755) 12
        WRITE(2,755) 12
        WRITE(2,755) 12
755     FORMAT(A)
        COMSTR='Circular polarization components'
        CALL RPHEAD(2,.FALSE.,BFILEL,DATET,TIMET,COMSTR,0,1,1)
        WRITE(2,760)
760     FORMAT(' EL')
        WRITE(2,765)
        WRITE(2,765)
765     FORMAT()
```

```
      DO 770,I=1,3
      CALL RPAXIS(2,.FALSE.,'UNUSED          ',0.D0,0.D0,
     *            '    ',0,'     ','    ')
770   CONTINUE
      CALL RPAXIS(2,.FALSE.,AZTXTT,AZFRMT,AZTOT,AZDIMT,ARANGT,
     *            AZXT,AZYT)
      WRITE(2,765)
      CALL RPAXIS(2,.FALSE.,FTXTT,FFRMT,FTOT,FDIMT,FRANGT,
     *            FXT,FYT)
      CLOSE(2)
C
      OPEN(2,STATUS='UNKNOWN',FILE=RFILER)
      WRITE(2,755) 12
      WRITE(2,755) 12
      WRITE(2,755) 12
      COMSTR=' '
      COMSTR='Circular polarization components'
      CALL RPHEAD(2,.FALSE.,BFILER,DATET,TIMET,COMSTR,0,1,1)
      WRITE(2,800)
800   FORMAT(' ER')
      WRITE(2,765)
      WRITE(2,765)
      DO 810,I=1,3
      CALL RPAXIS(2,.FALSE.,'UNUSED          ',0.D0,0.D0,
     *            '    ',0,'     ','    ')
810   CONTINUE
      CALL RPAXIS(2,.FALSE.,AZTXTT,AZFRMT,AZTOT,AZDIMT,ARANGT,
     *            AZXT,AZYT)
      WRITE(2,765)
      CALL RPAXIS(2,.FALSE.,FTXTT,FFRMT,FTOT,FDIMT,FRANGT,
     *            FXT,FYT)
      CLOSE(2)
C
      OPEN(2,STATUS='UNKNOWN',FILE=RFILAX)
      WRITE(2,755) 12
      WRITE(2,755) 12
      WRITE(2,755) 12
      COMSTR=' '
      COMSTR='Axial ratio pattern'
      CALL RPHEAD(2,.FALSE.,BFILAX,DATET,TIMET,COMSTR,0,1,1)
      WRITE(2,830)
830   FORMAT(' Axial ratio')
      WRITE(2,765)
      WRITE(2,765)
```

```
      DO 840,I=1,3
      CALL RPAXIS(2,.FALSE.,'UNUSED          ',0.D0,0.D0,
     *            '    ',0,'     ','    ')
840   CONTINUE
      CALL RPAXIS(2,.FALSE.,AZTXTT,AZFRMT,AZTOT,AZDIMT,ARANGT,
     *            AZXT,AZYT)
      WRITE(2,765)
      CALL RPAXIS(2,.FALSE.,FTXTT,FFRMT,FTOT,FDIMT,FRANGT,
     *            FXT,FYT)
      CLOSE(2)
C
C
      OPEN(2,STATUS='UNKNOWN',FILE=BINET,ACCESS='DIRECT',RECL=8*FRANGT)
      OPEN(3,STATUS='UNKNOWN',FILE=BINEP,ACCESS='DIRECT',RECL=8*FRANGT)
     OPEN(7,STATUS='UNKNOWN',FILE=BFILEL,ACCESS='DIRECT',RECL=8*FRANGT)
     OPEN(8,STATUS='UNKNOWN',FILE=BFILER,ACCESS='DIRECT',RECL=8*FRANGT)
     OPEN(9,STATUS='UNKNOWN',FILE=BFILAX,ACCESS='DIRECT',RECL=8*FRANGT)
      j=(0.,1.)
      DO 1000,I=1,ARANGT
      READ(2,REC=I) (ETHETA(K1),K1=1,FRANGT)
      READ(3,REC=I) (EPHI(K2),K2=1,FRANGT)
      DO 1010,K=1,FRANGT
      EL(K)=0.5*(ETHETA(K)-(j*EPHI(K)))
      ER(K)=0.5*(ETHETA(K)+(j*EPHI(K)))
      ABSEL=CABS(EL(K))
      ABSER=CABS(ER(K))
      AXRAT=ABS((ABSEL+ABSER)/(ABSEL-ABSER))
      CAXRAT(K)=CMPLX(AXRAT,0.)
1010  CONTINUE
      WRITE(7,REC=I) (EL(K3),K3=1,FRANGT)
      WRITE(8,REC=I) (ER(K4),K4=1,FRANGT)
      WRITE(9,REC=I) (CAXRAT(K5),K5=1,FRANGT)
1000  CONTINUE
      CLOSE(2)
      CLOSE(3)
      CLOSE(7)
      CLOSE(8)
      CLOSE(9)
      STOP
      END
```

The summation (5.55), resulting in (5.61) remains to be proved.

$$Y_{JJ'} = Y_o \sum_{i=0}^{N-1} \frac{1 - z\, e^{-j\frac{4\pi i}{N}}}{1 + z\, e^{-j\frac{4\pi i}{N}}} = \begin{cases} N Y_o \dfrac{1 + (-z)^{N/2}}{1 - (-z)^{N/2}} & \text{N even} \\ N Y_o \dfrac{1 - z^N}{1 + z^N} & \text{N odd} \end{cases} \qquad \text{(C.1)}$$

We make use of the series

$$\sum_{k=0}^{\infty} (-1)^k \alpha^k = \frac{1}{1+\alpha} \qquad (|\alpha| < 1) \qquad \text{(C.2)}$$

This summation is applied to the separate terms in (C.1), resulting in

$$\frac{1}{1 + z\, e^{-j\frac{4\pi i}{N}}} = \sum_{k=0}^{\infty} (-1)^k z^k e^{-j\frac{4\pi i k}{N}} \qquad \text{(C.3.a)}$$

$$\frac{-z\, e^{-j\frac{4\pi i}{N}}}{1 + z\, e^{-j\frac{4\pi i}{N}}} = \sum_{k=0}^{\infty} (-1)^{k+1} z^{k+1} e^{-j\frac{4\pi i (k+1)}{N}} \qquad \text{(C.3.b)}$$

Rewriting (C.3.b) with $\ell = k + 1$ gives

$$\frac{-z\, e^{-j\frac{4\pi i}{N}}}{1 + z\, e^{-j\frac{4\pi i}{N}}} = \left\{ \sum_{\ell=0}^{\infty} (-1)^{\ell} z^{\ell} e^{-j\frac{4\pi i \ell}{N}} \right\} - 1 \qquad \text{(C.4)}$$

Substitution of (C.3.a) and (C.4) in (C.1) gives

$$Y_{JJ'} = Y_o \left\{ \left[2 \sum_{i=0}^{N-1} \sum_{k=0}^{\infty} (-1)^k z^k e^{-j\frac{4\pi i k}{N}} \right] - N \right\}$$

$$= Y_o \left\{ \left[2 \sum_{k=0}^{\infty} (-1)^k z^k \sum_{i=0}^{N-1} e^{-j\frac{4\pi i k}{N}} \right] - N \right\} \qquad \text{(C.5)}$$

The finite summation in (C.5) can be written as

$$\sum_{i=0}^{N-1} e^{-j\frac{4\pi ik}{N}} = \begin{cases} 0 & \frac{2k}{N} \neq p \\ N & \frac{2k}{N} = p \end{cases} \qquad \text{(C.6)}$$

with p an integer . The terms in (C.5) thus only give a contribution to the summation as

$$k = \frac{Np}{2} \qquad \text{(C.7)}$$

is an integer.
Substituting (C.6) and (C.7) in (C.5) gives

$$Y_{JJ'} = NY_0 \left\{ 2\left[\sum_{p=0}^{\infty} (-1)^{\frac{Np}{2}} z^{\frac{Np}{2}} \right] - 1 \right\} \qquad \text{(C.8)}$$

Let's first consider the case N is even. This means that $\frac{Np}{2}$ is always an integer number. Rewriting (C.8) gives

(N even)

$$Y_{JJ'} = NY_0 \left\{ 2\left[\sum_{p=0}^{\infty} (-z)^{\frac{Np}{2}} \right] - 1 \right\} = NY_0 \left\{ \frac{2}{1-(-z)^{N/2}} - 1 \right\}$$

$$= NY_0 \left\{ \frac{1+(-z)^{N/2}}{1-(-z)^{N/2}} \right\} \qquad \text{(C.9)}$$

which is (5.61.a)

For N is odd the situation is different. In this case $\frac{Np}{2}$ is only an integer for p even.
If we substitute p = 2q, we obtain with (C.8)

(N odd)

$$Y_{JJ'} = Ny_o \left\{ \left[2 \sum_{q=0}^{\infty} (-1)^{Nq} z^{Nq} \right] - 1 \right\} \qquad (C.10)$$

resulting in

$$Y_{JJ'} = Ny_o \left\{ 2 \left[\sum_{q=0}^{\infty} (-1)^q (z^N)^q \right] - 1 \right\} = Ny_o \left\{ \frac{2}{1+z^N} - 1 \right\}$$

$$= Ny_o \left\{ \frac{1-z^N}{1+z^N} \right\} \qquad (C.11)$$

which is (5.61.c).

q.e.d.

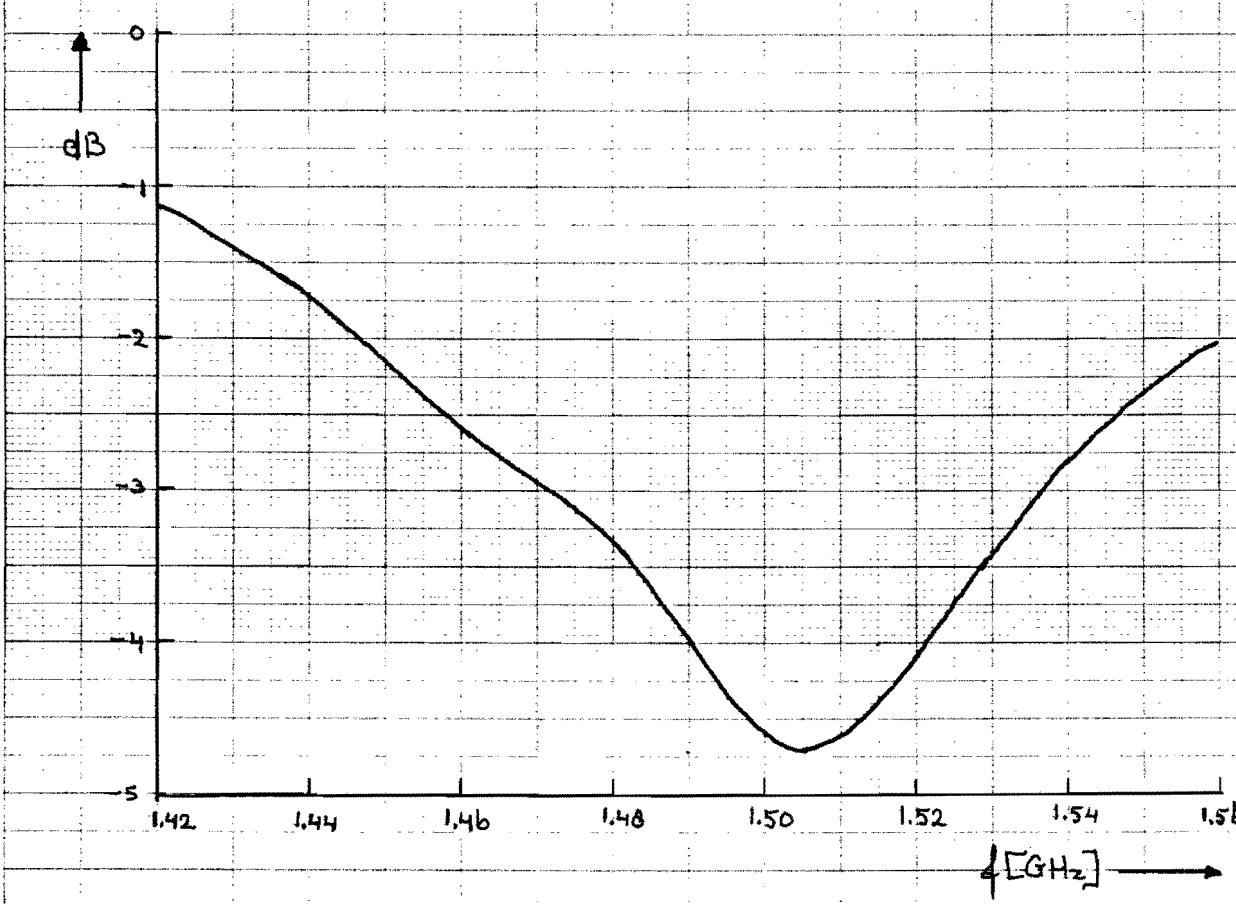

(a) Reflection coefficient.

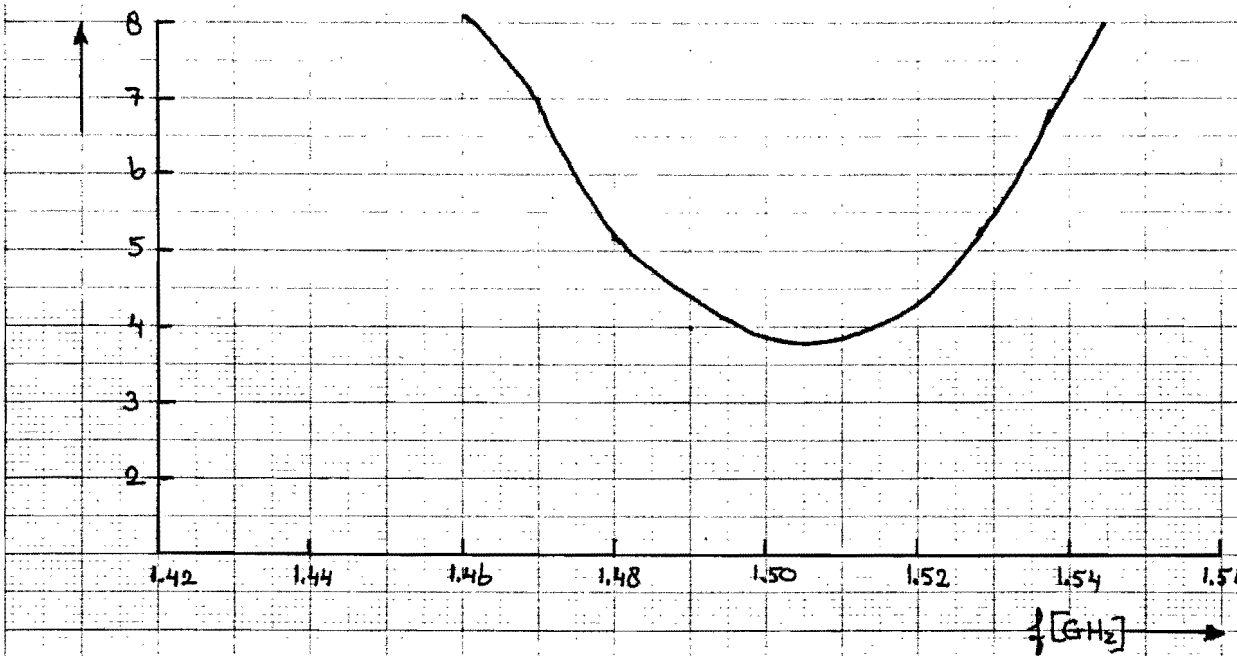

(b) Corresponding VSWR

Fig. D.1 Reflection measurements port 1a and 1b.

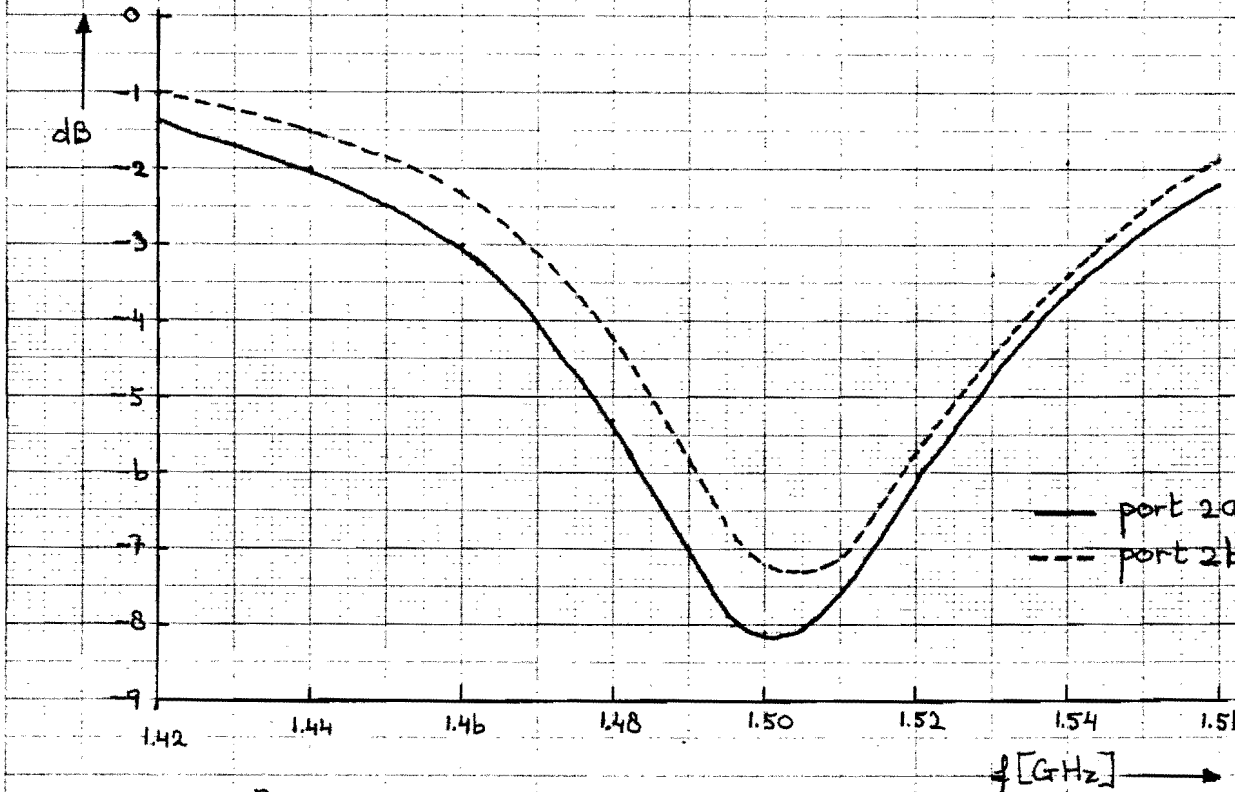

(a) Reflection coefficient.

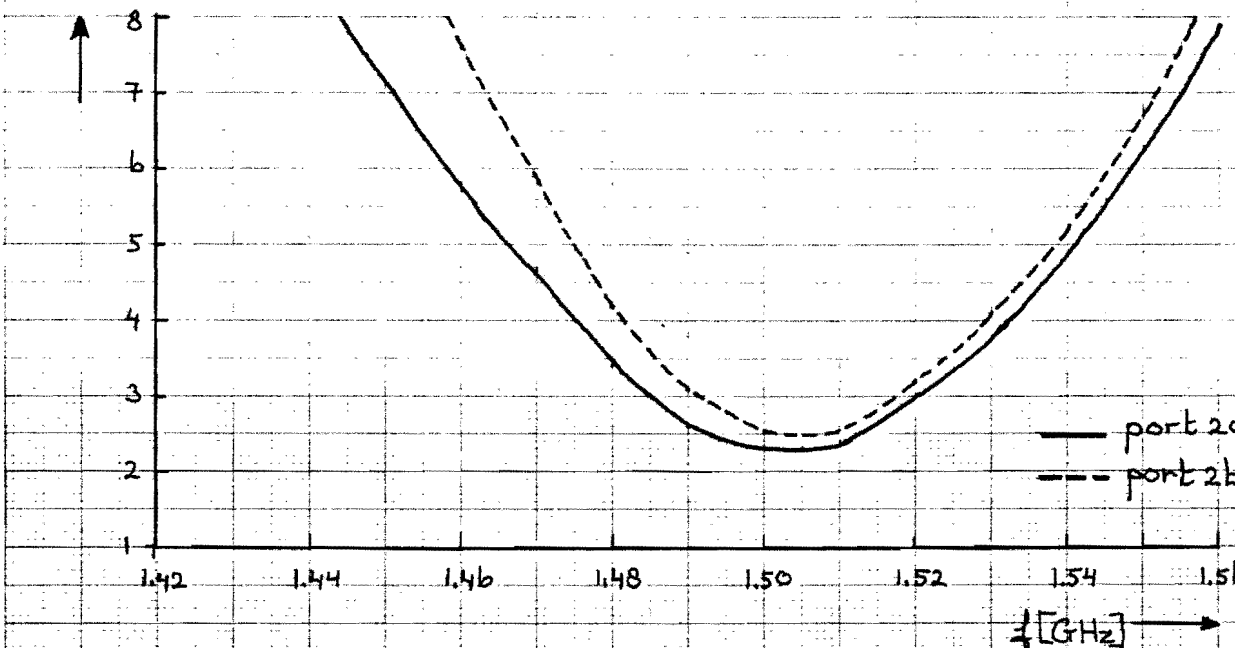

(b) Corresponding VSWR.

Fig. D.2 Reflection measurements port 2a and 2b.

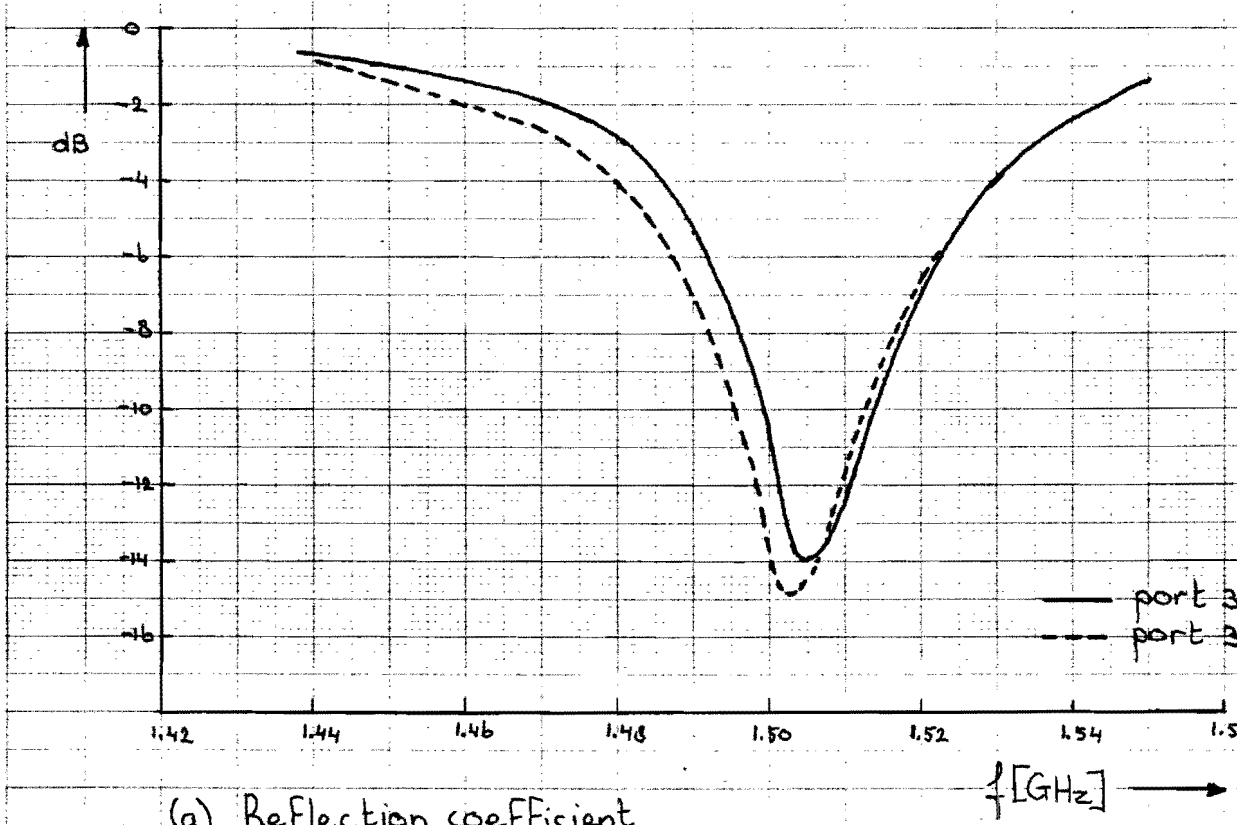

(a) Reflection coefficient.

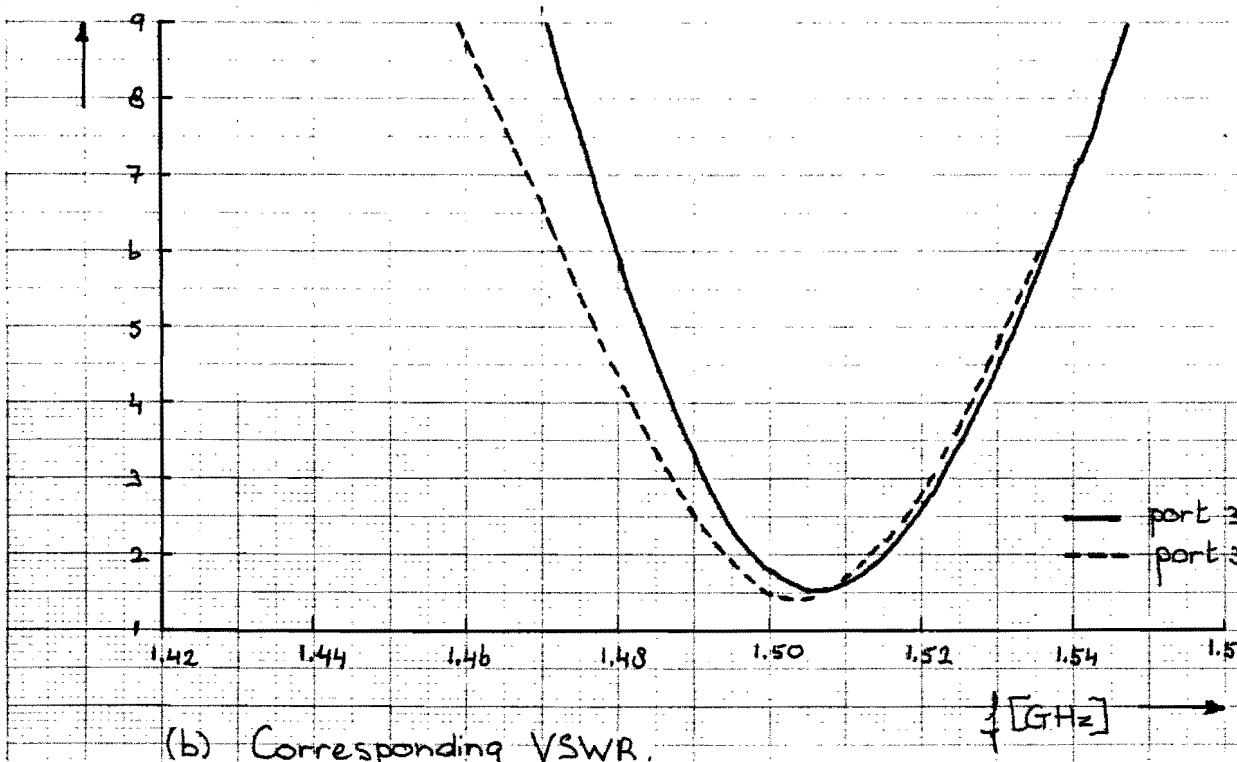

(b) Corresponding VSWR.

Fig. D.3 Reflection measurements port 3a and 3b.

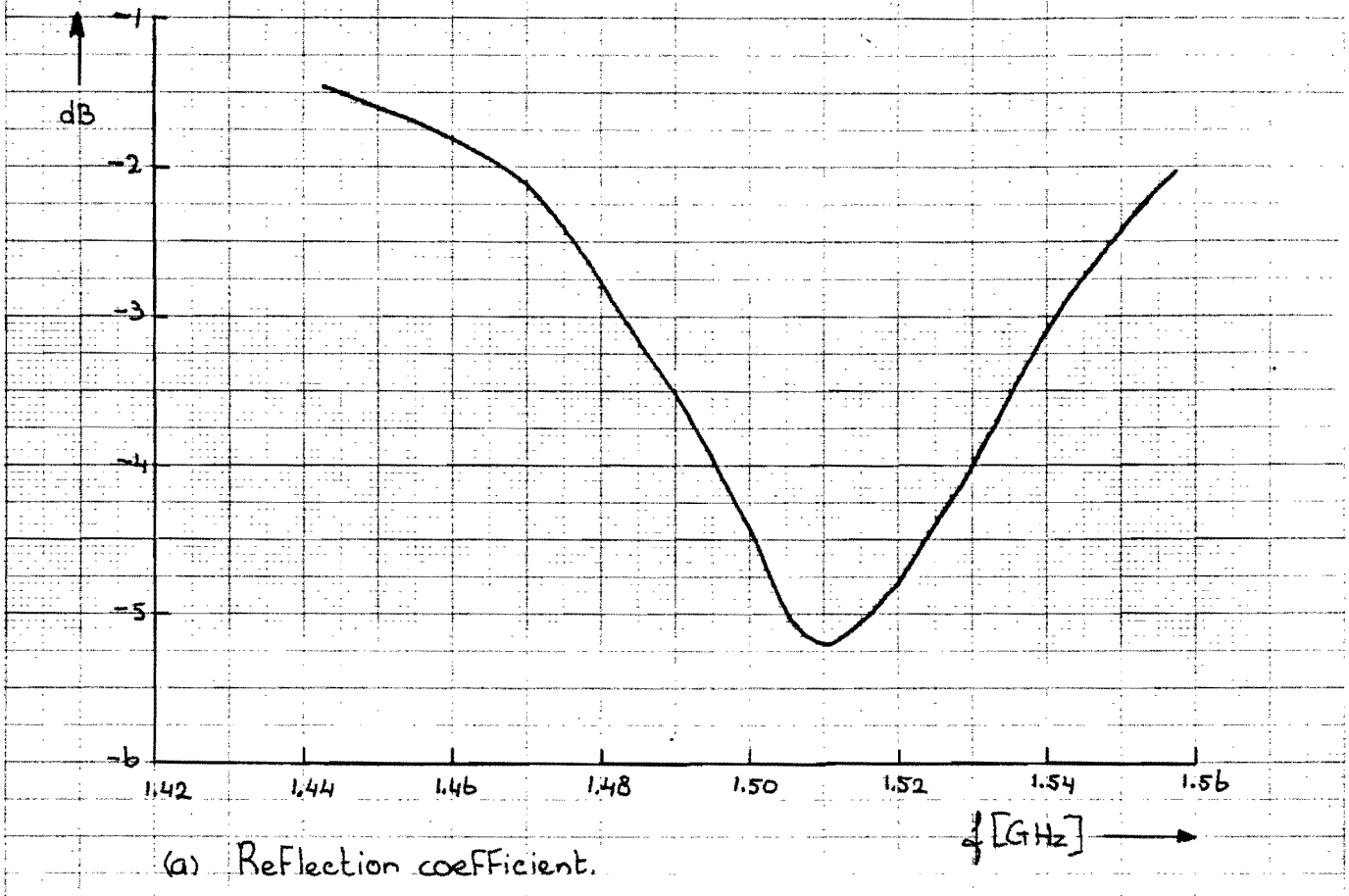

(a) Reflection coefficient.

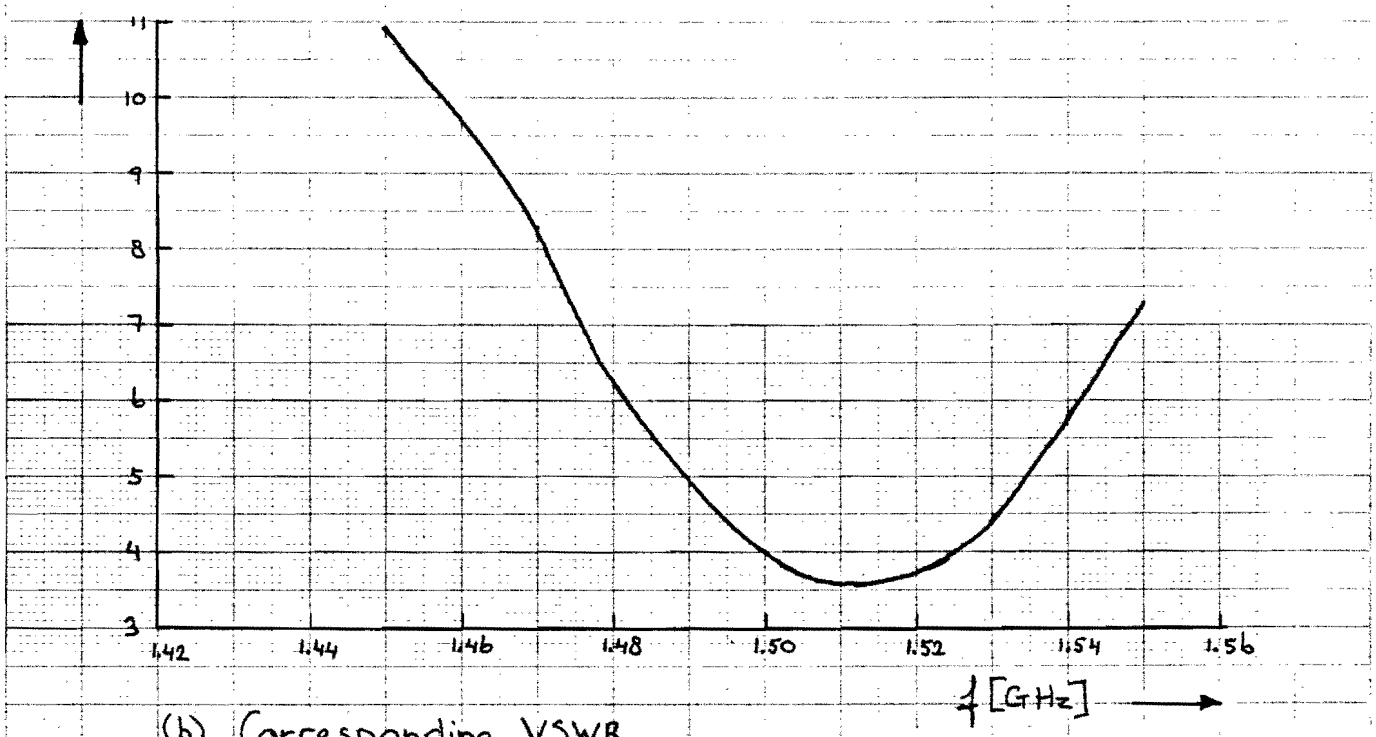

(b) Corresponding VSWR

Fig. D.4 Reflection measurements port 4a and 4b.

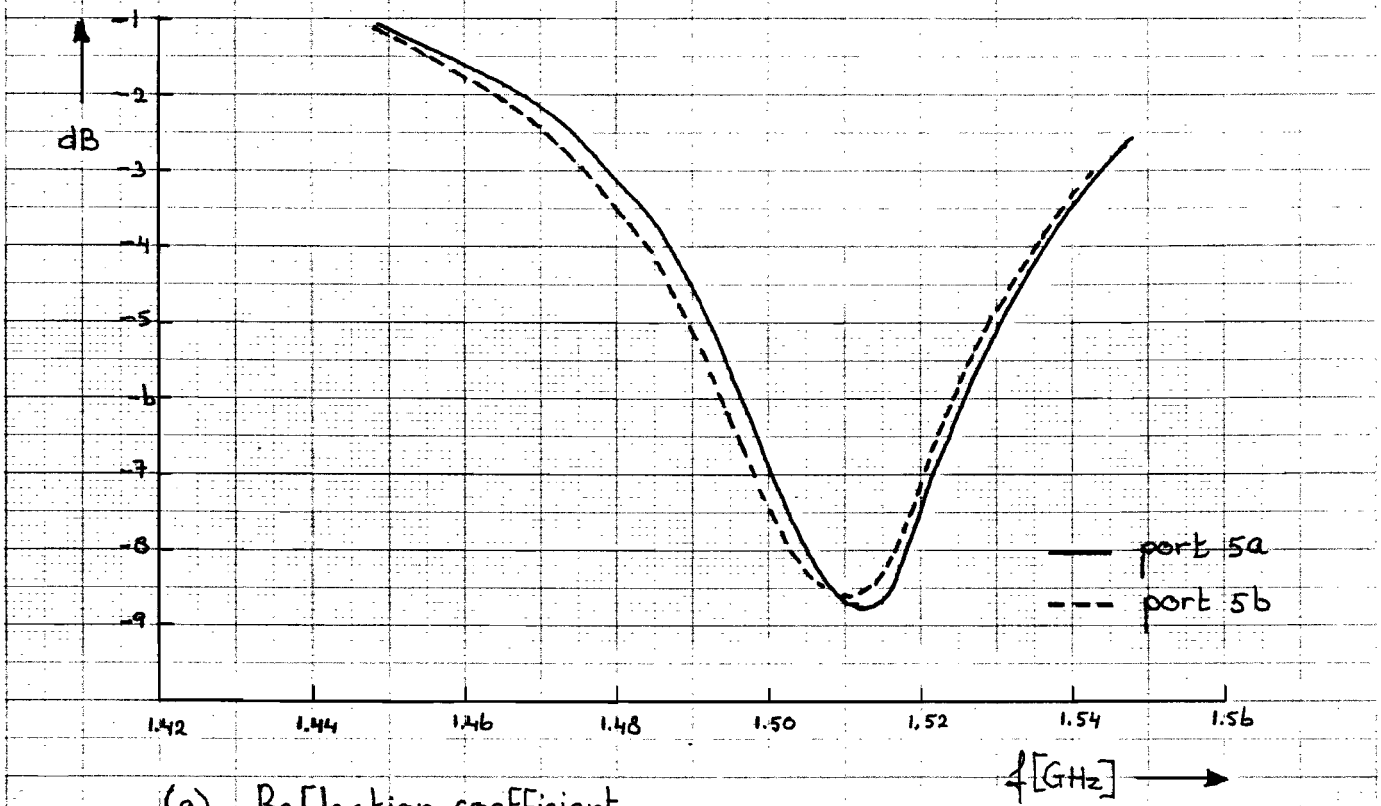

(a) Reflection coefficient.

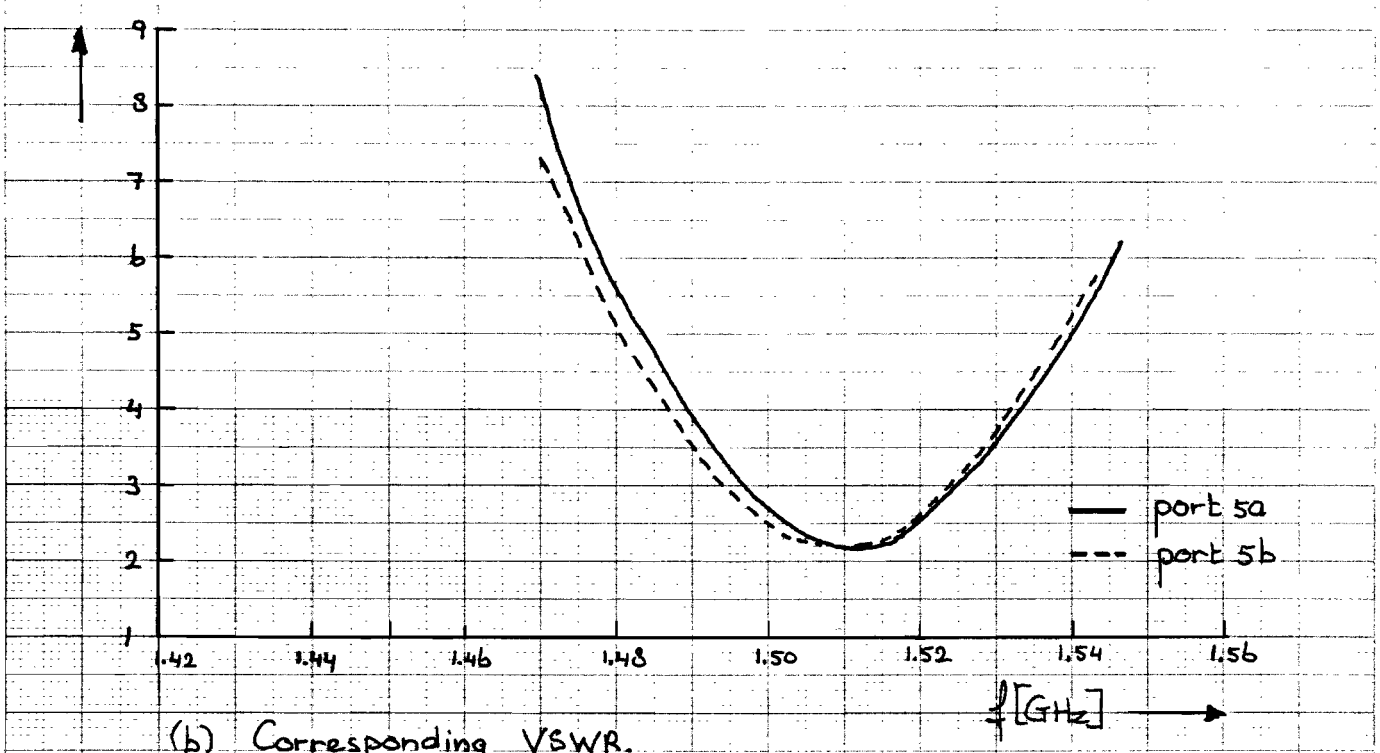

(b) Corresponding VSWR.

Fig. D.5 Reflection measurements port 5a and 5b.

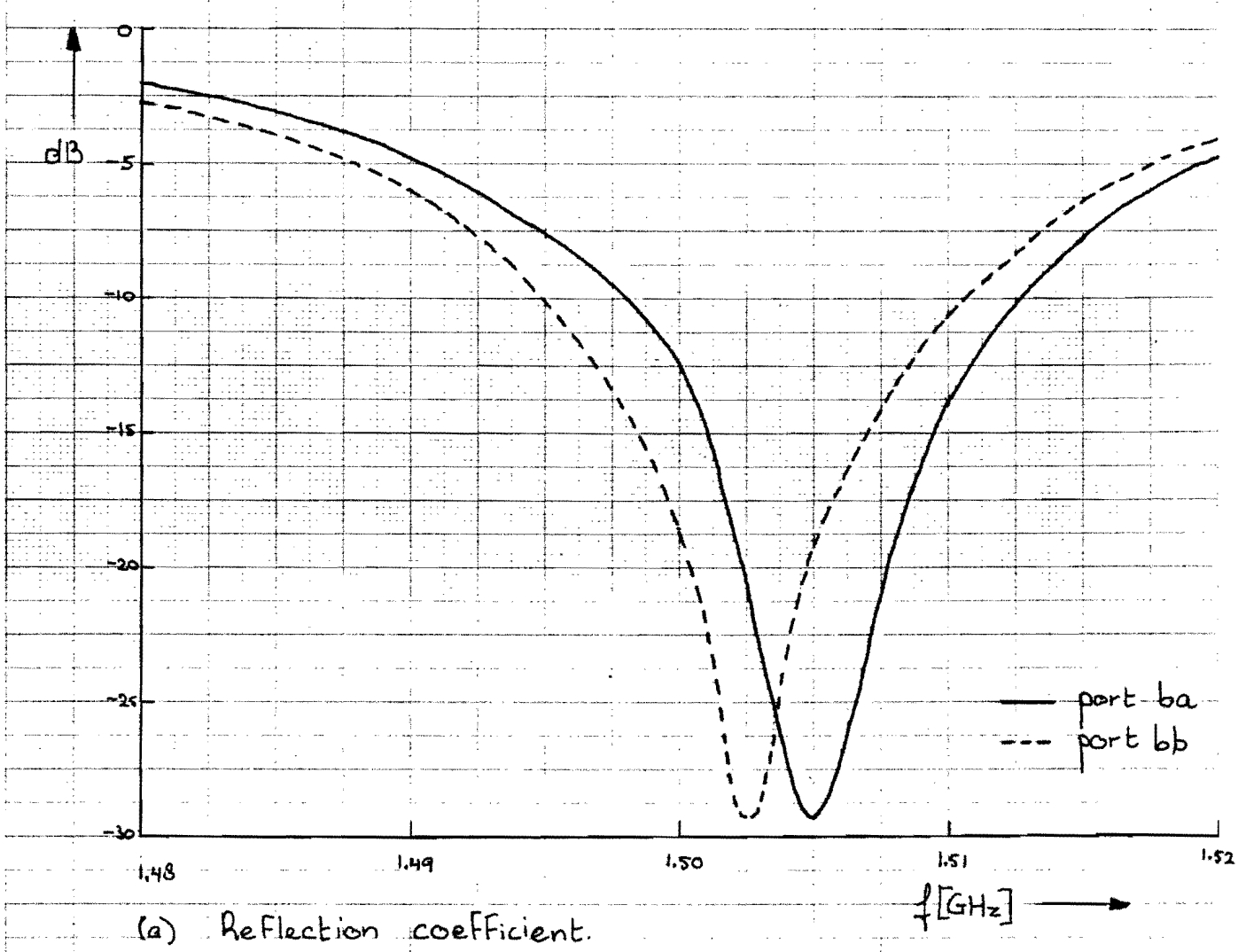

(a) Reflection coefficient.

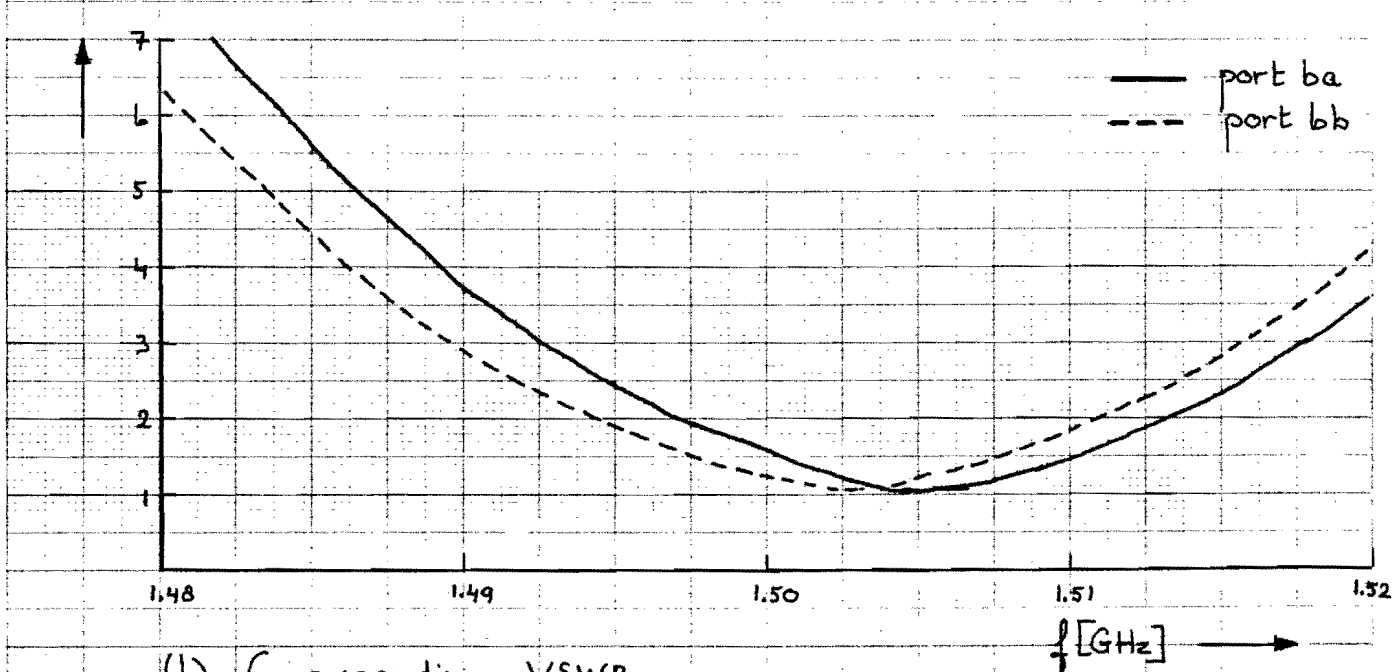

(b) Corresponding VSWR.

Fig D.6 Reflection measurement port ba and bb.

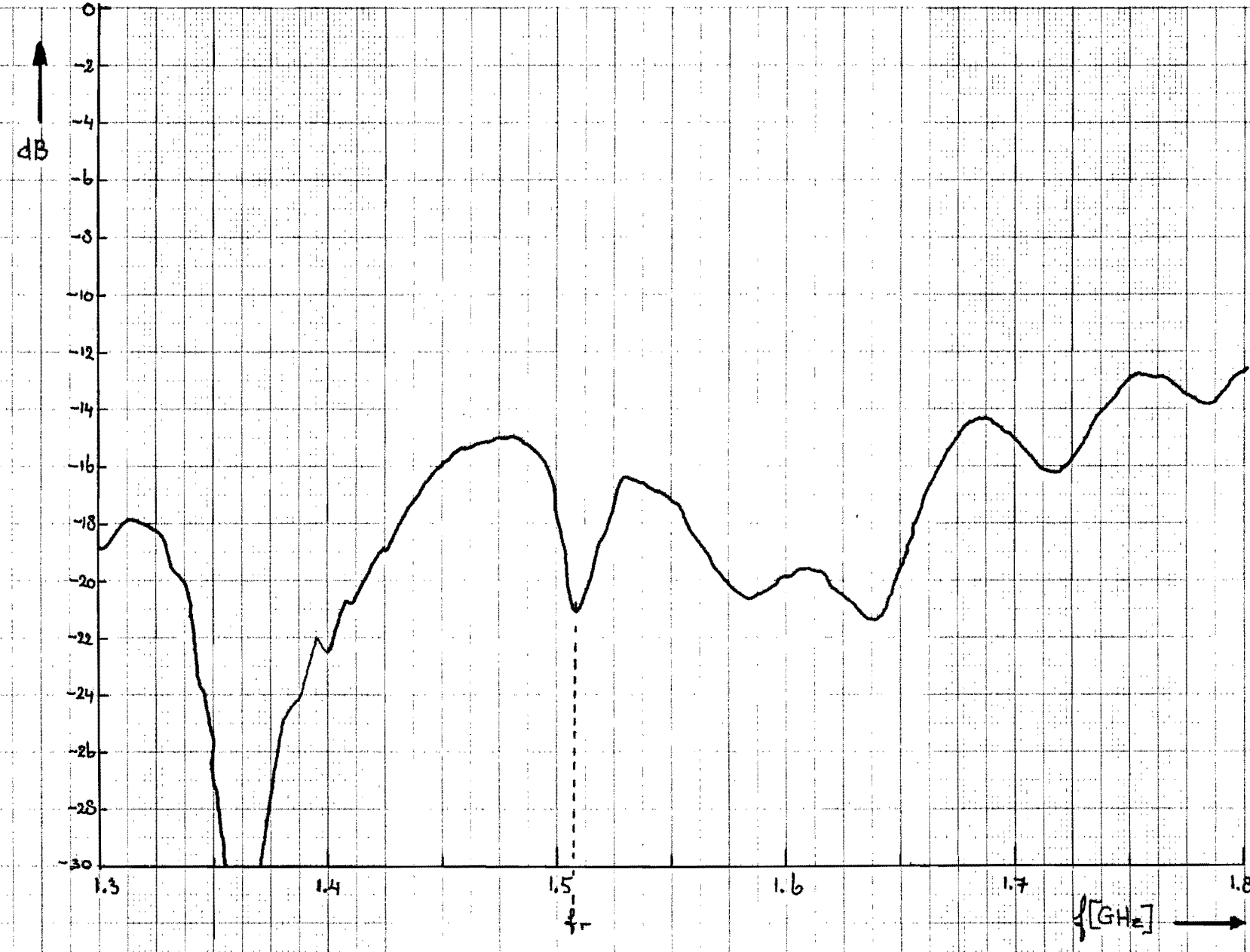

Fig. D.7 Measured reflection coefficient of circularly polarized dual feed square patch antenna.

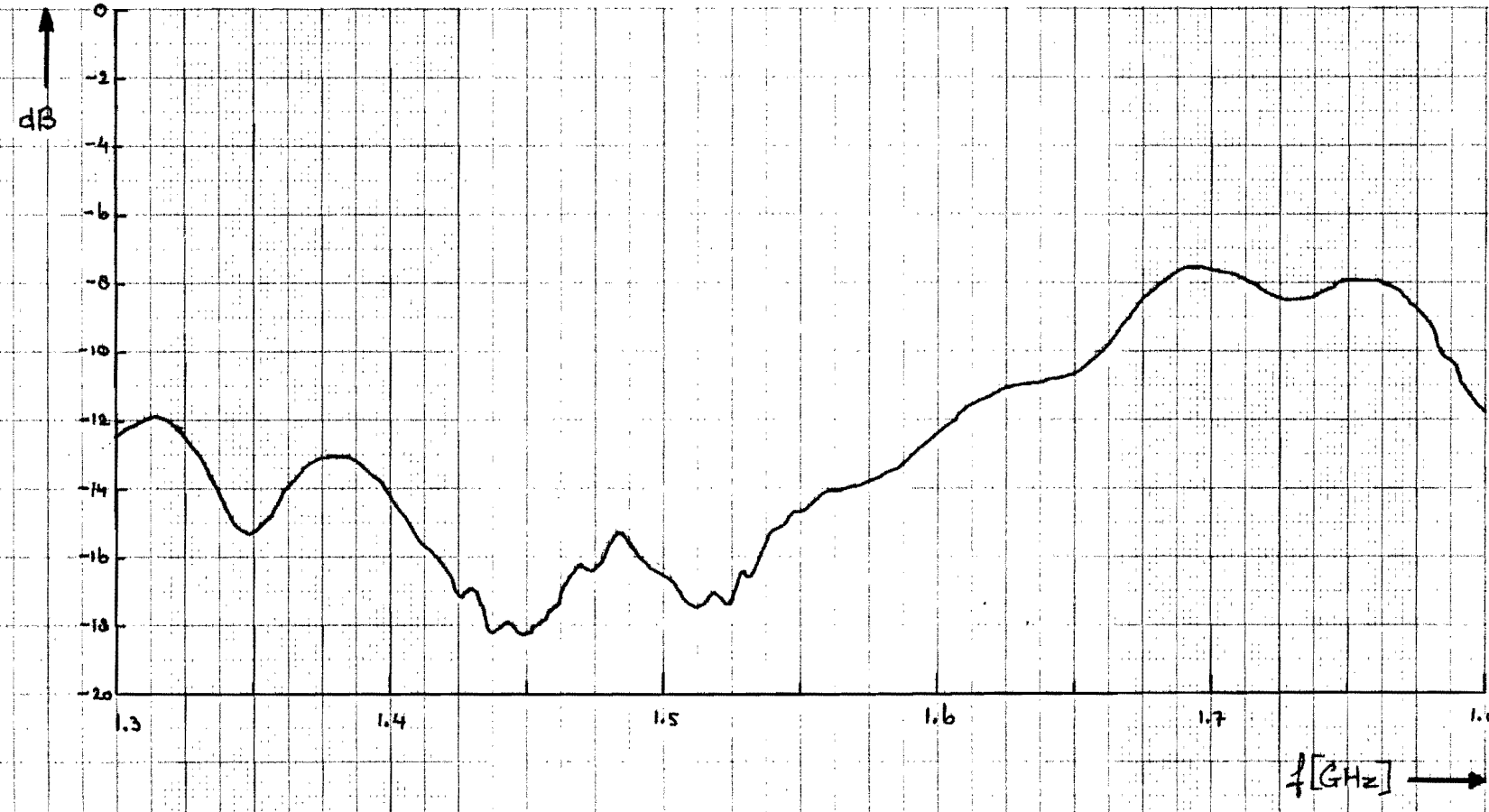

Fig. D.8 Measured reflection coefficient versus frequency of four element circularly polarized antenna array.

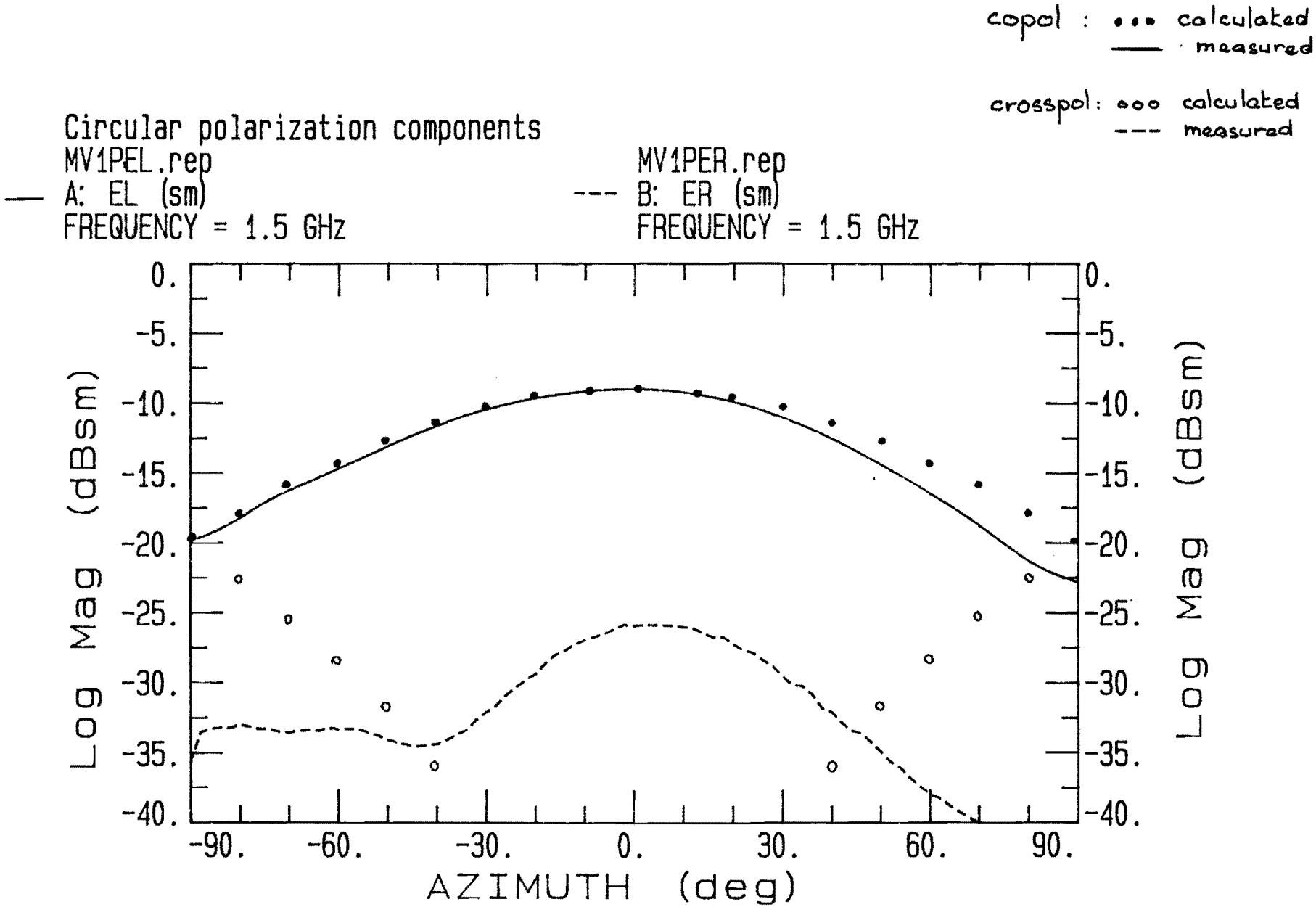

Fig. E.1 Single circularly polarized element. (Principal plane)

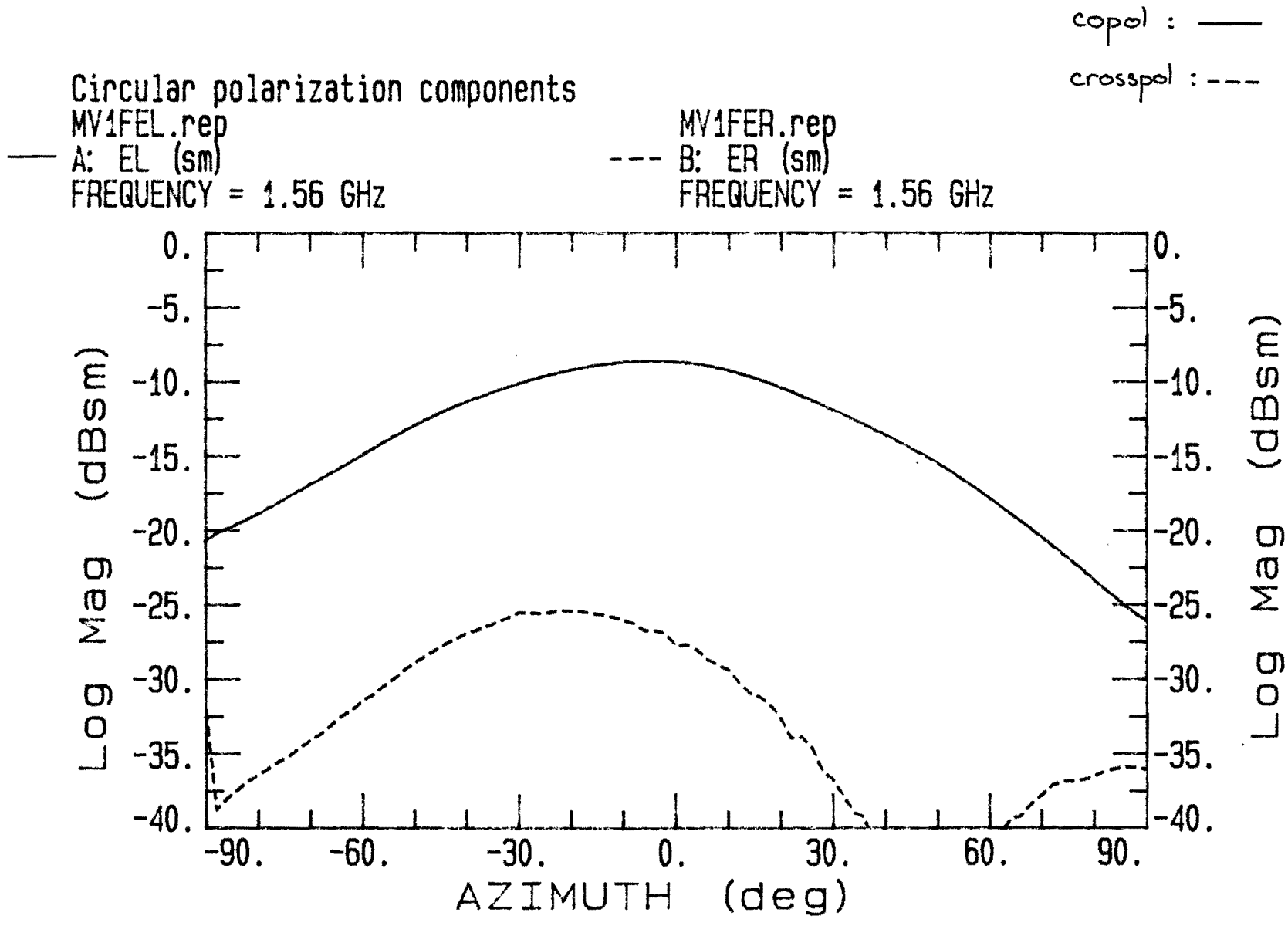

Fig. E.4 Single circularly polarized element. (Diagonal plane)

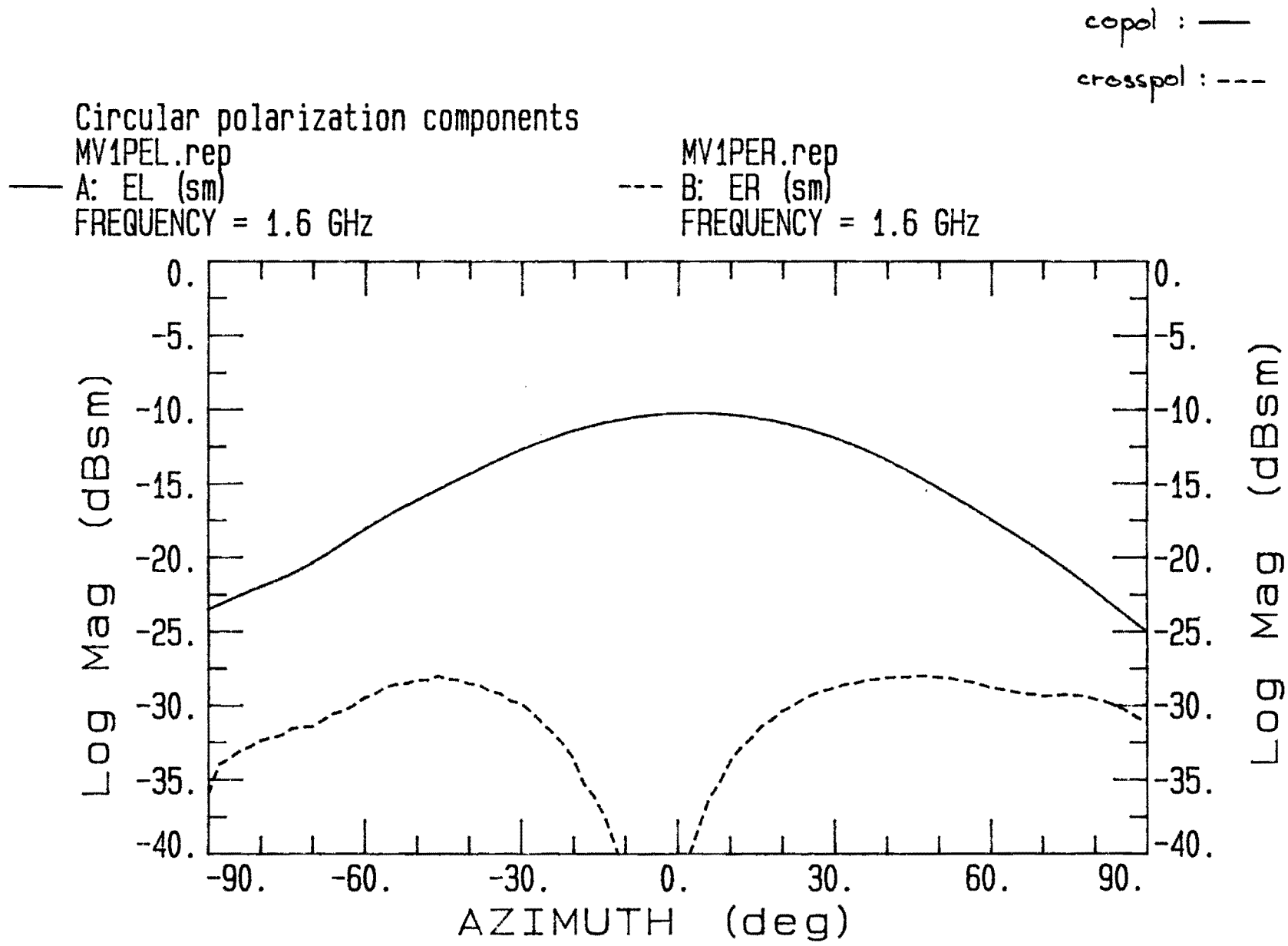

Fig. E.5 Single circularly polarized element. (Principal plane)

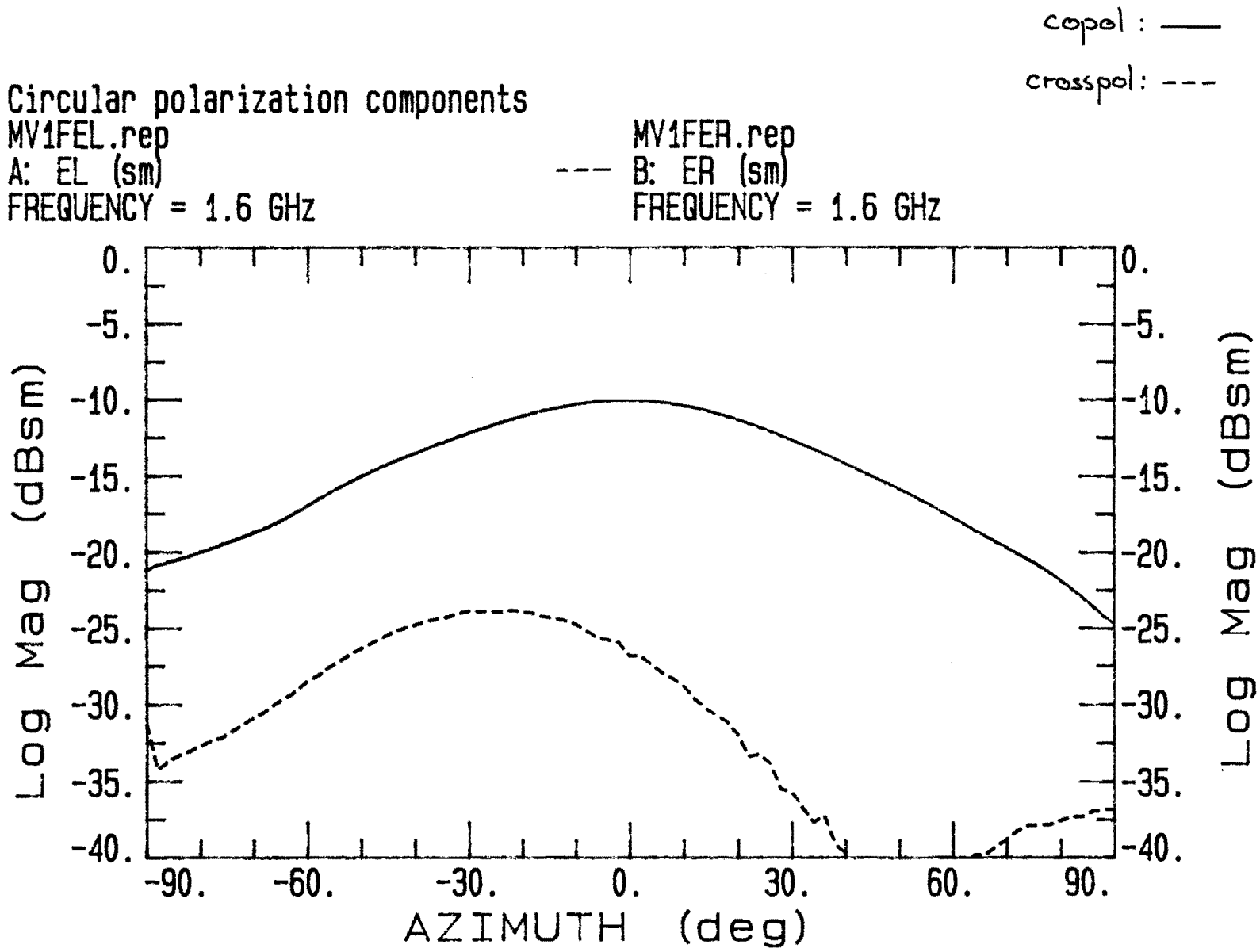

Fig. E.6 Single circularly polarized element. (Diagonal plane)

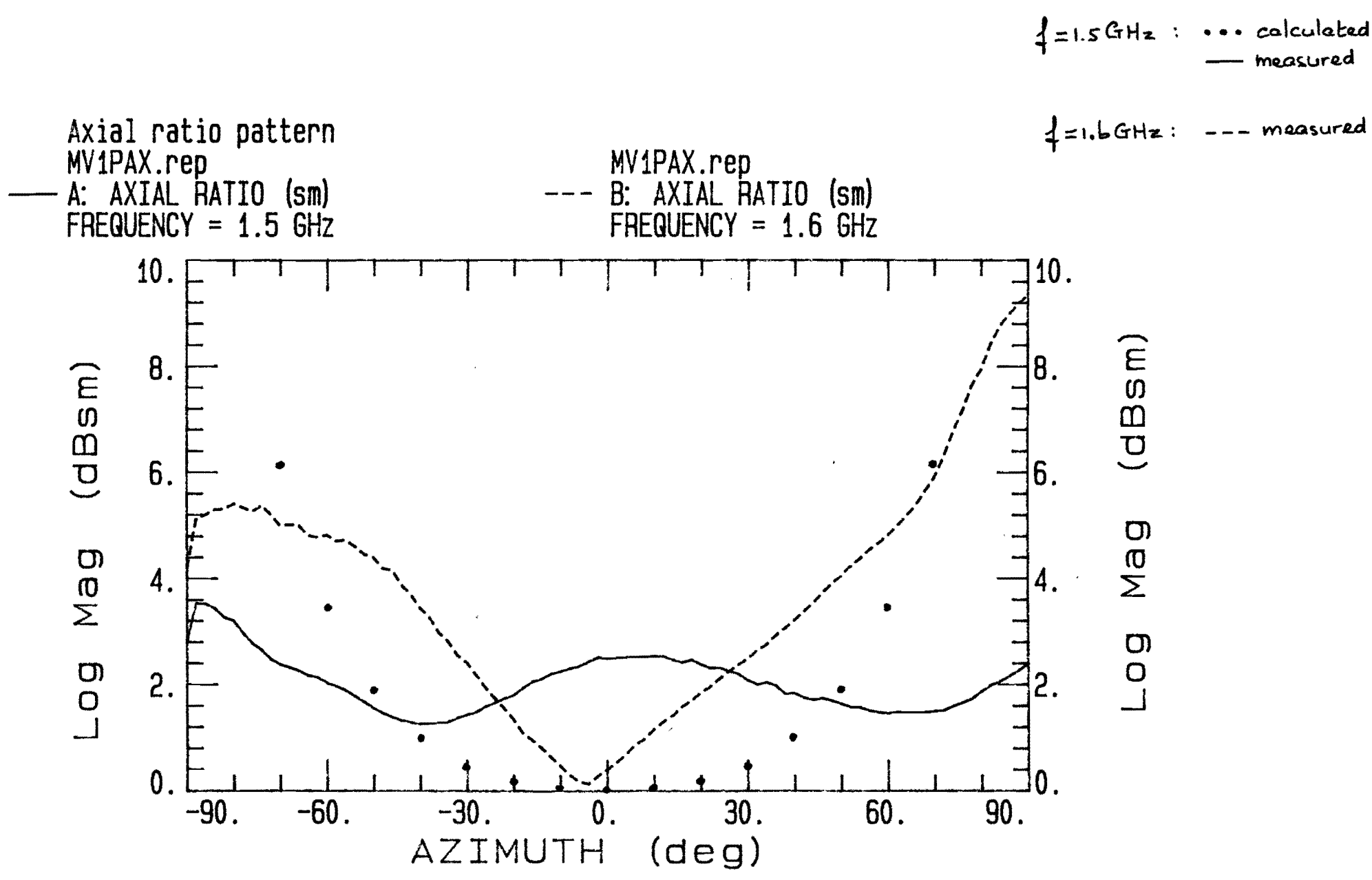

Fig. E.7 Single circularly polarized element. (Principal plane)

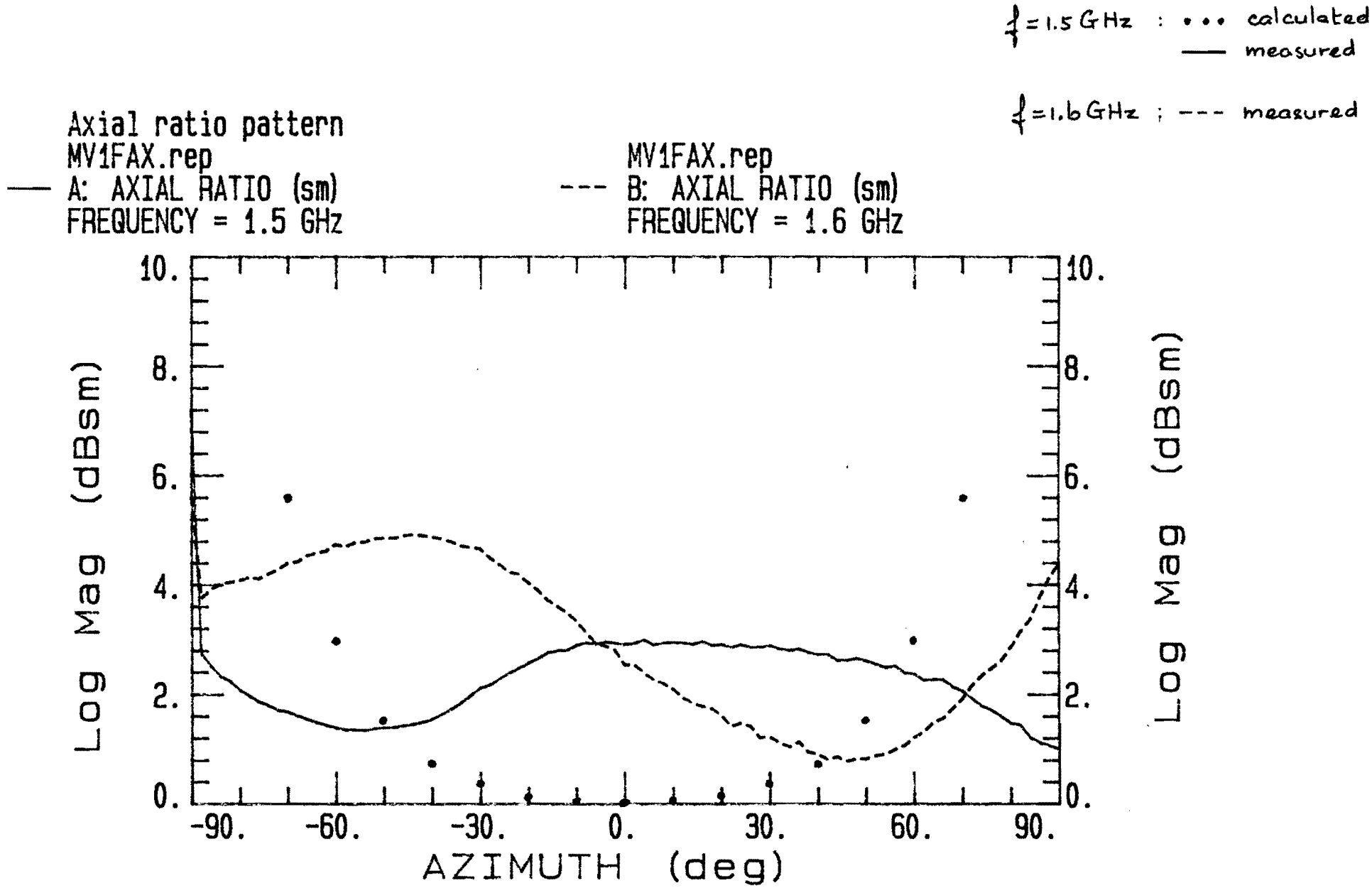

Fig. E.8 Single circularly polarized element. (Diagonal plane)

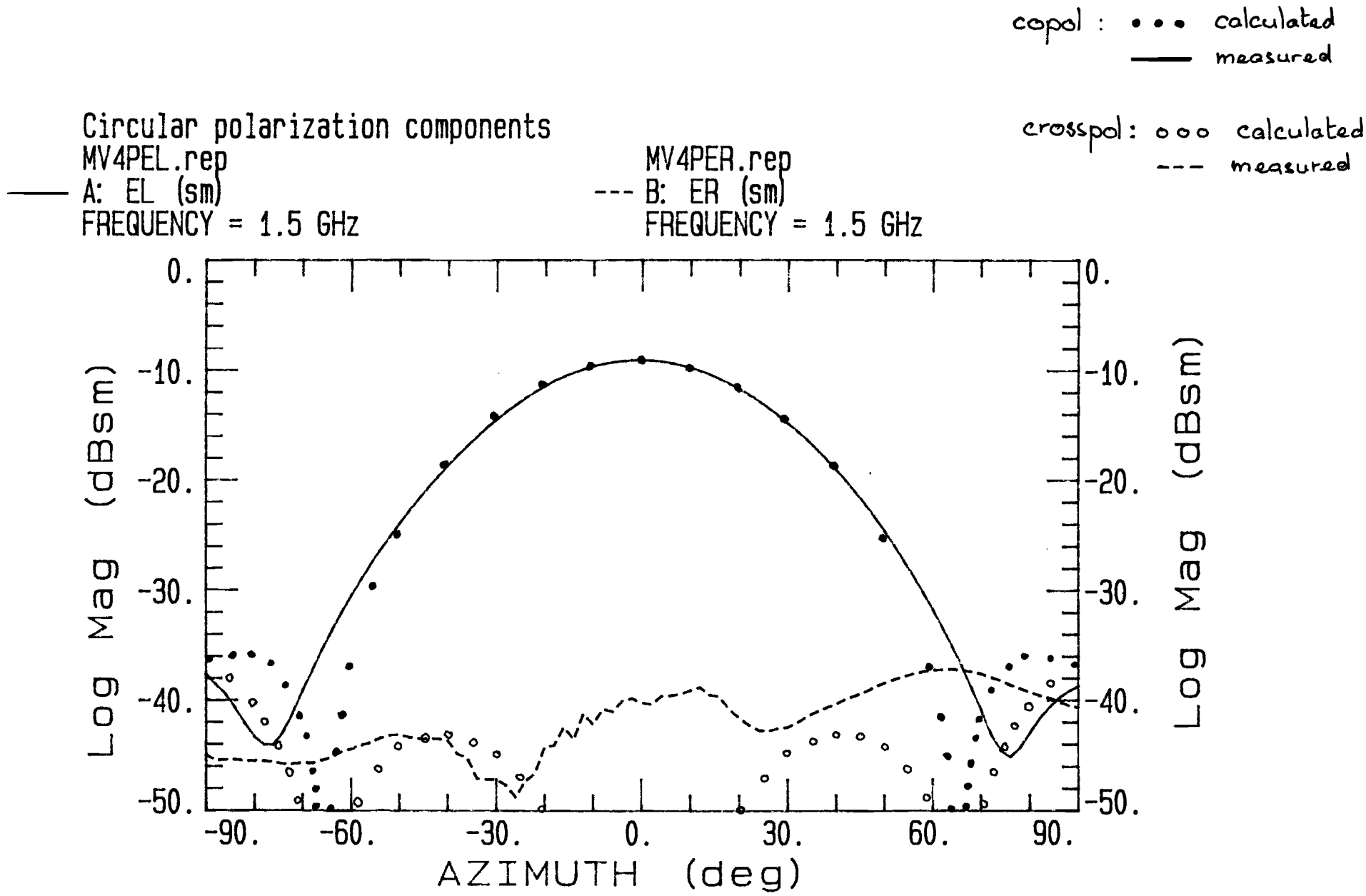

Fig.E.9 Four element circularly polarized antenna array.
(Principal plane)

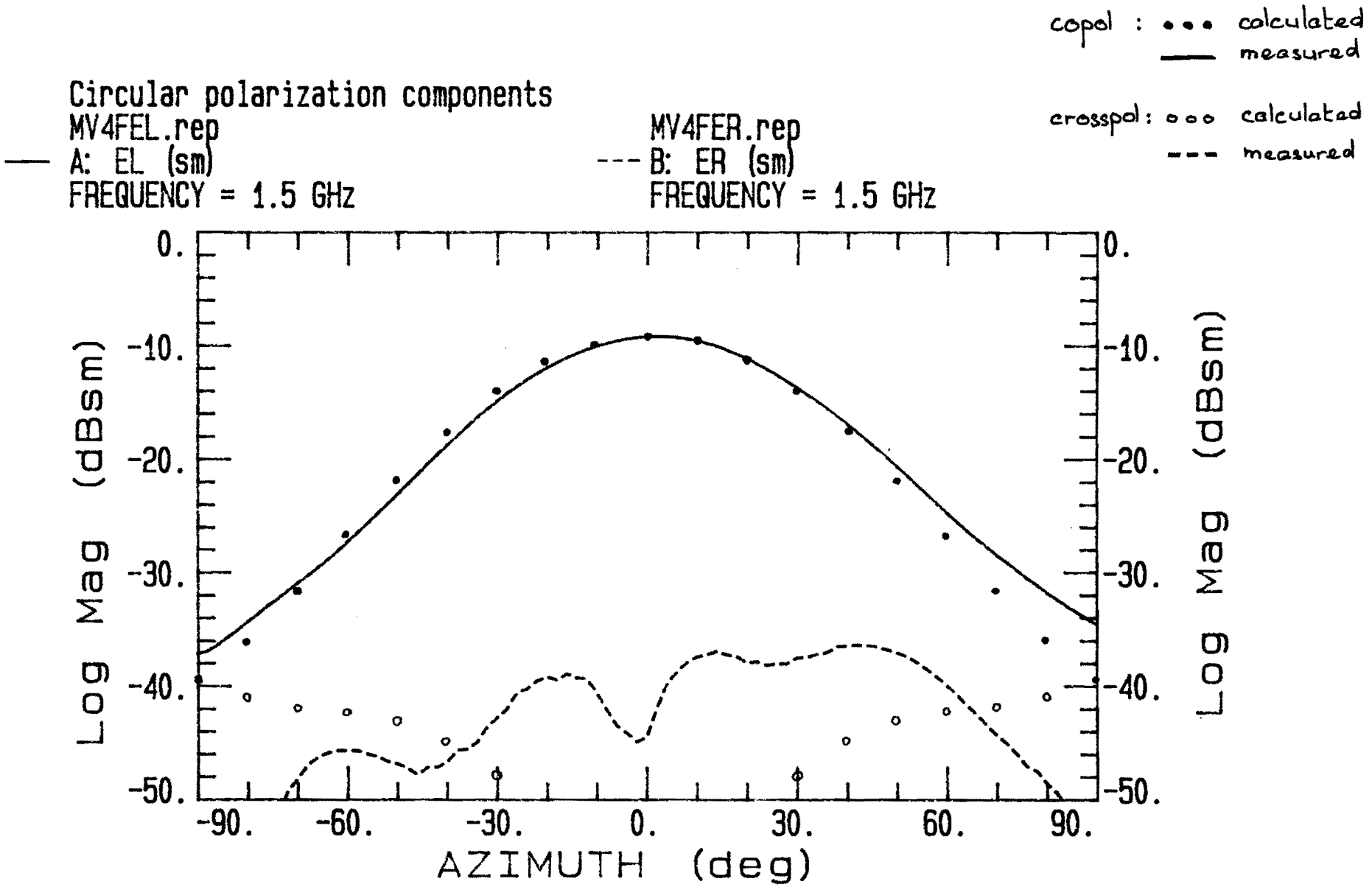

Fig. E.10 Four element circularly polarized antenna array.
(Diagonal plane)

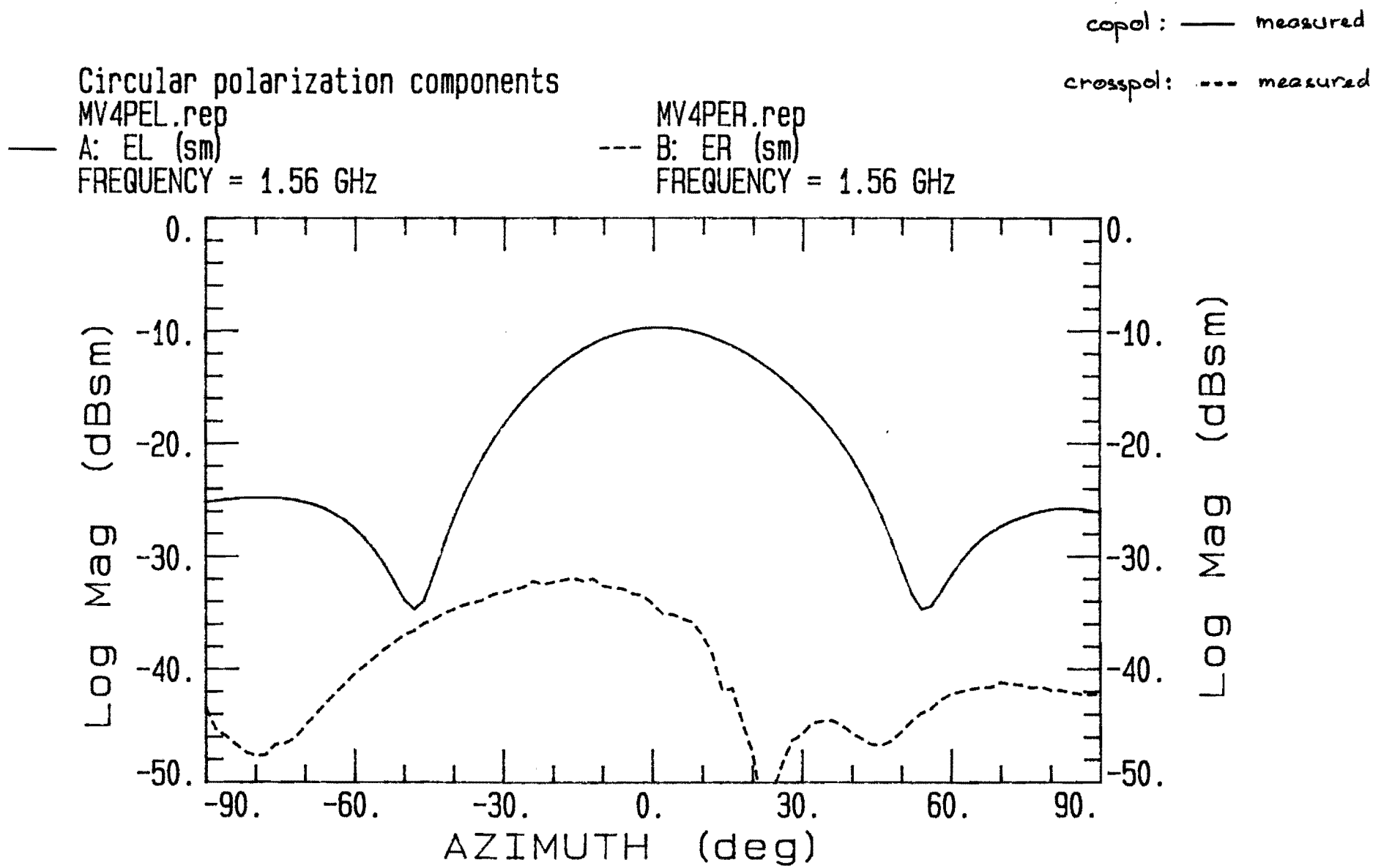

Fig. E.11 Four element circularly polarized antenna array.
(Principal plane)

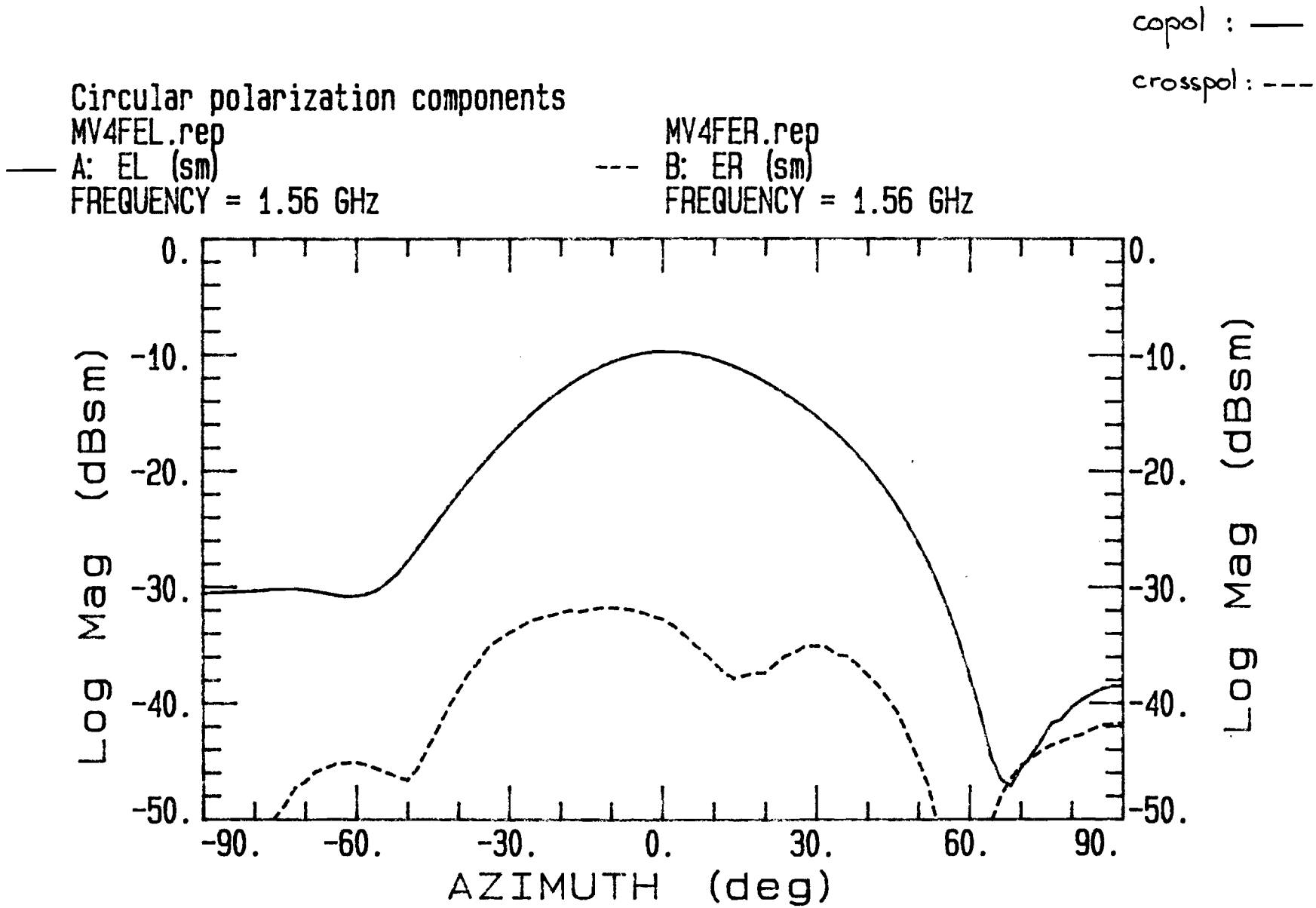

Fig. E.12 Four element circularly polarized antenna array.
(Diagonal plane)

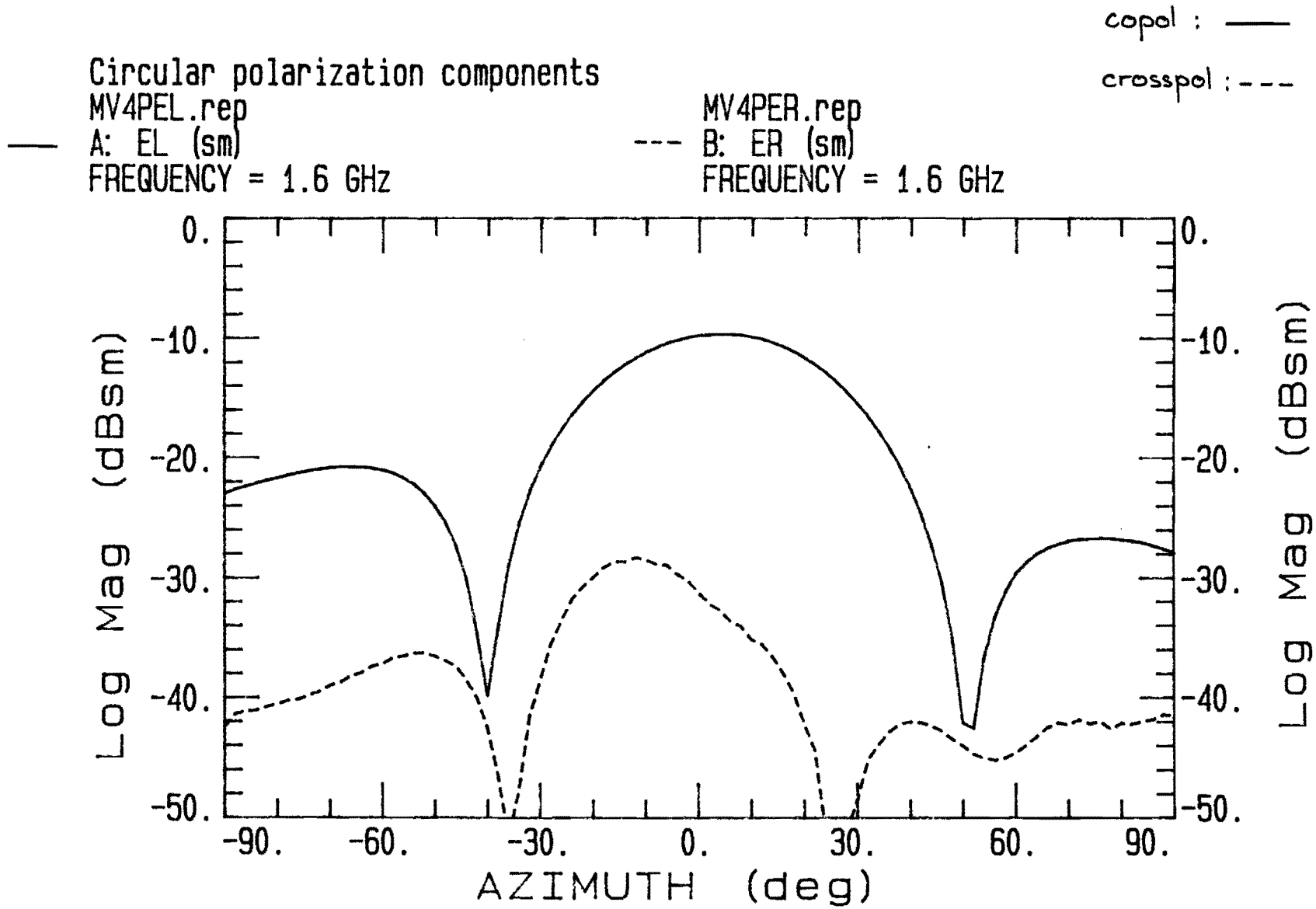

Fig. E.13 Four element circularly polarized antenna array.
(Principal plane)

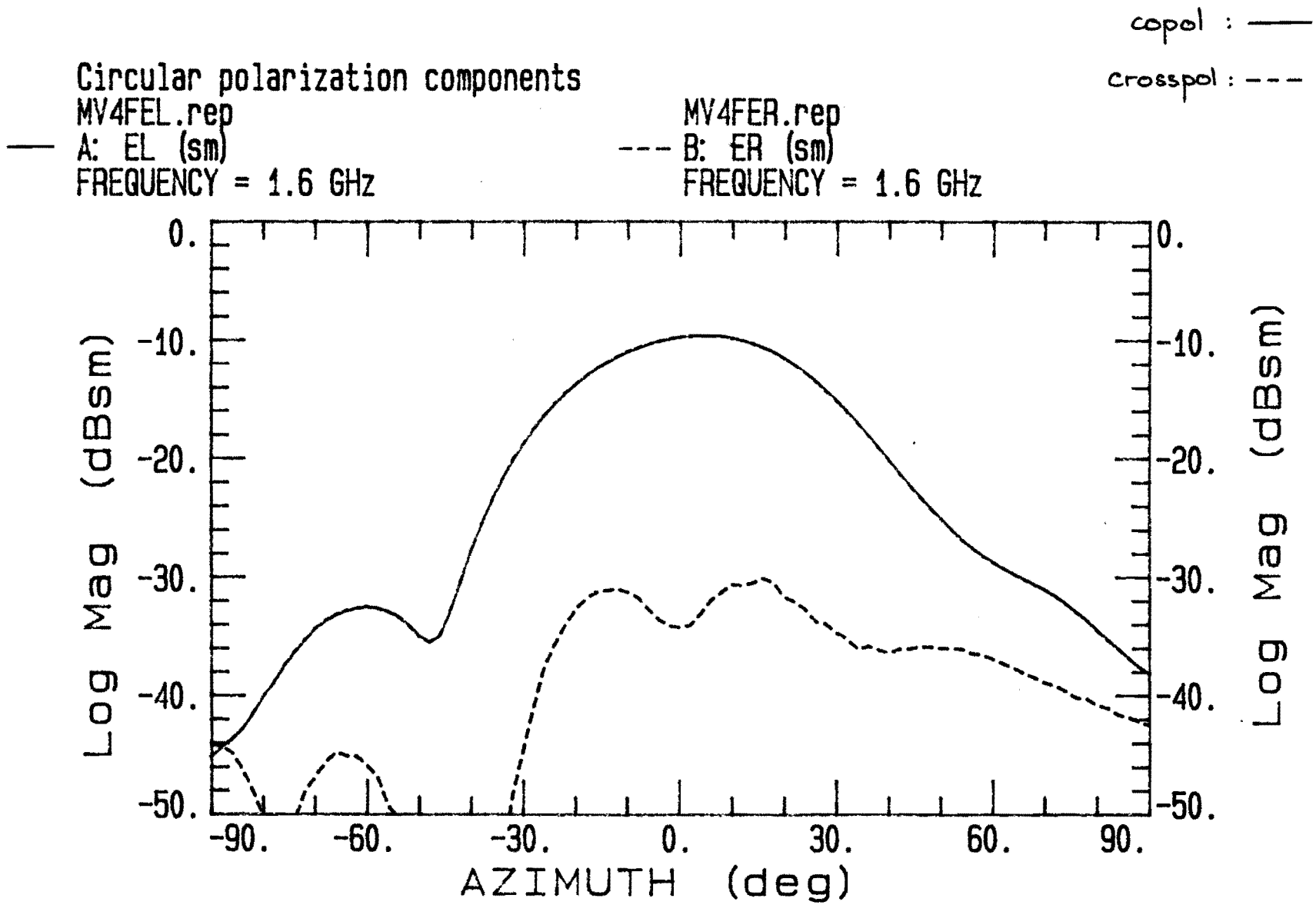

Fig. E.14 Four element circularly polarized antenna array.
(Diagonal plane)

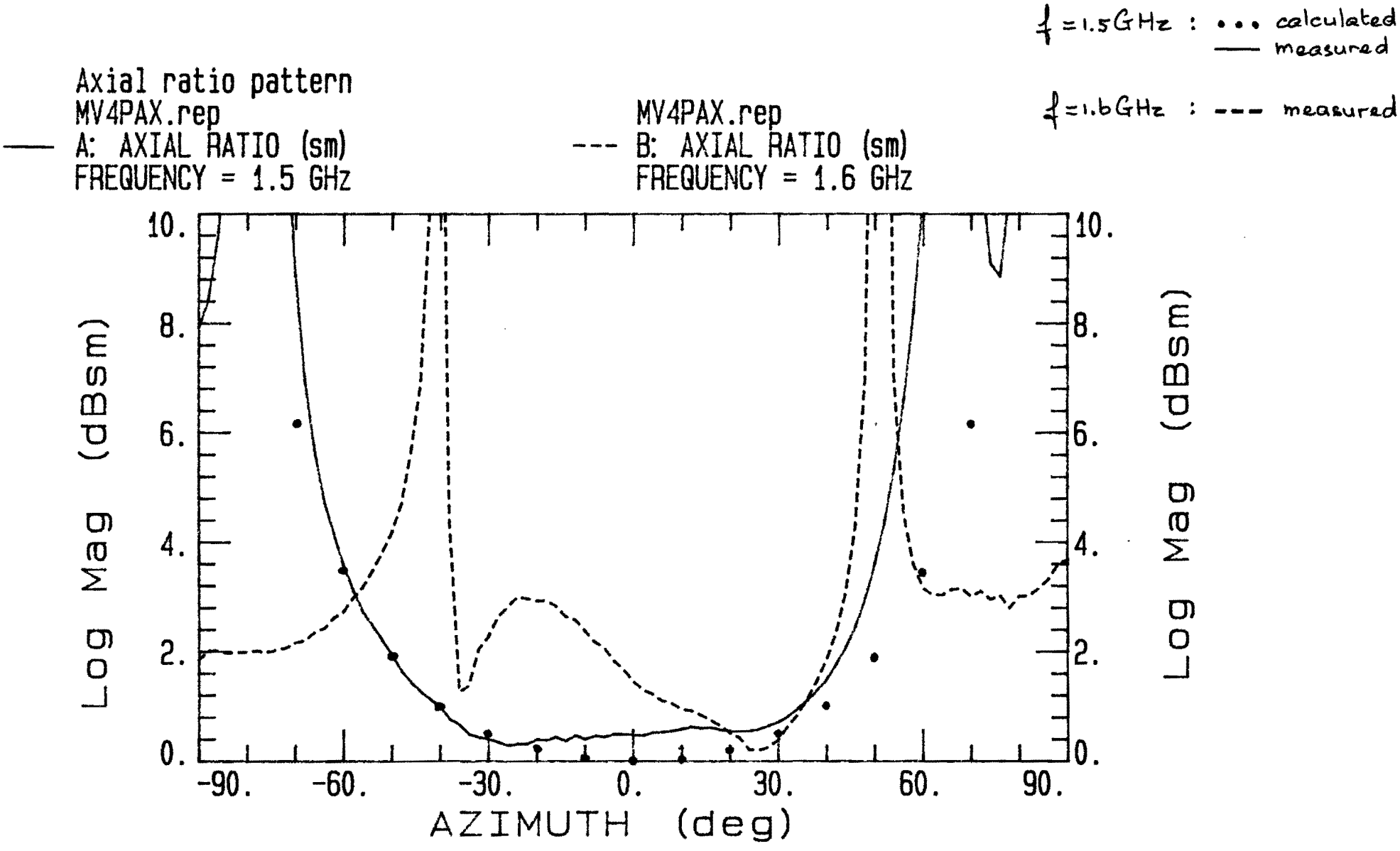

Fig. E.15 Four element circularly polarized antenna array.
(Principal plane)

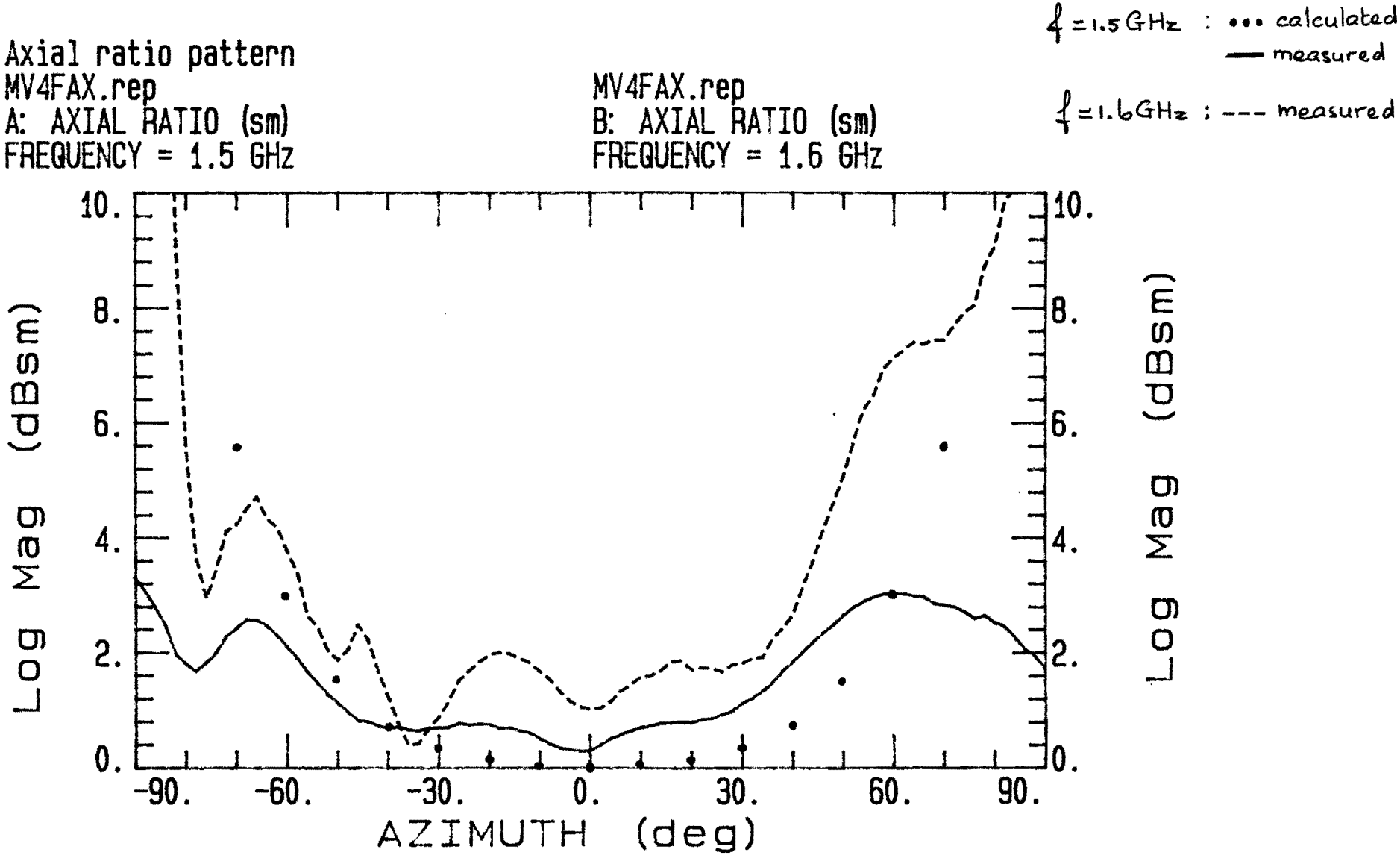

Fig. E.16 Four element circularly polarized antenna array.
(Diagonal plane)

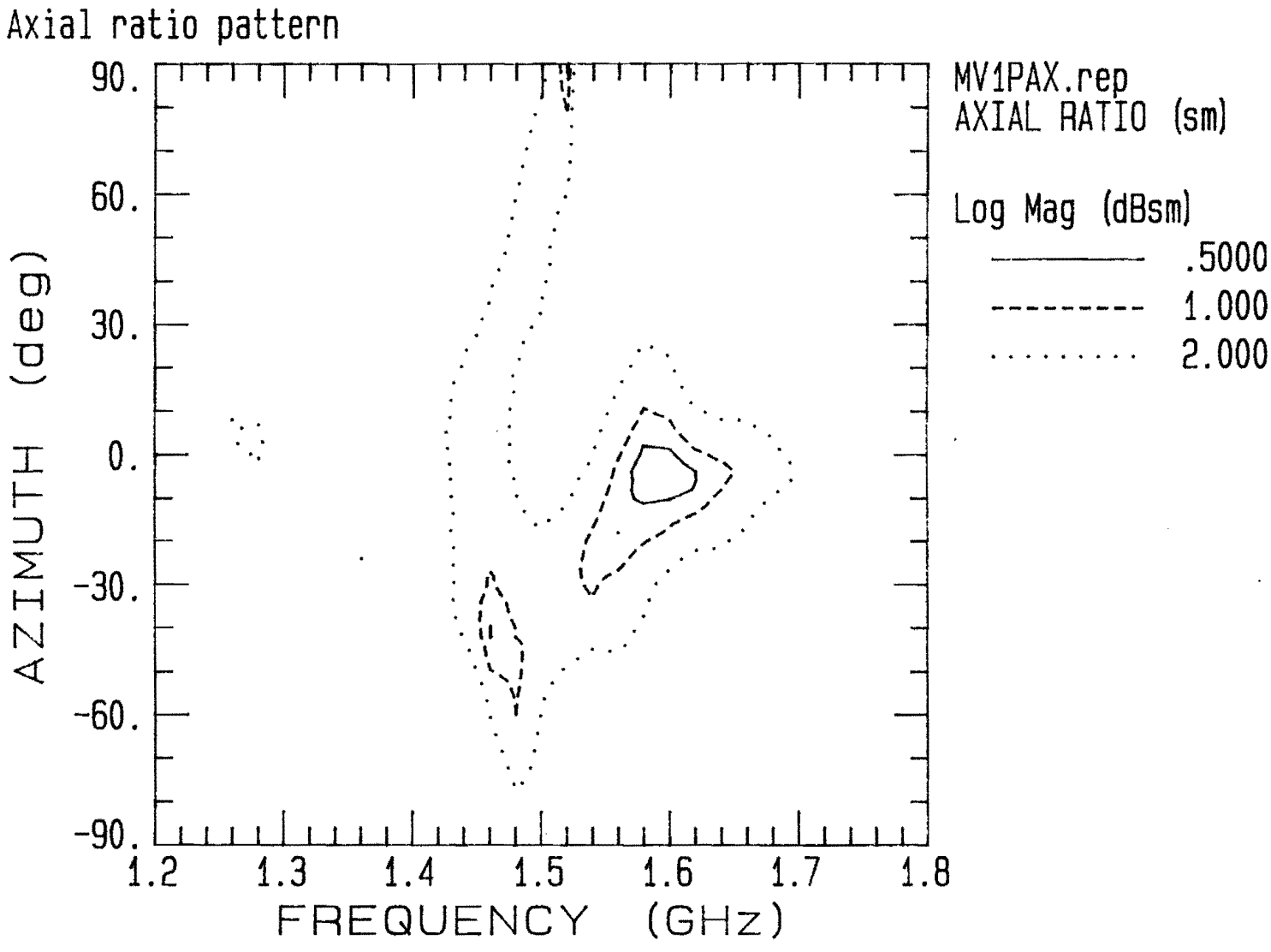

Fig. E.17 Contourplot axial ratio. Single element, circularly polarized. (Principal plane)

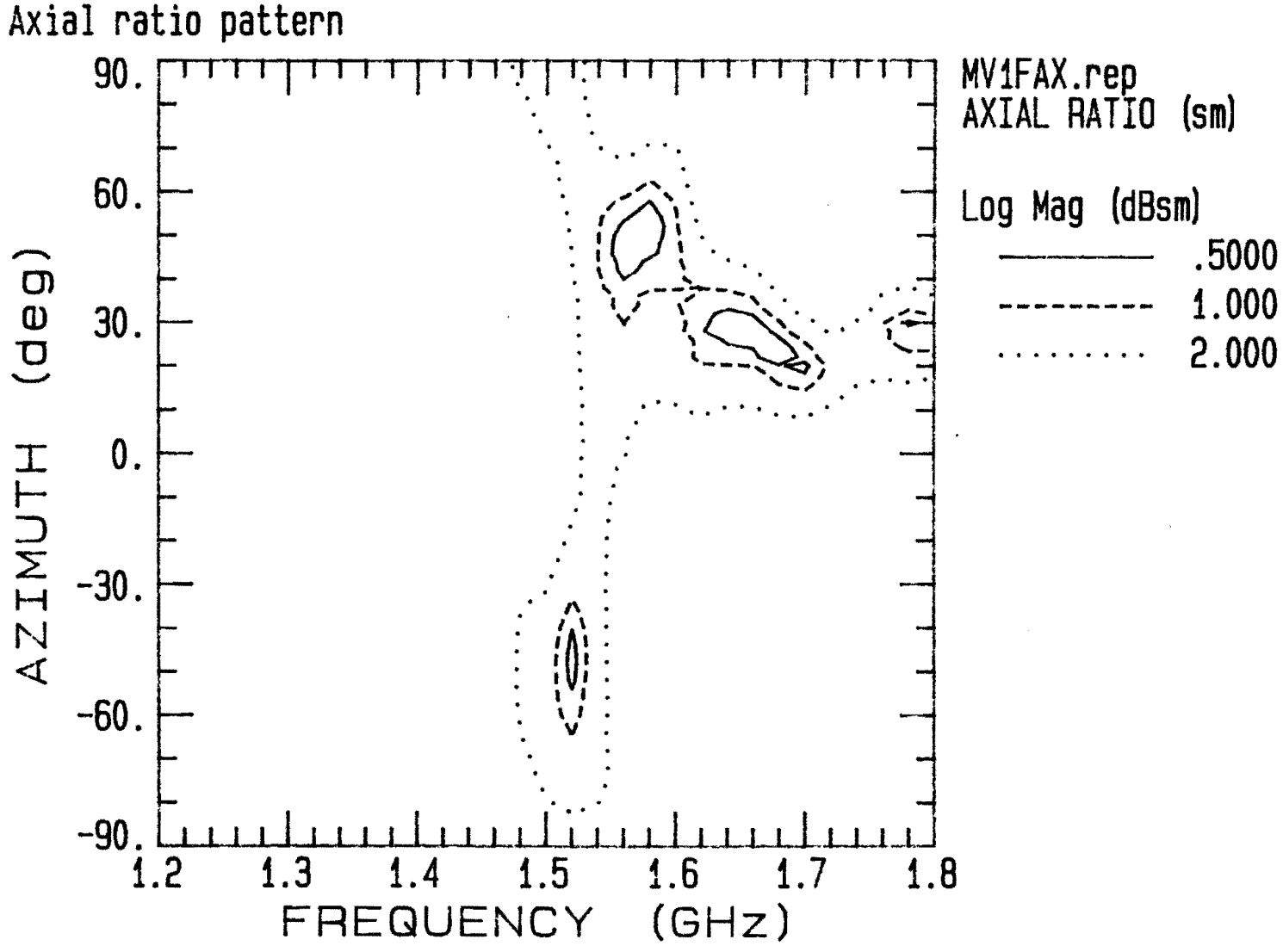

Fig. E.18 Contourplot axial ratio. Single circularly polarized antenna. (Diagonal plane)

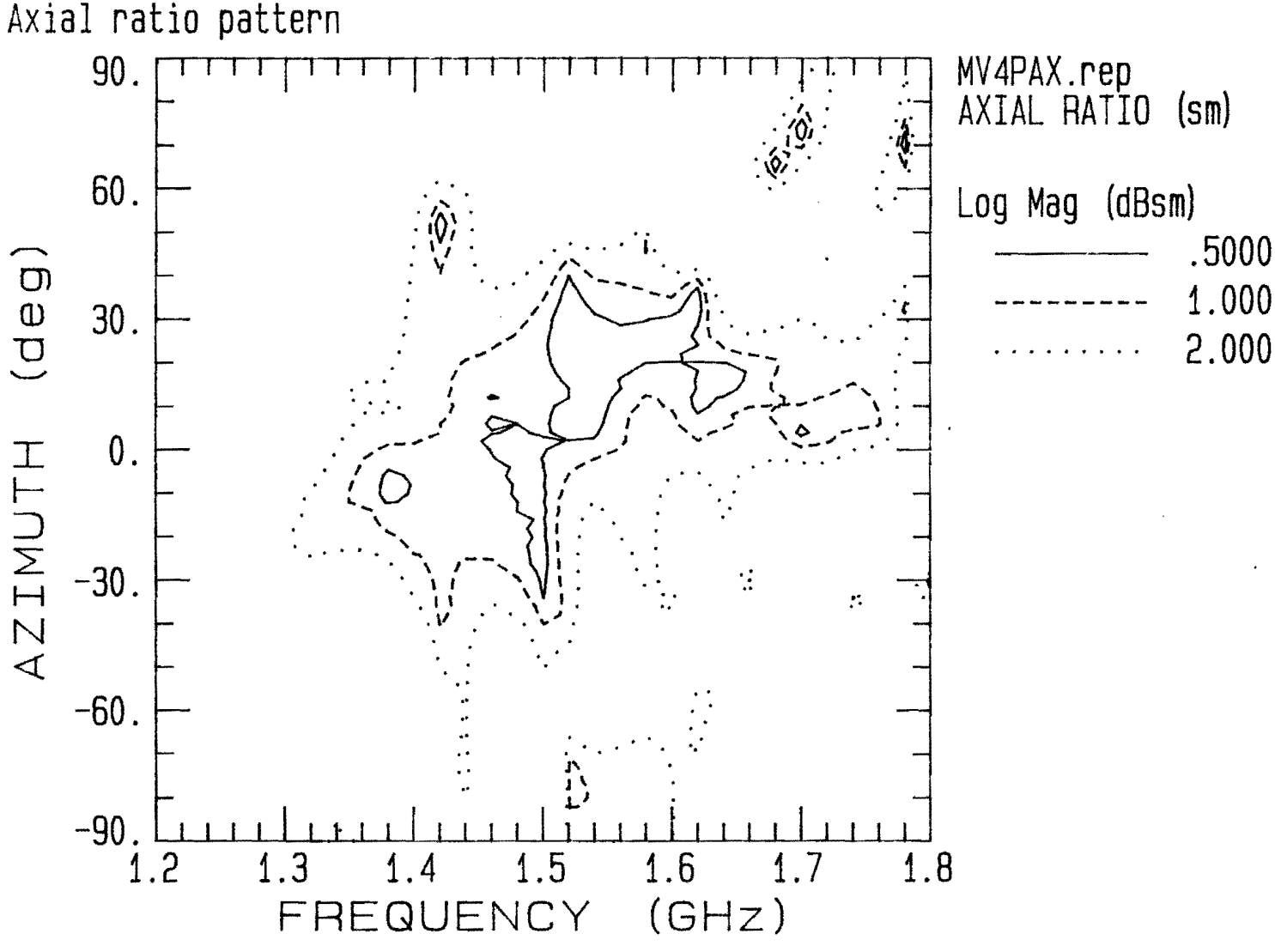

Fig. E.19 Contourplot axial ratio. Four element circularly polarized antenna array. (Principal plane).

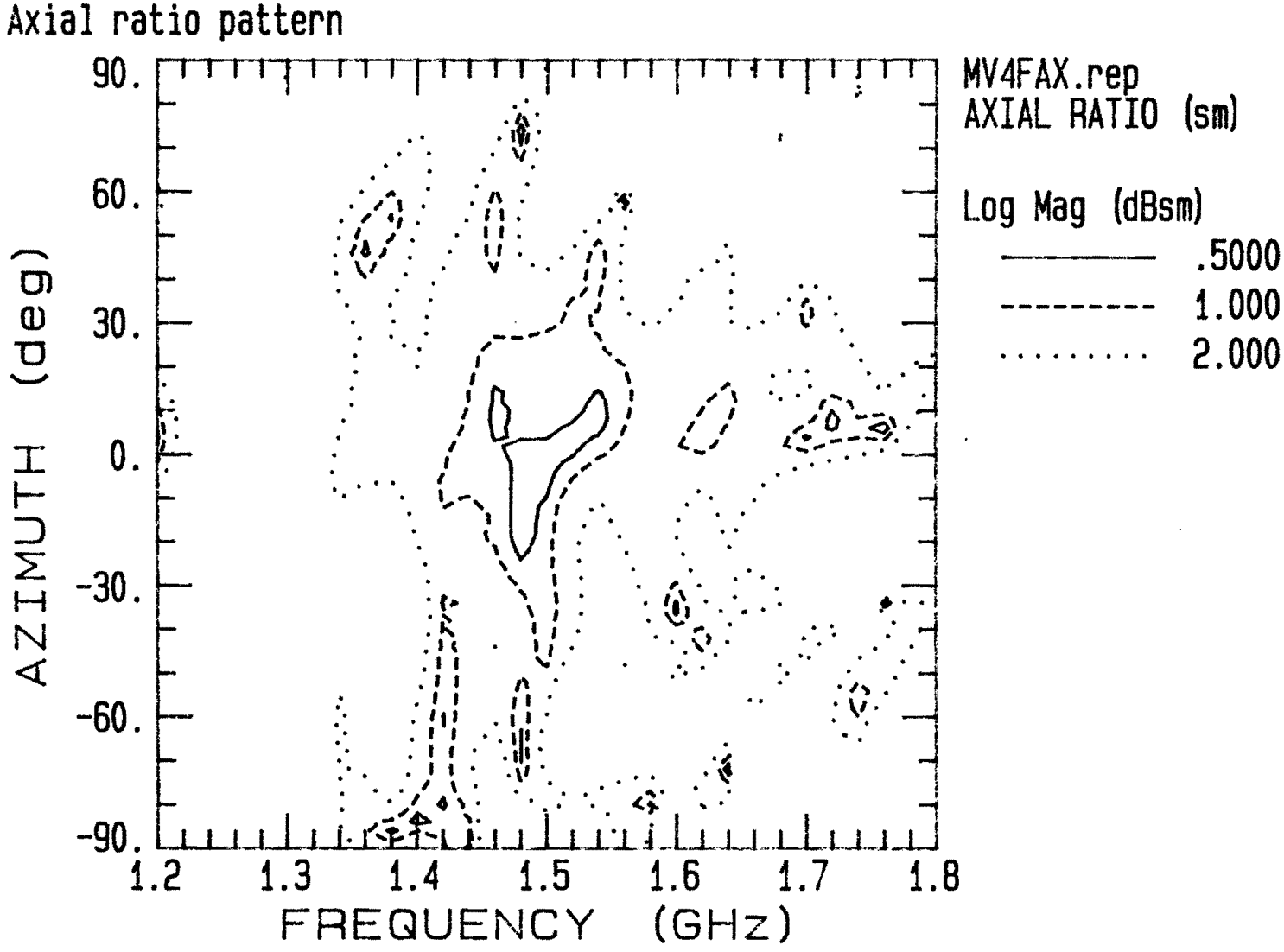

Fig. E.20 Contour plot axial ratio. Four element circularly polarized antenna array. (Diagonal plane)

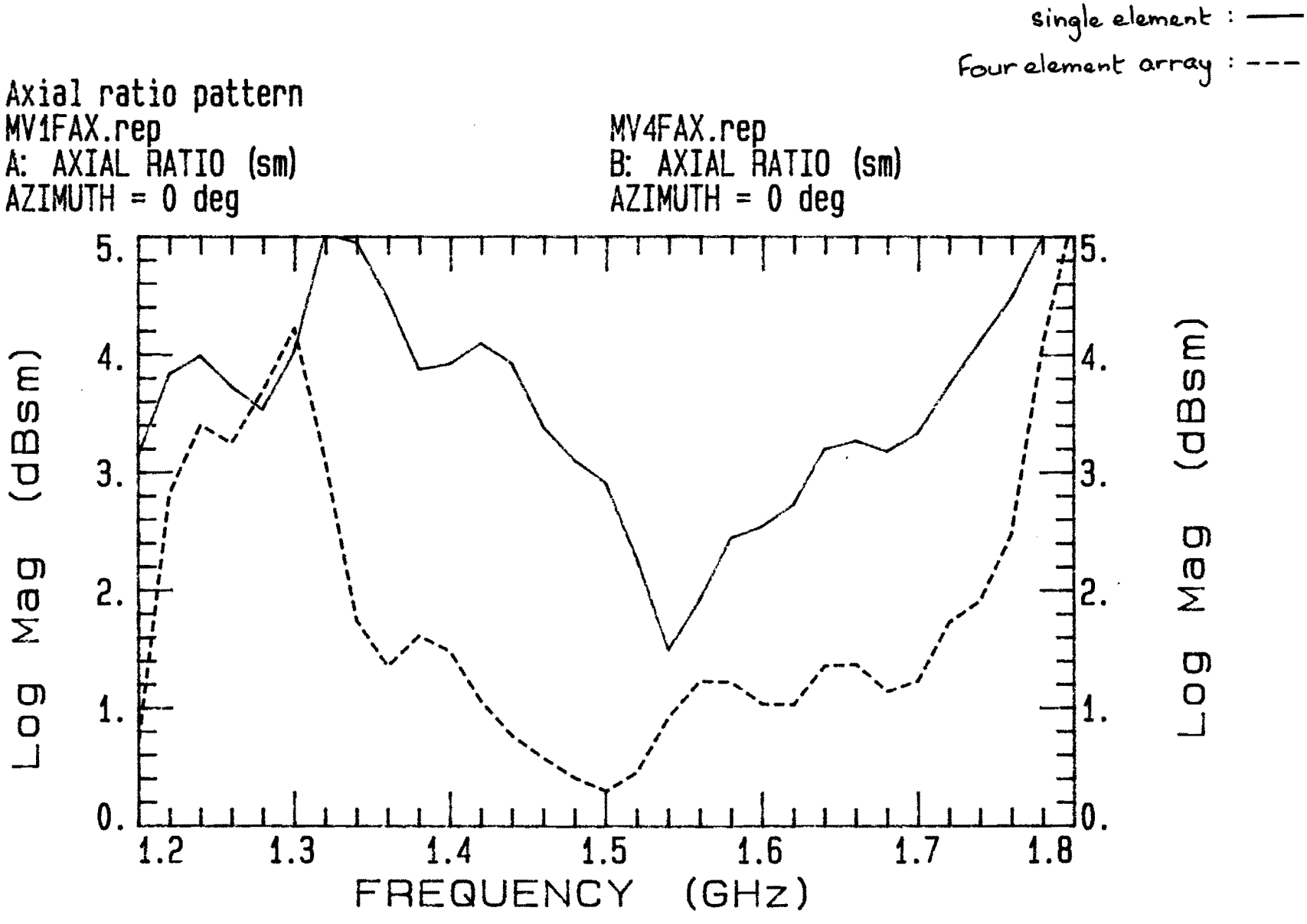

Fig. E. 21 Axial ratio versus Frequency For single element and Four element array.